

QCD

E. Laenen

Nikhef, Amsterdam, The Netherlands

Institute for Theoretical Physics, University of Amsterdam, The Netherlands

Institute of Theoretical Physics, Utrecht University, The Netherlands

Abstract

In these lecture notes I describe the theory of QCD and its application, through perturbation theory, at particle colliders.

1 Introduction

In particle physics, we encounter QCD nearly everywhere. The main collider of our time, the LHC, collides protons, which are made up of quarks, antiquarks and gluons, collectively called partons. Every proton collision involves partons, which readily produce a multitude of further partons, all turning into hadrons of one type or another. At present we are however mostly interested in *rare* final states, faint signals involving Higgs bosons, top quarks, vector bosons, possibly new particles. Hence we must understand very well how to separate the new from the known, to “remove the foreground”, in cosmology-speak; particle physicists call it background.

But it would do gross injustice to QCD and its dynamics to see it as merely a background engine. It really is a beautiful theory by itself. It is the only unbroken non-abelian gauge theory we know exists in Nature. Its Lagrangian is compact, and elegant

$$\mathcal{L}_{\text{QCD}} = -\frac{1}{4}\text{Tr}(G_{\mu\nu}G^{\mu\nu}) - \sum_{f=1}^{n_f} \bar{\psi}_f(\not{D} + m_f)\psi_f. \quad (1)$$

We shall discuss the meaning of the various symbols in this expression shortly, but one should not forget to be amazed at the complex outcomes that this relatively simple expression generates¹. For this reason, QCD dynamics is very interesting to study *sui generis*. In these lecture notes I shall visit a number² of aspects of QCD, as relevant in collider physics. The structure of these notes is as follows. In the next section the fundamental degrees of freedom and symmetries of QCD are discussed. In section 3 we discuss aspects of perturbative QCD when going to higher fixed orders. Section 4 contains an exposition of some modern methods of calculations, focussing in particular on helicity methods. Section 5 discusses aspects of all-order resummation, the underlying reasons and some applications. I conclude in Section 6. An appendix contains conventions and useful formulae.³

2 Partons and hadrons

In this section we discuss both the spectroscopic evidence for the presence of quarks and gluons in hadrons, as well as the partonic picture relevant for high-energy collisions.

2.1 Spectroscopy and symmetries of QCD

Six types (or flavours) of quarks are presently known to exist. They are fermions and are denoted by u , c , t and d , s , b , respectively, abbreviations of the names ‘up’, ‘charm’, ‘top’, and ‘down’, ‘strange’,

¹Of course, for that matter, the QED Lagrangian is even simpler, and yet it governs all of atomic physics, chemistry etc.

²Some of the notes correspond to a forthcoming book: *Field Theory in Particle Physics*, by B. de Wit, E. Laenen and J. Smith.

³*Caveat emptor*: though I tried to avoid them, there might be errors and inconsistencies in the equations below. In addition, I made no effort to be exhaustive in references.

‘bottom’. Three (u, c, t) have electric charge $\frac{2}{3}$ and three (d, s, b) charge $-\frac{1}{3}$ (measured in units of the elementary charge). Because quarks are not detected as separate physical particles (they are confined into hadrons), their masses are not exactly known, but can be estimated from hadron spectroscopy once the hadron composition in terms of quarks is given. The mass values thus obtained are called "constituent masses". One commonly introduces quantum numbers such as isospin or strangeness to distinguish the quark flavour, which then explains the corresponding quantum numbers of the hadronic bound states. Of course, there are also corresponding antiquarks $\bar{u}, \bar{c}, \bar{t}$ and $\bar{d}, \bar{s}, \bar{b}$, with opposite charges. The lightest-mass mesons and baryons are bound states of quarks and/or antiquarks with zero angular momentum.

For the moment let us restrict our attention to a single quark flavour, whose interactions are given by a non-abelian gauge theory. This choice is motivated by the fact that only such theories have the property that the interactions become strong at low energies, and can therefore explain confinement. We shall return to this further below. In order to let a non-abelian gauge group act on the quark field, we are forced to extend the number of fields. According to QCD, this gauge group is $SU(3)$. We shall try to justify this choice for the gauge group in a little while and first consider the definition of the theory. In order that $SU(3)$ can act nontrivially on the quark field $q(x)$, this field must have at least three components, so we write $q_\alpha(x) = (q_1(x), q_2(x), q_3(x))$. Hence for a given quark flavour, we have three different fields. These three varieties are called *colours* and are commonly denoted by ‘red’, ‘green’ and ‘blue’. Of course, at first sight, this assumption seems to make matters worse. We started with one quark for each flavour, which cannot be observed as a free particle; now we have three times as many unobservable quarks. Actually, the problem is even more vexing. Because quarks rotate under an $SU(3)$ symmetry group, one should expect a corresponding degeneracy for the observed bound states. In other words, each hadronic state should in general be degenerate and carry colour, while all other properties such as mass, electric charge and the like are independent of colour. We clearly do not observe such an exact degeneracy in Nature. Nevertheless, let us for now ignore this apparent proliferation of degrees of freedom and turn to the other ingredients of the model. Because the group $SU(3)$ is eight-dimensional ($SU(3)$ has eight generators), we must have eight gauge fields, denoted by V_μ^a . Under $SU(3)$ the quark fields transform in the fundamental, triplet representation, viz.

$$q(x) \rightarrow q'(x) = \exp\left(\frac{1}{2}i_a \xi^a(x)\right) q(x), \quad (2)$$

where $\xi^a(x)$ are the eight transformation parameters of $SU(3)$, and $q(x)$ represents the three-component column vector q_α consisting of the three quark colours. The conjugate quark fields are represented by the row vector $\bar{q}_\alpha = (\bar{q}_1, \bar{q}_2, \bar{q}_3)$ and transform according to

$$\bar{q}(x) \rightarrow \bar{q}'(x) = \bar{q}(x) \exp\left(-\frac{1}{2}i_a \xi^a(x)\right). \quad (3)$$

The invariant Lagrangian now takes the form

$$L = -\frac{1}{4}(G_{\mu\nu}^a)^2 - \bar{q} \not{D}q - m \bar{q}q, \quad (4)$$

with

$$\begin{aligned} G_{\mu\nu}^a &= \partial_\mu V_\nu^a - \partial_\nu V_\mu^a - g f_{bc}^a V_\mu^b V_\nu^c, \\ D_\mu q &= \partial_\mu q - \frac{1}{2}ig V_\mu^a t_a q. \end{aligned} \quad (5)$$

The $SU(3)$ generators $t_a = \frac{1}{2}i_a$ are expressed in terms of a standard set of matrices t_a , the Gell-Mann matrices, which are generalizations of the Pauli matrices τ_a . The $SU(3)$ structure constants f_{bc}^a follow from the commutators of these generators. Note that, we choose our generators to be anti-hermitian.

For other flavours, the QCD Lagrangian takes the same form as in (4), except that the actual value for the quark-mass parameter is different. The full Lagrangian thus depends on the QCD coupling constant g and on the mass parameters m , one for each flavour (quarks of different colour but of the same

flavour should have the same mass in order to conserve the $SU(3)$ gauge symmetry). Here we stress that the mass parameter in the Lagrangian *cannot* be identified directly with the constituent mass, which should follow from solving the full QCD field equations. Obviously, the QCD interactions leave the flavour of the quarks unchanged, and thus also strangeness and similar quantum numbers. However, with the exception of the electric charge, these quantum numbers are not conserved by the weak interactions, and quarks can change their flavour by emitting weak interaction bosons. The gluons do not carry flavour, but they do carry colour, since they transform under the $SU(3)$ gauge group. We therefore see that the quark content of the hadrons can be probed by weak and electromagnetic interactions through deep-inelastic scattering experiments.

Of course, quarks also carry spin indices, as they are normal Dirac spinor fields, so they are quite rich in indices. One index is the spinor index, which takes four values. Then there is the colour index, denoted above by α, \dots , which takes three values. Finally we can assign a flavour index, which takes six values corresponding to the different flavours. As we shall discuss colour further below, let us here explore aspects of quark flavour. By construction the QCD Lagrangian is invariant under *local* $SU(3)$. However, depending on the values for the mass parameters, there can also be a number of *global* flavour symmetries. The presence of these flavour symmetries has direct consequences for the hadronic bound states. The flavour symmetries are most relevant for the light quarks. As the mass parameters of the u and d quarks are comparable in size, the QCD Lagrangian is nearly invariant under global unitary rotations of the u and d quarks. These rotations form the group $U(1) \otimes SU(2)$. The invariance under $U(1)$ is related to the conservation of baryon number (quarks carry baryon number $\frac{1}{3}$, antiquarks $-\frac{1}{3}$). The $SU(2)$ transformations mix up and down quarks and are called isospin transformations. The breaking of isospin invariance is thus due to the fact that the u and d mass parameters are not quite equal (an additional but small breaking is caused by the electroweak interactions, which we do not consider in this chapter). The u and d mass parameters are not only nearly equal, they are also very small, which implies that the Lagrangian has in fact even more approximate flavour symmetries. To wit, for vanishing quark mass the Lagrangian is also invariant under unitary transformations of the u and d fields that contain the matrix γ_5 . Such transformations are called *chiral* transformations. Because of the presence of γ_5 , these transformations of the quarks will depend on their spin. We shall discuss these symmetries further below. These extra transformations involving γ_5 actually quite subtle because the chiral symmetry is realized in a so-called spontaneously broken way. The fact that the pion mass is so small (as compared to the other hadron masses) can then be explained by an approximate chiral symmetry in Nature. Obviously, we may follow the same strategy when including the s quark and consider extensions of the flavour symmetry group. Apart from the phase transformations one then encounters an $SU(3)$ flavour group (not to be confused with the $SU(3)$ colour group). In view of the fact that the s quark has a much higher mass, flavour $SU(3)$ is not as good a symmetry as isospin. Symmetry breaking effects are usually of the order of 10%. Of course one may consider further extensions by including γ_5 into the transformation rules or by including even heavier quarks. However, these extensions of the flavour symmetries tend to be less and less useful as they are affected by the large quark masses and thus no longer correspond to usefully approximate symmetries of Nature.

In order to realize the $SU(3)$ gauge transformations on the quark fields, we introduce three varieties of quarks, prosaically denoted by colours. However, it seems inevitable that the observed hadrons, bound states of quarks and antiquarks, will also exhibit the colour degeneracy. For instance, the pions are thought of as bound states of a u or a d quark with a \bar{u} or a \bar{d} antiquark. Since quarks and antiquarks come in three different colours, one has in principle *nine* types of pions of given electric charge, which must have equal mass. Altogether there should then be twenty-seven types of pions, rather than the three found in Nature!

The reason why this colour degeneracy is not observed in Nature is a rather subtle one. To explain this phenomenon, let us start by considering quarks of a single flavour, say u quarks, and construct the possible states consisting of three quarks, all at rest. Together they form a state with zero angular

momentum. Depending on the properties of the forces acting between these quarks, the three quarks may or may not cluster into a hadronic bound state. By comparing the properties of these three-quark states to those of the low-mass hadrons in Nature (in view of the centrifugal barrier one expects that states with nonzero angular momentum acquire higher masses) one may hope to unravel the systematics of quark spectroscopy and understand the nature of the forces that hold the hadrons together.

Hence, when considering the possibility of the three quarks forming a bound state, one may expect the emergence of a spin- $\frac{3}{2}$ bound state and/or one or two spin- $\frac{1}{2}$ bound states. Of course, whether or not they are actually realized as bound states depends on the properties of the interquark forces.

However, the above conclusions are invalidated as we are dealing with bound states of *identical* spin- $\frac{1}{2}$ particles. Being fermions they satisfy Pauli's exclusion principle, according to which the resulting state should be *antisymmetric* under the exchange of any two such particles. It turns out that the spin- $\frac{3}{2}$ bound state is, however, *symmetric* under the interchange of two fermions. This is easy to see for the states with $S_z = \pm\frac{3}{2}$, as they correspond to the situation where all three quark spins are aligned in the same direction. Hence a spin- $\frac{3}{2}$ bound state cannot be realized because of Pauli's exclusion principle. However, the spin- $\frac{1}{2}$ states cannot be realized either, as they are neither symmetric nor antisymmetric under the interchange of any two particles, but are of mixed symmetry (i.e., they can be (anti)symmetric under the exchange of two of the quarks, but not with respect to the third quark). Therefore, bound states of three identical spin- $\frac{1}{2}$ particles with zero angular momentum cannot exist, it would seem.

Surprisingly enough, when comparing the result of such quark model predictions to the low-mass baryons in Nature, one finds that there is in fact a bound state of three u quarks with spin- $\frac{3}{2}$, namely the Δ^{++} baryon with a mass of $1232 \text{ MeV } c^{-2}$, which is unstable and decays primarily into $p\pi^+$ with an average lifetime of $0.59 \times 10^{-23} \text{ s}$. On the other hand, no spin- $\frac{1}{2}$ bound states of three u quarks are found. At this point one could of course question the quark interpretation of the Δ^{++} , were it not for the fact that this phenomenon is universal! When comparing the quark model to the data, it turns out that the baryons always correspond to bound states of quarks that are *symmetric* rather than antisymmetric under the interchange of two quarks. Therefore, one would conclude, the Pauli principle is violated in the simple quark model.

Before resolving this puzzle, let us once more exhibit this phenomenon, but now for the slightly more general case of low-mass baryons consisting of u and d quarks. Each quark in the baryon now comes in four varieties: a u quark with spin 'up' or 'down' (measured along some direction in space) or a d quark with spin 'up' or 'down'. Assuming again zero total angular momentum, there are thus $4^3 = 64$ possible spin states, twenty of which are symmetric under the interchange of two particles. These symmetric states decompose into sixteen states with both isospin and ordinary spin equal to $\frac{3}{2}$, and four states with both isospin and ordinary spin equal to $\frac{1}{2}$. The first sixteen states correspond to the baryons $\Delta^{++}(uuu)$, $\Delta^+(uud)$, $\Delta^0(udd)$ and $\Delta^-(ddd)$, which carry spin- $\frac{3}{2}$ so that each one of them appears in four possible spin states (we listed the quark content in parentheses). The latter four states correspond to the nucleons $p(uud)$ and $n(udd)$, which carry spin- $\frac{1}{2}$ and thus appear in two varieties.⁴ No other states corresponding to bound states of three u or d quarks can be identified with baryons in Nature (for higher masses such bound states can be found, but those will have nonzero angular momentum).

Let us now stop exploring in detail the subtleties of the simple quark model, and turn to quantum chromodynamics. Because the quarks carry colour one can make the three-quark state antisymmetric by postulating total antisymmetry in the three colour indices. In this way the exclusion principle is preserved. This conjecture may seem rather ad hoc, and one may wonder whether there is an a priori reason for assuming antisymmetry in the colour indices. Indeed, it turns out that there is a principle behind this. When antisymmetrizing over the colour indices of a three-quark state, this state is a singlet

⁴As explained above, the spin- $\frac{1}{2}$ states are of mixed symmetry. However, the mixed symmetry in terms of the spin indices of the quarks can be combined with the mixed symmetry of the isospin indices in such a way that the resulting state becomes symmetric.

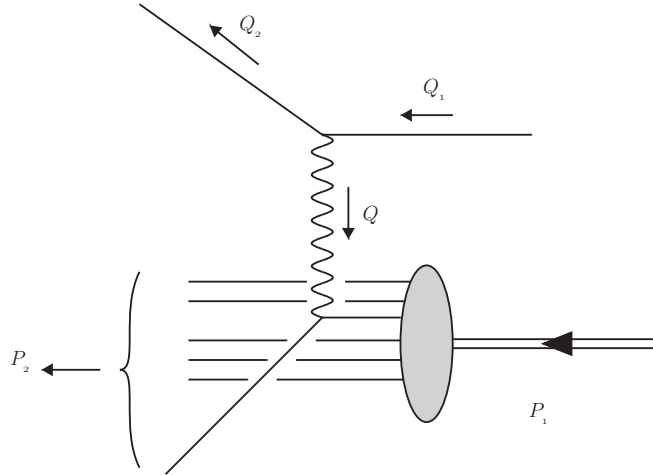


Fig. 1: Parton picture of a deep-inelastic collision process. Note that in the diagram time runs from right to left.

under the $SU(3)$ colour group. This follows from the tensor product of three triplets

$$\mathbf{3} \otimes \mathbf{3} \otimes \mathbf{3} = \mathbf{1} \oplus \mathbf{8} \oplus \mathbf{8} \oplus \mathbf{10}, \quad (6)$$

which yields a singlet state under colour $SU(3)$ that is fully antisymmetric.⁵ Assuming that no hadrons carry colour (so that they are *invariant* under the colour gauge group) requires the three-quark states to be antisymmetric in the colour indices. By virtue of Pauli's exclusion principle, they must therefore be *symmetric* with respect to all other quantum numbers, such as spin and isospin.

The principle that hadrons should be colourless can be put to a test when considering the low-mass mesons. As we mentioned at the beginning of this section, the mesons are bound states of a quark and an antiquark. Because of the three-fold degeneracy of the quarks associated with colour, each meson should appear in nine varieties, which differ in colour, but not in electric charge and mass. However, one particular combination of these states is again colourless. This follows from the tensor product rule

$$\mathbf{3} \otimes \bar{\mathbf{3}} = \mathbf{1} \oplus \mathbf{8}, \quad (7)$$

according to which the nine colour states decompose into a singlet state and eight states belonging to the octet representation. Only the singlet state is realized as a physical particle, so that the colour degeneracy is avoided. This turns out to be a universal feature of all hadrons. We simply never observe the colour degrees of freedom, but only bound states of quarks that are singlets of the colour symmetry group. In other words if we assign the primary colours to $\alpha = 1, 2, 3$ then the observed hadrons must be "white". Of course, this analogy is mostly picturesque and by no means necessary.

2.2 Parton model

We mentioned above that deep-inelastic scattering reveals the presence of weakly bound point-like parton constituents inside the nucleon, which we will shortly identify as spin- $\frac{1}{2}$ fractionally charged quarks (gluons are neutral with respect to weak and electromagnetic interactions, so they are not directly involved in this process). To see this, we first examine a simple model in which the fast-moving nucleon

⁵The interpretation of this product rule is as before. The $3^3 = 27$ states formed by all possible products of $SU(3)$ triplet states decompose under the action of $SU(3)$ in four different representations: the singlet representation, which is completely antisymmetric, the $\mathbf{10}$ representation, which is completely symmetric, and two $\mathbf{8}$ representations, which have mixed symmetry (the $SU(3)$ representations are denoted by their dimension, unlike the representations of the rotation group, which are denoted by the value of the spin). To derive such product rules is more complicated for $SU(3)$ than for the $SU(2)$, the relevant group for spin and isospin.

consists of a finite number of particles, each carrying a certain fraction of its momentum. These constituents are so weakly bound that they may be regarded as free. For simplicity we assume also that just one parton is subject to the interaction with the photon that is exchanged in the inelastic process; the others are neutral and play the role of spectators (see Fig. 1). The charged constituent with momentum $p_\mu = \xi P_{1\mu}$ (we neglect the transverse parton momenta) and mass $m = \xi M$ ($0 < \xi < 1$) changes its momentum to $(\xi P_1 + Q)_\mu$ in the interaction with the virtual boson; the mass-shell condition requires $(\xi P_1 + Q)^2 = (\xi P_1)^2$ or $2\xi P_1 \cdot Q + Q^2 = 0$. We have then

$$\xi = -\frac{Q^2}{2P_1 \cdot Q} \equiv x, \quad (8)$$

where we have introduced the Bjorken scaling variable x , whose meaning is clear from (8).

Defining also the variable y by the fractional energy loss of the incoming lepton, i.e. in de target restframe by $(E' - E)/E$, one may write the differential cross section for deep-inelastic scattering (DIS), mediated by a photon, in terms of dimensionless structure functions as

$$\left(\frac{d^2\sigma}{dx dy}\right)^\gamma = \frac{8\pi\alpha^2 ME}{(Q^2)^2} \left[\frac{1 + (1-y)^2}{2} 2xF_1^\gamma(x, Q^2) + (1-y)[F_2^\gamma(x, Q^2) - 2xF_1^\gamma(x, Q^2)] - \frac{M}{2E}xy F_2^\gamma(x, Q^2) \right], \quad (9)$$

where M is the nucleon mass. The accumulated data for this process, mostly from the HERA collider at DESY, are displayed in Fig. 2. Notice that to first approximation the structure function $F_2(x, Q^2)$ only

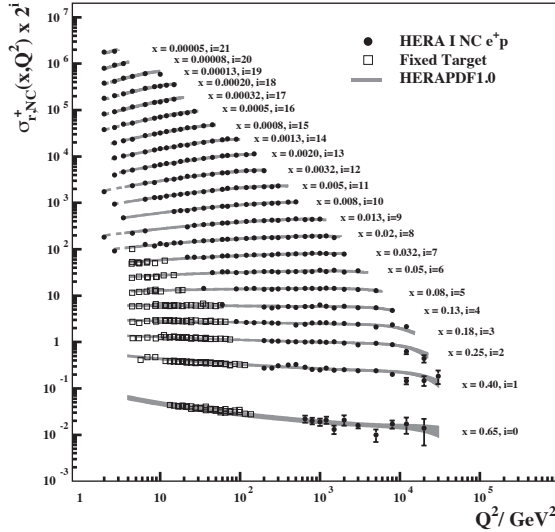


Fig. 2: The reduced cross section (corresponding to $F_2(x, Q^2)$ up to a small correction due to weak interaction effects). The data have been taken at the HERA collider [1].

depends on x , a phenomenon known as scaling. The parton model, to which we now turn, provides an explanation for this phenomenon.

After the interaction with the virtual boson has taken place, the charged constituent will move in a different direction than the spectator particles. However, during recoil it feels the influence of the binding mechanism, which forces the constituents to recombine into a new hadronic state, such as an excited nucleon or a nucleon with one or several pions (on a much longer time scale than that of the primary collision). Confinement dictates that the nature of this final-state interaction is such that the

partons cannot be produced as isolated particles, and that the binding force does not interfere with the primary interaction with the vector bosons.

Because the spectators do not participate in the primary interaction the cross section for inelastic lepton-nucleon scattering is given directly in terms of the cross section for lepton-parton scattering. Assuming that the parton is point-like and that the beam energy in the laboratory frame is large compared to the masses, one can compute, using the rules of QED

$$\left(\frac{d\sigma}{dy}\right)^\gamma = \frac{8\pi\alpha^2 ME}{(Q^2)^2} q^2 \frac{(1-y)^2 + 1}{2} \xi. \quad (10)$$

where the factor ξ arises because we have replaced the parton mass m by $M\xi$. Comparing (10) to (9), we conclude that the contribution from elastic parton scattering via photon exchange to the nucleon structure functions is given by

$$F_2^\gamma(x) = 2xF_1^\gamma(x) = q^2 x \delta(x - \xi), \quad (11)$$

The structure functions thus satisfy the Callan-Gross relation [2]

$$F_2(x) = 2xF_1(x), \quad (12)$$

which is characteristic for (massless) spin- $\frac{1}{2}$ partons. Although we have now found structure functions that depend only on x , in agreement with the phenomenon of scaling discussed above, the model is clearly unrealistic as x remains restricted to a single value ξ . Therefore, to improve the situation one now assumes that the nucleon contains many partons interacting with the intermediate photon and carrying a fraction of the nucleon momentum according to a probability distribution $f(\xi)$. To be precise, $f_i(\xi)d\xi$ measures the number of partons of type i (e.g. a u-quark or a gluon) in the momentum range from ξP_1 to $(\xi + d\xi)P_1$. As the nucleon may also contain anti-partons there is a corresponding distribution $\bar{f}_i(\xi)$ to measure the number of anti-partons in the same momentum range. In doing so we will keep ignoring the effect of transverse parton momenta. Furthermore we assume that the scattering on the partons is *incoherent* (i.e. quantum-mechanical interference effects between scattering reactions on different partons are ignored) so that we can simply sum and/or integrate (10) over the various (anti-)parton distributions,

$$\left(\frac{d\sigma}{dy}\right)^\gamma = \frac{8\pi\alpha^2 ME}{(Q^2)^2} \frac{(1-y)^2 + 1}{2} \sum_i q_i^2 \int_x^1 d\xi \xi f_i(\xi), \quad (13)$$

where the sum is over (anti-)quark flavours i having fractional charge q_i (either $\frac{2}{3}$ or $-\frac{1}{3}$). Let us discuss a few more consequences of the parton model. Identifying the partons as quarks⁶ we can directly derive the following parton model expression for the electromagnetic structure functions

$$\begin{aligned} x^{-1}F_2^\gamma(x) &= 2F_1^\gamma(x) \\ &= \frac{4}{9}[u(x) + \bar{u}(x) + c(x) + \bar{c}(x)] + \frac{1}{9}[d(x) + \bar{d}(x) + s(x) + \bar{s}(x)]. \end{aligned} \quad (14)$$

One may now also immediately state the charge sum rule

$$\begin{aligned} Q^{\text{nucleon}} &= \int_0^1 dx \left[\frac{2}{3}[u(x) - \bar{u}(x) + c(x) - \bar{c}(x)] \right. \\ &\quad \left. - \frac{1}{3}[d(x) - \bar{d}(x) + s(x) - \bar{s}(x)] \right], \end{aligned} \quad (15)$$

which the parton distribution functions must obey. Furthermore we note that by interchange of u and d quarks a proton becomes a neutron and vice versa (this interchange can be realized by a special isospin transformation). Therefore all neutron quark distributions follow from those of the proton: $u(x)^N = d(x)^P$, $d(x)^N = u(x)^P$, whereas the s- and c-distributions are equal. Henceforth we will therefore use the notation where $u(x)$, $d(x)$, $s(x)$ and $c(x)$ refer to the proton structure functions only. In Fig. 3

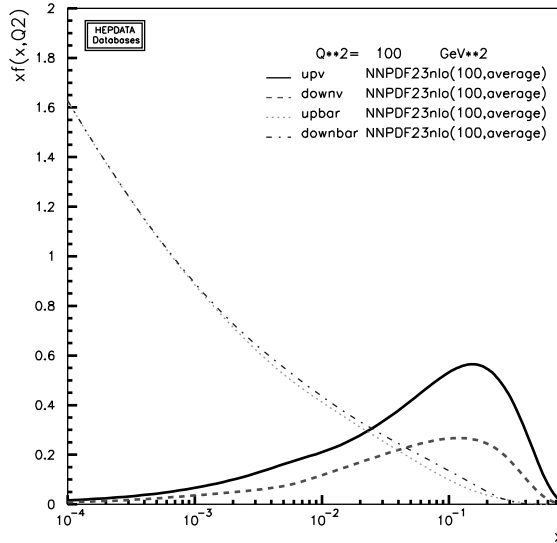


Fig. 3: The distributions of $x[u(x) - \bar{u}(x)]$ and $x[d(x) - \bar{d}(x)]$ (the valence quarks), as well as those of the anti-up $x\bar{u}(x)$ and anti-down $x\bar{d}(x)$ in the proton. The plots correspond to the NNPDF set, version 2.3 [3] for a value of $Q^2 = 100 \text{ GeV}^2$ [4].

we show some examples of quark distribution functions in the proton. Unlike the quarks, the gluons are neutral under weak and electromagnetic interactions, so they are not directly observed in the deep-inelastic process. Their presence can, however, already be inferred from the naive model discussed above, because the total fraction of the nucleon momentum carried by the quarks (which is given by the areas under the curves of Fig. 3) is roughly $\frac{1}{2}$. This is an indirect indication that gluons carry the remaining nucleon momentum.

As stated above, if the nucleon is probed at large Q^2 the quarks inside will behave as free point-like objects. The QCD interactions will dissipate the momentum transfer Q^2 to other quarks, and in this process gluons will be radiated which may again interact with quarks or gluons or annihilate into quark-anti-quark pairs. This effect becomes more sizeable if the momentum transfer Q^2 is shared by many quarks and gluons, as the average momenta are then smaller so that the effective QCD coupling grows in strength. The timescale that is relevant for the final state interaction is therefore much larger than that for the primary interaction. Incorporating these quark-gluon interactions into the naive quark-parton model leads in principle to a consistent field-theoretic set-up for calculating quantum corrections in deep-inelastic scattering, and other processes.

We finally remark that the universal nature of the parton distribution functions $f_i(\xi)$ should allow us to apply the parton model also to the Drell-Yan process, in which a quark and an anti-quark inside the nucleons collide to form a lepton-anti-lepton pair. This we shall do further below in these notes.

2.3 Renormalization and asymptotic freedom

The examination of the quantum corrections in a theory can provide crucial insight into the structure of the theory, and its consistency. For example, if they break the gauge symmetries of a theory (so that these symmetries are anomalous), the theory can be inconsistent. It can also teach us about the predictive power of the theory. If the higher order corrections for some observable are so large that the very concept of perturbation theory for this case becomes doubtful, we have a crisis of the theory's predictive power

⁶We include u,d,s and c quarks here as they can be treated as massless quarks in most high-energy processes. Bottom and top quarks, being heavier, are often not treated as partons.

for this observable. Higher order corrections may contain ultraviolet divergences (we will discuss other divergences later). Here we discuss how one may handle them and account for them.

2.3.1 Regularization

In order to handle divergences one must first regularize the quantum field theory in such a way that the infinities become temporarily finite (would-be infinities). If done consistently, one can apply the renormalization procedure, upon which for appropriate quantities the would-be infinities cancel, so that the regularization can be removed. A number of regularization have been invented in the past, let us review some of them.

Cut-off

In this method one imposes a uniform upper limit Λ on the loop momenta

$$\int^{\Lambda} \frac{dq}{q} + \dots = \ln \Lambda + \text{finite terms} \quad (16)$$

The would-be infinity is represented here by $\ln \Lambda$. When all would-be infinities have cancelled and only $1/\Lambda^p$ terms are left, one can remove the regulator by $\Lambda \rightarrow \infty$. The advantage of this method is that it is very intuitive, the (serious) disadvantage is that it is very cumbersome in higher orders, in particular for gauge theories. It is therefore mostly used in high energy physics for didactical purposes.

Lattice

In this method one discretizes spacetime, and defines fields to live only on the lattice points (or on the links between them). In this way momenta cannot be larger than $1/a$ where a is the lattice spacing. A major advantage of this method is that it can actually be used for computer simulation, so that the full path integral can be evaluated, without need to expand it in perturbation theory. Among the drawbacks are difficulties in maintaining continuum symmetries on the lattice. It is however a widely used method, mostly for lower energy observables, such as hadron masses and decay constants.

Dimensional regularization

This is the regularization that is most powerful in perturbative quantum field theory, and therefore also most widely used. It consists of the temporary extension of the number of dimensions in spacetime, or conversely, momentum space, from 4 to $4 + \varepsilon$

$$\int d^4x \mathcal{L}(x) \rightarrow \int d^{4+\varepsilon}x \mathcal{L}(x) \quad (17)$$

How does this method regularize ultraviolet divergences⁷? A careful dimensional analysis shows that (i) momentum space propagators continue to look like $1/(q^2 + m^2)$, and (ii) gauge couplings now get dimension $-\varepsilon/2$. Then a one-loop integral is extended as follows

$$\int d^4q \frac{1}{q^4} \rightarrow \int d^{4+\varepsilon}q \frac{1}{q^4} \quad (18)$$

In $n = 4 + \varepsilon$ dimensional polar coordinates this may be written as (introducing a lower limit Q on the q integral)

$$\int d\Omega_{3+\varepsilon} \int_Q^\infty dq q^{3+\varepsilon} \frac{1}{q^4} \quad (19)$$

These d dimensional integrals can be carried out to yield

$$\frac{2\pi^{2+\varepsilon/2}}{\Gamma(2 + \varepsilon/2)} \frac{-1}{\varepsilon} Q^\varepsilon \quad (20)$$

⁷A more careful treatment of dimensional regularization, including the conditions on the complex parameter ε can be found in [5].

The Euler gamma function $\Gamma(2 + \varepsilon/2)$ makes a frequent appearance in this regularization method. The would-be infinity is $1/\varepsilon$. Removing the regulator would correspond to taking the limit $\varepsilon \rightarrow 0$.

2.3.2 Renormalization

Now that we know how to regularize a quantum field theory we are ready to understand conceptually the renormalization procedure. At its heart is the question how to have a predictive theory when higher-order corrections contribute an infinite amount to various Green functions.

Let us first form a physical picture for the case of the QED lagrangian

$$\mathcal{L}_{\text{QED}} = -\frac{1}{4}(\partial_\mu A_\nu - \partial_\nu A_\mu)^2 - \bar{\psi} \not{\partial} \psi - m \bar{\psi} \psi + ie A_\mu \bar{\psi} \gamma^\mu \psi, \quad (21)$$

with A_μ representation the photon field, ψ the electron field, and e the electric charge. For QCD the conceptual points are the same, if a bit more complicated. At lowest order, and after gauge-fixing, the lagrangian provides an electron 2-point function (leading to the electron propagator), a photon 2-point function (leading to the photon propagator), and a photon-electron 3-point function (leading to the QED interaction vertex), see Fig. 4. Let us now look at some of their one-loop correction when the

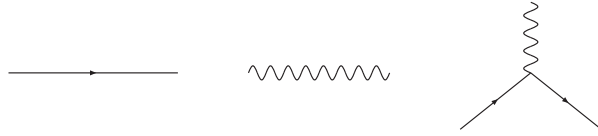


Fig. 4: Lowest order Green's functions provided by lagrangian

loop-momentum q becomes very large. In Fig. 5 we indicate how these corrections may be viewed. Be-

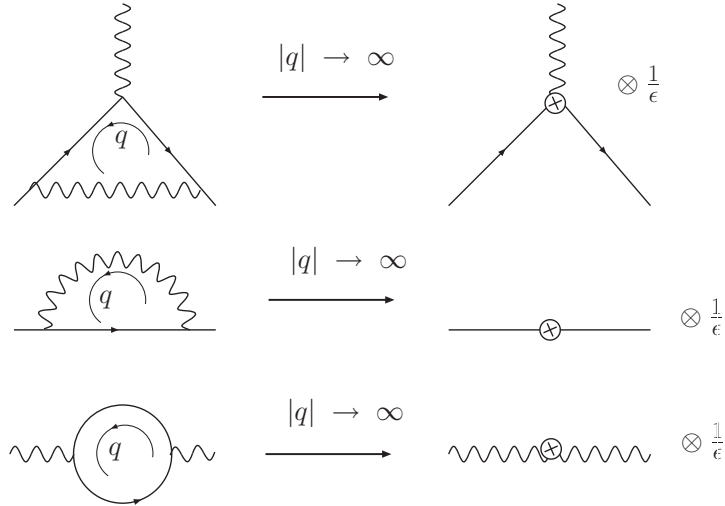


Fig. 5: One-loop corrections to lowest order Green's functions and their UV limit.

cause the loop momentum becomes so large, the loop reduces to a very local effect, of would-be infinite strength. It should be noticed that the result is simply a would-be infinite coefficient times the lowest order Green function. This is an important result. For example in Fig. 6 we see that the UV limit of the box graph, while leading to local 4-photon vertex which does *not* occur in the lagrangian, is also *not* would-be infinite. This suggests that we can absorb in this case the $1/\varepsilon$'s into the couplings and field normalizations of the lagrangian, without need to introduced new types of interactions. Quantum Electrodynamics is in fact a renormalizable theory. This means that it is sufficient to renormalize e, m, ψ, A_μ

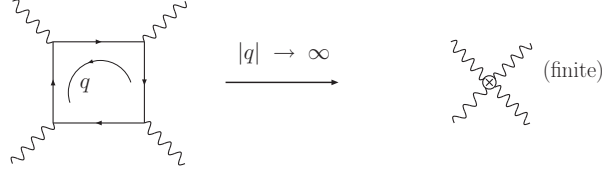


Fig. 6: UV limit of QED box graph

to absorb/cancel all would-be infinities for any Green function in QED. Let us see how this absorption works, using dimensional regularization.

First, let us recall that in dimensional regularization the dimension of the gauge coupling is no longer zero, but rather

$$[e] = \frac{2-d}{2} = -\frac{\varepsilon}{2} \quad (22)$$

To keep count of such dimensionalities, and to be able to define a dimensionless coupling, we introduce a mass scale μ , whose value is intrinsically arbitrary, such that

$$e = e(\mu)\mu^{-\varepsilon/2} \quad (23)$$

We now *renormalize* e by a factor Z_e that contains would-be infinities

$$e = e_R(\mu)\mu^{-\varepsilon/2}Z_e\left(\frac{1}{\varepsilon}, e_R(\mu)\right) = \left(1 + e_R(\mu)^2\frac{1}{\varepsilon}z_e^{(1)} + e_R(\mu)^4\left[\frac{1}{\varepsilon^2}z_e^{(2)} + \frac{1}{\varepsilon}z_e^{(1,1)}\right] + \dots\right) \quad (24)$$

The renormalized coupling $e_R(\mu)$ is finite, and it can be directly related to an actual physical quantity like the fine-structure constant. How this works when what is supposed to be a number actually depends on μ we will see below.

We have not yet specified the constants $z_e^{(1)}, z_e^{(2)}, z_e^{(1,1)}$ etc. Let us now consider an observable O which we have computed to 1-loop, using the QED Feynman rules

$$O = eC + e^3\left[A\frac{1}{\varepsilon}(Q^2)^{-\varepsilon/2} + B\right] \quad (25)$$

where Q is the typical energy scale of the observable. We now renormalize the coupling according to (24) and obtain, to order $e_R(\mu)^3$ and obtain

$$O = \mu^{-\varepsilon/2}\left\{e_R(\mu)C + e_R(\mu)^3\left[A\frac{1}{\varepsilon}\left(\frac{Q^2}{\mu^2}\right)^{-\varepsilon/2} + C\frac{1}{\varepsilon}z_e^{(1)} + B\right]\right\} \quad (26)$$

We can now choose $z_e^{(1)} = -A/C$. Then the poles in ε will cancel, and we can expand the result in ε

$$O = \left\{e_R(\mu)C + e_R(\mu)^3\left[A\ln\left(\frac{Q^2}{\mu^2}\right) + B\right]\right\} \quad (27)$$

One might think that it is not so hard to cancel divergences if one can simply choose to do so by picking $z_e^{(1)} = -A/C$. The remarkable fact, and the essence of the renormalizability of a theory, is however that this same choice works for all cases. One would always, for QED, find the same answer for $z_e^{(1)}$. Similarly for $Z_\psi\left(\frac{1}{\varepsilon}, e_R(\mu)\right), Z_\alpha\left(\frac{1}{\varepsilon}, e_R(\mu)\right), Z_m\left(\frac{1}{\varepsilon}, e_R(\mu)\right)$. To find their coefficients in the $e_R(\mu)$ expansion one can take some relatively simple observables, and compute them once and for all.

Based on the example just discussed it should not be too great a surprise to learn that the generic structure of the observable, after renormalization, is

$$O(Q, \mu) = e_R(\mu)^2 [O_1] + \quad (28)$$

$$e_R(\mu)^4 \left[O_{10} + O_{11} \ln \left(\frac{Q^2}{\mu^2} \right) \right] + \quad (29)$$

$$e_R(\mu)^6 \left[O_{20} + O_{21} \ln \left(\frac{Q^2}{\mu^2} \right) + O_{20} \ln^2 \left(\frac{Q^2}{\mu^2} \right) \right] + \dots \quad (30)$$

where the O_{ij} are various constants. We note that (i) $O(Q, \mu)$ is finite, and (ii) it depends on the determined scale μ both directly, via the logarithms, and implicitly, via the renormalized coupling $e_R(\mu)$. The last point is problematic: if we have consistently cancelled the divergences only for O to depend on an arbitrary scale it seems we have not gained much predictive power. However, the μ dependence is precisely such that for Eq. (28)

$$\mu \frac{d}{d\mu} O(Q, \mu) = \mathcal{O}(e_R^8(\mu)) \quad (31)$$

i.e. one order beyond the one calculated. Should one add another order to the result in (28) the residual dependence on μ would be $\mathcal{O}(e_R^{10}(\mu))$ and therefore progressively less, and the prediction ever more precise. Some uncertainty will however remain, and it is customary to estimate it by varying μ/Q from 2 to 1/2.

2.3.3 Running coupling, β function

What is the origin of this conspiratorial μ dependence? It is in fact the renormalization procedure itself. In the problem sets it was shown that from the relation (24) one can derive (by acting with $d/d \ln \mu$ on both side) a first order differential equation for the μ dependence of the finite renormalized coupling

$$\mu \frac{d}{d\mu} e_R(\mu) = \beta_0 e_R(\mu)^3 + \beta_1 e_R(\mu)^5 + \dots \equiv \beta(e_R(\mu)) \quad (32)$$

known as the β function equation, or sometimes also as the renormalization group equation for the running coupling.

The β -function equation plays an important role in the Standard Model. It should be clear that its occurrence is generic. Because each coupling in the Standard Model requires renormalization, each will have its own β -function. The β functions are only known in form of a perturbative expansion, as in Eq. (32). For non-abelian gauge theory no less than the first four terms are known (five for the case of SU(3) [6]!). The first term

$$\beta_0 = - \frac{11C_A - 4T_F N_F}{12\pi} \quad (33)$$

was calculated in the early 70's. The 2004 Nobel Prize was awarded for this calculation, in particular for the interpretation for the fact that the term is *negative*, about which more below. From eq. (32) we can already see that if the function has negative coefficients, as non-abelian gauge theories such as QCD do, the coupling decreases for a positive increment in the scale μ , i.e. when $\mu \rightarrow \mu + d\mu$, leading to asymptotic freedom in the ultraviolet, and strong binding at low scales μ .

2.3.4 Symmetries of QCD

Before diving further into the perturbative aspects of QCD, let us devote now a bit of space to considering the fundamental symmetries of QCD. We discussed some of this already qualitatively in section 2.1, here we discuss these from a field-theoretical point of view. The defining symmetry of QCD is the local SU(3) symmetry, under which the quark transform as

$$\psi(x) \rightarrow \psi'(x) = U(x) \psi(x), \quad U = \exp(\xi^a t_a), \quad (34)$$

where the matrices t_a are called the *generators* of the group defined in the representation appropriate to ψ , and the ξ^a constitute a set of linearly independent *real* parameters in terms of which the group

elements can be described. The number of generators is obviously equal to the number of independent parameters ξ^a and therefore to the dimension of the group, but is not necessarily related to the dimension of the matrices U and t_a ⁸. Hence, U is a square matrix whose dimension is equal to the number of components in ψ (3 in the case of QCD). The covariant derivative should be such that when acting on a field that already transforms covariantly, the result will transform covariantly also

$$D_\mu \psi(x) \rightarrow (D_\mu \psi(x))' = U(x) D_\mu \psi(x). \quad (35)$$

To this end one introduces a (set of) gauge field(s)

$$D_\mu \psi \equiv \partial_\mu \psi - W_\mu \psi, \quad W_\mu = W_\mu^a t_a, \quad (36)$$

so that also W_μ is matrices, and the number of gauge fields equals the number of generators (8 in the case of SU(3)). With the property (35) it is easy to construct non-abelian gauge theory. The rule (35) holds if W_μ transforms as

$$W_\mu \rightarrow W'_\mu = U W_\mu U^{-1} + (\partial_\mu U) U^{-1}, \quad (37)$$

i.e. inhomogeneously (the second term does not contain W_μ), and non-covariantly (the second term depends on the derivative of $U(x)$). With the covariant derivative one can also construct the field strength tensor

$$G_{\mu\nu} = -[D_\mu, D_\nu] = \partial_\mu W_\nu - \partial_\nu W_\mu - [W_\mu, W_\nu], \quad (38)$$

The field strength transforms covariantly and homogeneously

$$G_{\mu\nu} \rightarrow G'_{\mu\nu} = U G_{\mu\nu} U^{-1}. \quad (39)$$

Finally, the QCD coupling constant can be introduced by replacing

$$W_\mu^a \rightarrow g W_\mu^a, \quad G_{\mu\nu}^a \rightarrow g G_{\mu\nu}^a. \quad (40)$$

With this we can write down the QCD Lagrangian for one quark flavour, with mass m

$$\begin{aligned} \mathcal{L} &= \mathcal{L}_W + \mathcal{L}_\psi \\ &= \frac{1}{4} \text{Tr} [G_{\mu\nu} G^{\mu\nu}] - \bar{\psi} \not{D} \psi - m \bar{\psi} \psi. \end{aligned} \quad (41)$$

Thanks to the rules in (34,35) and (39), it is straightforward to check its local SU(3) invariance

We now turn to a global symmetry of the QCD Lagrangian, that is relevant because there is more than one quark flavour. The full QCD Lagrangian reads

$$\mathcal{L}_{\text{QCD}} = -\frac{1}{4} \text{Tr} (G_{\mu\nu} G^{\mu\nu}) - \sum_{f=1}^{n_f} \bar{\psi}_f (\not{D} + m_f) \psi_f. \quad (42)$$

Besides having local symmetry, this Lagrangian has an interesting global symmetry if the masses of the quarks may be neglected. We can use the chiral projector $P_L = (1 + \gamma_5)/2$ and $P_R = (1 - \gamma_5)/2$ (it is easy to check that they are idempotent, that $P_L P_R = P_R P_L = 0$ and that they and sum to 1) to define left- and righthanded quarks

$$\psi_L = P_L \psi, \quad \psi_R = P_R \psi. \quad (43)$$

In these terms, the fermion sector of (42) reads

$$\sum_{f=1}^{n_f} \bar{\psi}_f (\not{D} + m_f) \psi_f = \sum_{f=1}^{n_f} (\bar{\psi}_{L,f} \not{D} \psi_{L,f} + \bar{\psi}_{R,f} \not{D} \psi_{R,f}) \sum_{f=1}^{n_f} m_f (\bar{\psi}_{L,f} \psi_{R,f} + \bar{\psi}_{R,f} \psi_{L,f}). \quad (44)$$

⁸For instance, for the three SU(2) generators one can choose 2,3,... dimensional matrices, corresponding to (iso)spin $\frac{1}{2}, 1, \dots$

When setting $m_f = 0$ one notes that the left- and righthanded quarks have no interactions. We may in fact mix them independently

$$\psi_{L,i} \rightarrow \psi'_{L,i} = U_{L,ij}\psi_{L,j}, \quad \psi_{R,i} \rightarrow \psi'_{R,i} = U_{R,ij}\psi_{R,j}, \quad (45)$$

with U_L and U_R independent unitarity matrices. The dimension of these matrices is equal to the number of quark flavours that is (approximately) massless. This is a good approximation for the up and down quarks, in general still reasonable for the strange quark, but for the heavy quarks not anymore. Note that the chiral symmetry $U_L \otimes U_R$ is a global symmetry, we do not make an effort to make this symmetry local. It relates many properties of pions and kaons.

But this symmetry becomes especially interesting when one accounts for the fact that the QCD nonperturbative vacuum should have the structure

$$\sum_f \langle \overline{\psi}_{L,f} \psi_{R,f} \rangle + (L \leftrightarrow R). \quad (46)$$

In words, in the QCD groundstate left- and righthanded projections of quark flavours are coupled, so that this chiral symmetry is spontaneously broken. By Goldstone's theorem, the spectrum of QCD (the set of actually realized particles) should feature massless spinless bosons. They must however be odd under parity, so that they are in fact pseudoscalar bosons. The obvious candidates for these would be the pions and kaons of the pseudoscalar meson octet. The reason is that the groundstate (46) is still invariant when choosing $U_L = U_R$ (so-called vector rotations), but when transforming left- and righthanded quarks differently, a γ_5 remains, which implies that the goldstone bosons behaves as $\overline{\psi}\gamma_5\psi$, i.e. as pseudoscalar mesons.

Though it still an unsolved problem how to compute the non-perturbative QCD spectrum fully analytically from the Lagrangian (42), one may set up an effective theory, Chiral Perturbation Theory (χ PT), for pions (and kaons) valid for low energy scattering. However, in these notes we shall not go further into this interesting subject.

2.4 Evidence for colour

Because the QCD colour quantum number is so central to its understanding and functioning, it would be interesting to verify it. This is not straightforward, as we discussed, since colour is confined (hadrons are "white"), so that its existence can only be inferred. Let's see how this might be done. Consider the total cross section for the production of a fermion-antifermion pair $f\bar{f}$ in an electron-positron collision, to lowest order in the electromagnetic coupling. The fermion has e.m. charge $Q_f e$ and mass m , and we approximate the electron to be massless. The answer is in fact quite simple

$$\sigma_f(s) = \frac{4\pi\alpha^2 Q_f^2}{3s} \beta \left(1 + \frac{2m_f^2}{s} \right) \theta(s - 4m_f^2) \quad (47)$$

where s is the center-of-mass energy squared. Note that we have attached a label f to the mass the type of fermion f . The factor involving the electric charges also depends on the fermion "flavour". Thus, for an electron, muon and tau $Q_f = -1$, for up, charm, and top quarks $Q_f = 2/3$, while for down, strange and bottom quarks $Q_f = -1/3$. The factor $\beta = \sqrt{1 - 4m_f^2/s}$ is a phase space volume factor; when s is just a little bit larger than $4m_f^2$ β is close to zero, i.e. near threshold the cross section is small. Far above threshold $\beta \sim 1$. The theta function ensures that the cross section is only non-zero if the center of mass energy is large enough to produce the quark pair.

How might we use this result? If the produced fermions are electrons, muons or taus we can directly confront the result with data, and agreement is in fact very good. There is a more interesting use

of the formula in Eq. (47). Consider the inclusive *quark* cross section

$$\sigma_{had}(s) = \sum_{f=u,d,s,c,\dots} \frac{4\pi\alpha^2 Q_f^2}{3s} \beta \left(1 + \frac{2m_f^2}{s}\right) \theta(s - 4m_f^2) N_c \quad (48)$$

The extra factor N_c at the end accounts for the fact that quarks come in $N_c = 3$ colours. We may interpret this in fact as a prediction for the inclusive *hadron* cross section, because the quark final state must, before they reach any detector, make a transition to a hadronic final state, see the illustration in Fig. 7. In Fig. 8 we see the confrontation of this result with data, and that the agreement is very good,

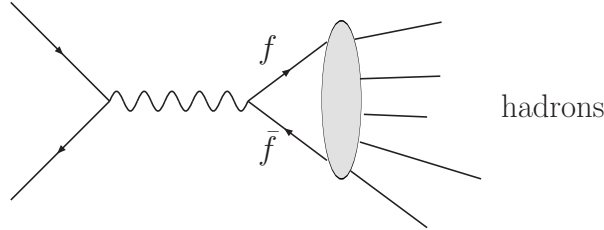


Fig. 7: $e^+e^- \rightarrow$ hadrons; the blob represents the "hadronization" process. Note that time runs from left to right in this diagram.

except that we did not anticipate the huge peak near $\sqrt{s} \simeq 90\text{GeV}$. That is because we did not include in our calculation of $\sigma_f(s)$ in eq. (47) a second diagram in which not a photon (as in Fig. 7) but a Z -boson of mass $M_Z \simeq 90\text{GeV}$ mediates the scattering. Had we done so, with the factor $1/s$ replaced $1/(s - M_Z^2 + \Gamma_Z^2)$, where Γ_Z is the Z -boson decay width (about 2 GeV). The good agreement also implies that the effect of higher order corrections to $\sigma(s)$ should be small, and indeed they turn out to be so, after calculation. We can now define an

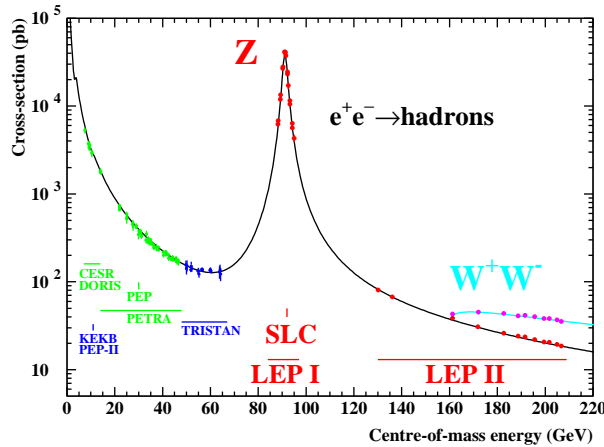


Fig. 8: Total cross section for e^+e^- to fermions.

observable traditionally called R

$$R(s) = \frac{\sigma(e^+e^- \rightarrow \text{hadrons})}{\sigma(e^+e^- \rightarrow \mu^+\mu^-)} \quad (49)$$

The benefit of defining such a ratio is that a many common factors cancel in the theoretical prediction, and that many experimental uncertainties cancel in the experimental measurement. We have then

$$R(s) = \frac{\sum_{f=u,d,s,c,\dots} \sigma(e^+e^- \rightarrow f\bar{f})}{\sigma(e^+e^- \rightarrow \mu^+\mu^-)} \quad (50)$$

For large center-of-mass energy \sqrt{s} we can derive from (48) that

$$R(s) \xrightarrow{s \rightarrow \infty} N_c \sum_{f=u,d,s,c,\dots} Q_f^2 \theta(s - 4m_f^2) \quad (51)$$

In Fig. 9 we confront this result with experiment. We can draw the conclusions that (i) there is again

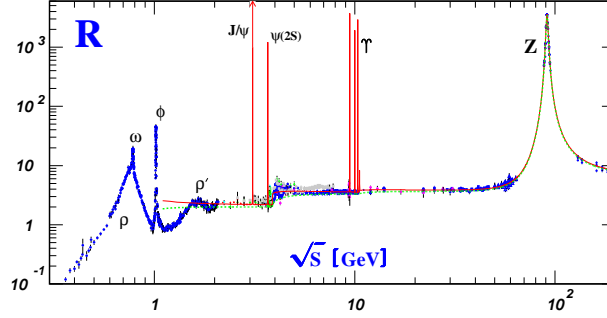


Fig. 9: R-ratio vs. center of mass energy

fairly good agreement between prediction and measurement; (ii) we see the effects of new quark flavour f being “turned on” as the energy increases beyond $2m_f$ ($m_c \simeq 1.5$ GeV, $m_b \simeq 5$ GeV); (iii) the larger step at charm than at bottom (proportional to $Q_c^2 = 4/9$ and $Q_b^2 = 1/9$, respectively) is well-predicted; (iv) the value of $R(s)$, say beyond the bottom quark threshold

$$R(s) = N_c \sum_{f=u,d,s,c,b} Q_f^2 \theta(s - 4m_f^2) = 3 \left(\frac{4}{9} + \frac{1}{9} + \frac{1}{9} + \frac{4}{9} + \frac{1}{9} \right) = \frac{11}{3} \quad (52)$$

agrees with experiment, and indicated that quarks come indeed in 3 colours.

3 Higher orders

In this section we discuss a number of key aspects relevant for computing higher-order effects in QCD. These are crucial to present-day applications of QCD for collider physics, so we provide a fair amount of detail.

3.1 Parton distribution functions (PDFs)

Before discussing how to compute higher-order partonic cross sections, let us discuss the quantities that form the interface of these to the hadronic cross sections: parton distribution functions. A recent, excellent review can be found in [7]. We already encountered the PDFs in section 2.2 in the context of the parton model, where they were functions of the momentum fraction variable (“ x ”) only. However, in the context of higher-order calculations they play a central role in the cancellation of initial state collinear divergences, and in that process also acquire (logarithmic) factorization scale dependence. It should be clear that, being the interface between hadronic and partonic cross sections, they play a crucial role at the hadron colliders such as the HERA, Tevatron and LHC, and the quality of theoretical predictions is directly tied to knowing the PDFs well. Thus, we need to understand how to determine the PDFs and their uncertainties. To be precise, 11 of them: 5 quark, 5 anti-quark and 1 gluon PDF, which we denote by $\phi_{i/P}(\xi, \mu_F)$, the number of partons of type i in the proton with momentum fraction ξ , at factorization scale μ_F .

Key to this determination is their universality: the QCD factorization theorems [8] ensure that it is same set PDFs that occurs in all well-defined partonic cross sections to any fixed order. Therefore, one may choose (with care) a set of observables (e.g. DIS structure functions, certain hadron collider cross

sections) to infer the PDFs from. Since each is described as a combination of PDFs and partonic cross sections we have the set of equations

$$[O_n + \Delta O_n]^{\text{exp}} = \sum_{i=1}^{11} \phi_{i/P} \otimes [\hat{\sigma}_{n,i} \pm \delta \hat{\sigma}_{n,i}]^{\text{theory}}, \quad (53)$$

where also the experimental and theoretical uncertainties are indicated. From this set of equations the PDFs may be inferred. Notice that if the calculations on the rhs are all of order N^kLO, then the PDFs inferred are also labelled N^kLO, even though there are intrinsically non-perturbative functions. The N^kLO PDFs can then be consistently used for other N^kLO (and of course also for lower *k*) calculations.

The determination of the PDFs is not a trivial matter, and is performed by various groups, each taking different approaches. The groups are known by acronyms of various lengths: MSTW, CTEQ, NNPDF, GJR, HERAPDF, ABKM, etc. Below we shall discuss briefly some features and results of some of these approaches.

First, a brief aside on the formal aspects of a PDF. Although they cannot yet be computed from first principles, it is possible to give a precise definition of PDFs in terms of operators. In essence, it is the expectation value of a parton counting operator (think of $a^\dagger a$ for a harmonic oscillator in quantum mechanics) in a proton state. For the quark case it is

$$\phi_{q/P}(\xi, \mu) = \frac{1}{4\pi} \int_{-\infty}^{+\infty} dy^- e^{-ip^+ y^-} \langle p | \bar{q}(0, y^-, 0_T) \gamma^+ q(0, 0, 0_T) | p \rangle. \quad (54)$$

We have introduced here also lightcone notation for 4-vectors

$$p^\pm = \frac{p^0 \pm p^3}{\sqrt{2}}, \quad p \cdot q = -p^+ q^- - p^- q^+ + p_T \cdot q_T. \quad (55)$$

so that $\gamma^+ = (\gamma^0 + \gamma^3)/\sqrt{2}$ in (54). The benefit of having a definition such as (54) is that one can compute now higher-order corrections to the operator, renormalize it, and then have a renormalization group equation for it. This is in fact then precisely the DGLAP equation. Note this can all be done in QCD perturbation theory. For the purposes of such calculations one can replace the proton states with parton states. Of course, the non-perturbative aspect comes in when evaluating the operator in a proton state. The DGLAP evolution equation reads

$$\mu \frac{d}{d\mu} \phi_{i/P}(\xi, \mu) = \sum_j \int_\xi^1 \frac{dz}{z} P_{ij}(z, \alpha_s(\mu)) \phi_{j/P} \left(\frac{\xi}{z}, \mu \right), \quad (56)$$

where the P_{ij} are the Altarelli-Parisi splitting functions, which act here as evolution kernels. With evolution is meant the change in form of the function as the energy scale μ evolves. They are now known to NNLO (3-loop) [9, 10]. The logic is thus not unlike that of the running coupling, but now we have “running functions”.

Returning now to how to extract the actual functional form of the PDFs from the equation (53), we see how the DGLAP equation is very useful. The data, on the lhs of (53), are taken at various energy scales. The theoretical description can for each observable be computed at the same energy scale because the scale evolution of the PDFs is known, so that meaningful comparison can be made.

The selection of observables to be used in eq. (53) must be done with care. Different observables should be sensitive in different ways to the various PDFs, so that a reliable extraction of a PDF is possible for each parton type. For instance, in DIS the most important partonic subprocess is $\gamma^* q \rightarrow q + X$ (where the off-shell photon is exchanged with the initial electron), so that associated observables are particularly sensitive to light quark PDFs. A nice overview of the main processes involved can be found in table 1, taken from Reference [11], which lists the processes that are included in a typical present-day

Process	Subprocess	Partons	x range
$\ell^\pm \{p, n\} \rightarrow \ell^\pm X$	$\gamma^* q \rightarrow q$	q, \bar{q}, g	$x \gtrsim 0.01$
$\ell^\pm n/p \rightarrow \ell^\pm X$	$\gamma^* d/u \rightarrow d/u$	d/u	$x \gtrsim 0.01$
$pp \rightarrow \mu^+ \mu^- X$	$u\bar{u}, d\bar{d} \rightarrow \gamma^*$	\bar{q}	$0.015 \lesssim x \lesssim 0.35$
$pn/pp \rightarrow \mu^+ \mu^- X$	$(u\bar{d})/(u\bar{u}) \rightarrow \gamma^*$	\bar{d}/\bar{u}	$0.015 \lesssim x \lesssim 0.35$
$\nu(\bar{\nu}) N \rightarrow \mu^- (\mu^+) X$	$W^* q \rightarrow q'$	q, \bar{q}	$0.01 \lesssim x \lesssim 0.5$
$\nu N \rightarrow \mu^- \mu^+ X$	$W^* s \rightarrow c$	s	$0.01 \lesssim x \lesssim 0.2$
$\bar{\nu} N \rightarrow \mu^+ \mu^- X$	$W^* \bar{s} \rightarrow \bar{c}$	\bar{s}	$0.01 \lesssim x \lesssim 0.2$
$e^\pm p \rightarrow e^\pm X$	$\gamma^* q \rightarrow q$	g, q, \bar{q}	$0.0001 \lesssim x \lesssim 0.1$
$e^+ p \rightarrow \bar{\nu} X$	$W^+ \{d, s\} \rightarrow \{u, c\}$	d, s	$x \gtrsim 0.01$
$e^\pm p \rightarrow e^\pm c\bar{c} X$	$\gamma^* c \rightarrow c, \gamma^* g \rightarrow c\bar{c}$	c, g	$0.0001 \lesssim x \lesssim 0.01$
$e^\pm p \rightarrow \text{jet} + X$	$\gamma^* g \rightarrow q\bar{q}$	g	$0.01 \lesssim x \lesssim 0.1$
$p\bar{p} \rightarrow \text{jet} + X$	$gg, qg, q\bar{q} \rightarrow 2j$	g, q	$0.01 \lesssim x \lesssim 0.5$
$p\bar{p} \rightarrow (W^\pm \rightarrow \ell^\pm \nu) X$	$ud \rightarrow W, \bar{u}\bar{d} \rightarrow W$	u, d, \bar{u}, \bar{d}	$x \gtrsim 0.05$
$p\bar{p} \rightarrow (Z \rightarrow \ell^+ \ell^-) X$	$uu, dd \rightarrow Z$	d	$x \gtrsim 0.05$

Table 1: The main processes, their dominant subprocesses and the parton types they mostly affect, and the relevant x range. that are included in the MSTW 2008 global PDF analysis. They are partitioned into fixed-target experiments, HERA and the Tevatron.

global fit (MSTW08), and the PDFs they constrain. A priori, the space of functions is too large to be constrained through a global fit implied by solving eq. (53) for the PDFs using a finite amount of data, so some assumptions must be made. The various groups differ in their approaches to this issue to varying degrees, and, related to this, also in their determination of the errors of the extracted PDFs.

A few constraints are taken along. First, charm and bottom PDF's can be determined from the light flavour ones, assuming that such heavy quark arise from gluon splittings in the proton. This can be done in different ways, known as variable flavour number schemes, see also [7] for further comments and references. Also, the already mentioned charge and momentum sum rules must be obeyed precisely.

The most common approach is to take a physically motivated form for the PDFs at a low fixed scale Q_0 such as

$$\phi_{i/P}(x, Q_0^2) = x^{\alpha_i} (1-x)^{\beta_i} g_i(x), \quad (57)$$

with the choice of function $g_i(x)$ differing per group (polynomials, exponentials etc). The form at other scales is found by solving the DGLAP evolution equation (56). Typically about 20-30 parameters are then to be fitted using χ^2 as goodness-of-fit

$$\chi^2 = \sum_{i,j=1}^{N_{data}} (D_i - T_i) (V^{-1})_{ij} (D_j - T_j), \quad (58)$$

where D_i, T_i are data and theoretical prediction, respectively, and V is the experimental covariance matrix. The uncertainties are determined by varying the parameters such that per variation along certain directions in parameter space (determined by the Hessian matrix) the χ^2 increased by a fixed amount. In this way, one generates a best-fit PDF set and a collection of one-sigma error sets, from which then uncertainties for physical observables may be determined.

Another approach is to use, instead of the fixed forms in (57), an approach that does not include theoretical bias at the outset, using neural networks. The number of free (architecture) parameters in this case is of order 200-300 and very redundant, but that's ok. The probability distribution in the space of function is modelled by a Monte Carlo sample of replica's, so that averages and standard deviations can be easily computed using sums over replicas.

Both approaches agree quite well, and differences are very instructive. A comparison of various recent sets for the LHC at 8 TeV is shown in Fig. 10. Clearly, the topic of PDF determination is highly

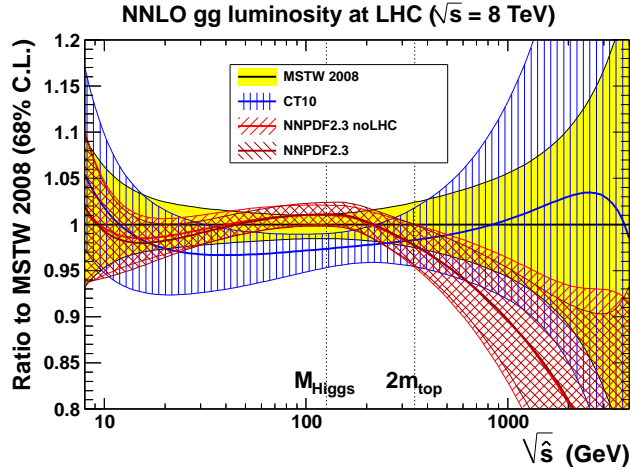


Fig. 10: Comparison of gluon-gluon luminosity functions for various PDFsets, relative to the MSTW08 set. Taken from [7].

important, and progress continues as data accumulate and understanding of subtle bias effects improves. A recent review [12] describes the state of affairs at the start of LHC run 2.

3.2 e^+e^- collisions and event shapes

Before continuing with aspects of QCD at hadron colliders, let us first have a look at issues in QCD at e^+e^- colliders, such as the former LEP collider at CERN. Such colliders are, in a sense, the cleanest place to study QCD, due to the pointlike, non-strongly interacting initial state particles. We already saw how the number of colours, and the masses of heavy quarks can be seen in in R -ratio. However, the R -ratio involves the total cross section, and is not sensitive to the particular shape or structure of the final state.

There are other observables or variables that can be, and were, measured, experimentally. and are also theoretically consistent (that is, they are infrared-safe, which we discuss in section 3), and are sensitive to the geometry or structure of the final state. These *event shape* observables describe properties of final state configurations differently from the total cross section in e^+e^- collisions (they have also been generalized to other collision types).

A well-known example of such an infrared safe event shape is the maximum directed momentum, or thrust T , in e^+e^- collisions. The thrust of an event is defined by

$$T = \max_{\hat{n}} \frac{\sum_i |\vec{p}_i \cdot \hat{n}|}{\sum_i |\vec{p}_i|}, \quad (59)$$

where the p_i are the momenta of the particles and the unit three-vector \hat{n} is varied until a maximum value of T is obtained. It varies between $T = \frac{1}{2}$ for a spherical energy flow and $T = 1$ for a pencil-like linear energy flow of two very narrow, back-to-back jets. Let us illustrate this discussion by the calculation of the thrust distribution for the reaction

$$e^+(k_1) + e^-(k_2) \rightarrow \gamma(q) \rightarrow q(p_1) + \bar{q}(p_2) + g(p_3). \quad (60)$$

The Feynman diagrams are shown in Fig. 11. The kinematical situation is that of an off-shell photon decaying into three massless partons, which allows us to use Dalitz plot variables to describe the final

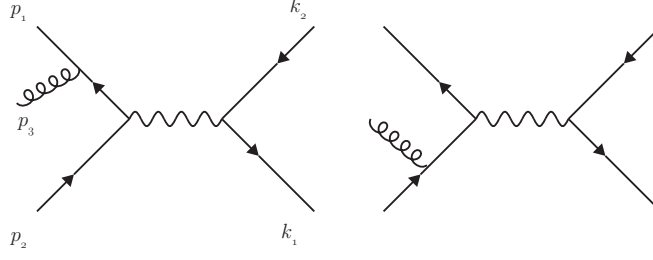


Fig. 11: Feynman diagrams for $e^+e^- \rightarrow \gamma \rightarrow q\bar{q}g$ at lowest order in the QCD coupling

state. The Dalitz plot for a decay into 3-particle final state is a scatterplot of events in a plane spanned by two of the final particle energies. The reason for plotting events this way is that the phase space measure is “flat” in those variables, so that any clustering of events represents an intermediate resonance in the decay.

Let us then choose two energies to specify the allowed region in a Dalitz plot, or, more conveniently and equivalently, choose invariant mass variables. Hence, using the particle name to represent its four momentum, we introduce $s_{13} = -(p_1 + p_3)^2$, $s_{23} = -(p_2 + p_3)^2$ and $s_{12} = -(p_1 + p_2)^2$. Since the three final particles are coplanar, the whole kinematics is specified by s_{13} , s_{23} and 3 angular variables. One angular variable θ specifies the polar angle between the beam axis and a line in the three-particle plane. Another azimuthal angular variable ϕ specifies the orientation of the plane with respect to this line and finally there is an overall azimuthal angle χ . The phase space for the final three particles therefore becomes

$$\frac{1}{(2\pi)^5} \int \frac{d^3p_1}{2E_1} \int \frac{d^3p_2}{2E_2} \int \frac{d^3p_3}{2E_3} = \frac{1}{(2\pi)^5} \int \frac{1}{32q^2} ds_{13} ds_{23} d\phi d\sin\theta d\chi. \quad (61)$$

The expression for the cross-section after squaring the matrix element for $e^+e^- \rightarrow q\bar{q}g$ and integrating over ϕ and χ turns out to be

$$\frac{d^3\sigma}{ds_{13} ds_{23} d\sin\theta} = \frac{\alpha_e^2 \alpha_s}{8 q^2} (x_1^2 + x_2^2) (2 + \cos^2\theta) \frac{1}{s_{13} s_{23}}, \quad (62)$$

where the variables $x_i = E_i/E$, with $E = \sqrt{q^2}/2$, are related to the invariant mass variables by $s_{13} = q^2(1 - x_2)$, $s_{23} = q^2(1 - x_1)$, $s_{12} = q^2(1 - x_3)$. Note that $x_1 + x_2 + x_3 = 2$. From (62) we see that the angular distribution of the normal to the plane with respect to the beam line is given by $2 + \cos^2\theta$. A final integration over $\sin\theta$ yields the two equivalent expressions.

$$\sigma_T^{-1} \frac{d^2\sigma}{ds_{13} ds_{23}} = \frac{2}{3\pi} \alpha_s \frac{x_1^2 + x_2^2}{s_{13} s_{23}}, \quad (63)$$

or

$$\sigma_T^{-1} \frac{d^2\sigma}{dx_1 dx_2} = \frac{2}{3\pi} \alpha_s \frac{x_1^2 + x_2^2}{(1 - x_1)(1 - x_2)}, \quad (64)$$

where we have divided both sides of the equation by $\sigma_T = \frac{4}{3}\pi\alpha_e^2/s$, the $e^+e^- \rightarrow \mu^+\mu^-$ cross section. These distributions diverge for small invariant masses, or, equivalently as the scaled energies $x_{1,2}$ of the quark and antiquark go to one. It is not very difficult to show that the thrust variable T for the present case is equal to $\max(x_1, x_2, x_3)$ for each event, with $\frac{2}{3} \leq T \leq 1$. For fixed T the allowed region in x_1, x_2 is then shown in Fig. 12. The lines EF, FD and DE are the lines $x_1 = 1$, $x_2 = 1$ and $x_3 = 1$, respectively. The figure shows the subdivision of the final phase space into three regions depending on which particle has the largest x value. Consider first the case $T = x_2$. Then we have

$$\sigma_T^{-1} \frac{d\sigma}{dT} = \frac{2\alpha_s}{3\pi} \int dx_1 dx_2 \delta(T - x_2) \theta(T - x_1) \theta(T - x_3)$$

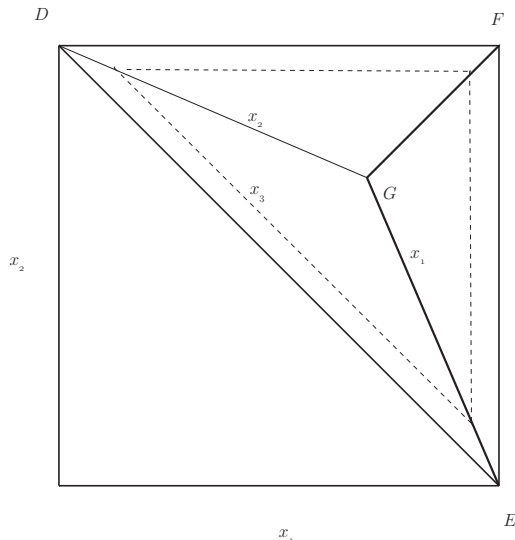


Fig. 12: Contributing regions in $x_{1,2}$ for a given value of thrust T . On the line DE $x_3 = 1$ (recall that $x_1 + x_2 + x_3 = 2$). At the point G all three x_i are equal to $2/3$. In each of the three triangles that join at G one of the three x_i is largest, as indicated. On the dashed line the value of T is constant.

$$\begin{aligned}
& \times \frac{x_1^2 + x_2^2}{(1-x_1)(1-x_2)} \\
& = \frac{2\alpha_s}{3\pi} \int_{2(1-T)}^T dx \frac{T^2 + x^2}{(1-T)(1-x)} \\
& = \frac{2\alpha_s}{3\pi} \left\{ \frac{1+T^2}{1-T} \ln \frac{2T-1}{1-T} + \frac{3T^2 - 14T + 8}{2(1-T)} \right\}, \tag{65}
\end{aligned}$$

with an identical result for $T = x_1$. The $T = x_3$ case is slightly different, and corresponds to integrating over the dashed line parallel to DE in Fig. 12. On this line we have that $x_1 = 2 - T - x_2$, while x_2 ranges from $2(1-T)$ to T . One then finds

$$\sigma_T^{-1} \frac{d\sigma}{dT} = \frac{4\alpha_s}{3\pi} \left\{ \frac{1 + (1-T)^2}{T} \ln \frac{2T-1}{1-T} + 2 - 3T \right\}. \tag{66}$$

Clearly there is different, interesting dependence on T for the various cases.

Note that the thrust distributions for the quark and antiquark are singular as $T \rightarrow 1$, signifying the appearance of soft and/or collinear singularities, where either the gluon is very soft, or the (anti-)quark-gluon splitting is essentially collinear (in the $T = x_3$ case (66) the distribution is singular but integrable). In these infrared and collinear regions of phase space non-perturbative effects must start playing a role in order to cure this apparent problem in perturbative QCD.

The different expressions for the thrust dependence for different regions in Fig. 12 allow us to make an interesting observation. Since the integral of the gluon T distribution in (66) is integrable at $T = 1$, we can integrate it from $T = 2/3$ to $T = 1$ to find the probability that the gluon is the most energetic particle. This yields

$$\sigma_T^{-1} \int_{2/3}^1 \frac{d\sigma}{dT} dT = 0.61 \frac{\alpha_s}{\pi}. \tag{67}$$

We can reasonably ⁹ assume that α_s is a function of q^2 , the center-of-mass energy squared, so that the

⁹A higher-order calculation of the thrust distribution [13–16], which requires renormalization of the QCD coupling, confirms this.

total probability that the gluon is the most energetic particle decreases with increasing q^2 . The probability that the quark or the antiquark is the most energetic particle is then given by $(1 - 0.61\alpha_s/\pi)$.

The total thrust distribution is twice the result (65) (accounting for the cases $T = x_1$ and $T = x_2$) added to the result (66), which yields

$$\sigma_T^{-1} \frac{d\sigma}{dT} = \frac{2\alpha_s}{3\pi} \left[\frac{2(3T^2 - 3T + 2)}{T(1-T)} \ln \frac{2T-1}{1-T} - \frac{3(3T-2)(2-T)}{1-T} \right]. \quad (68)$$

Because the integrand is integrable at $T = 1$ we can also compute the average value of $(1 - T)$ from this formula

$$\langle 1 - T \rangle \equiv \sigma_T^{-1} \int dT \frac{d\sigma}{dT} (1 - T) = 1.05 \frac{\alpha_s(q^2)}{\pi}. \quad (69)$$

We see that this average value of $(1 - T)$ decreases with increasing q^2 .

A comparison of higher-order calculations for thrust with data is shown in Fig. 13, showing the good quality of (but also the need for) the NNLO approximation.

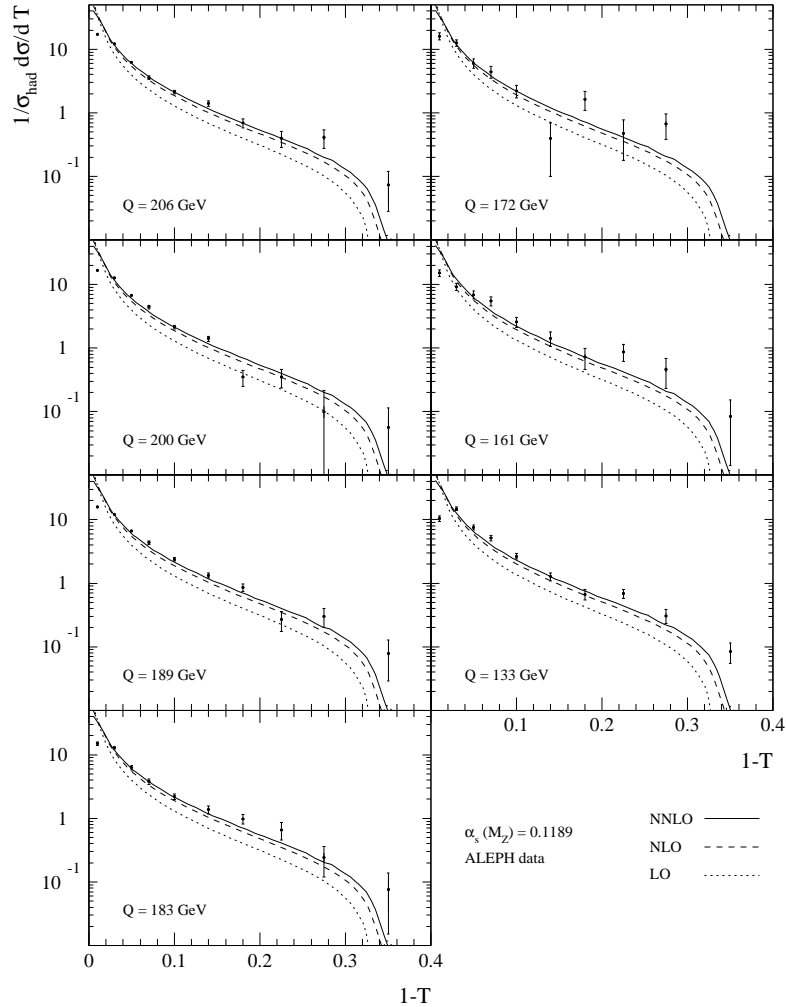


Fig. 13: A comparison of thrust data from the ALEPH collaboration, with LO, NLO and NNLO calculations for various LEP cm energies. Figure taken from [17].

This concludes our rather detailed look at event-shape variables, where we already saw the appearance of infrared and collinear singularities. We now turn to a more detailed discussion of these, as this is a central issue in the application of perturbative QCD for colliders.

3.3 More on e^+e^- cross sections, IR divergences, KLN theorem

The ratio $R = \sigma(e^+e^- \rightarrow \text{hadrons})/\sigma(e^+e^- \rightarrow \mu^+\mu^-)$ was already discussed in section 2.4 when discussing evidence for colour. In order to compute higher-order QCD corrections to this ratio, i.e. to the e^+e^- total cross section, we must deal with infrared and collinear divergences (often collectively called ‘‘infrared’’). This can be seen if one would integrate the expression (68) over T ; it would produce a divergence due to the $1/(1 - T)$ behaviour.

The Kinoshita-Lee-Nauenberg theorem [18, 19] (KLN) now states that, when summing over all contributions to the observable at that order (i.e. also the loop-corrections) the divergences cancel if the sum is over a sufficiently degenerate set of states.

This is a very powerful result, so let us discuss it a bit further. One of the crucial aspects of massless particles is indeed that one is dealing with degenerate states. For instance, in quantum electrodynamics, it is not meaningful to distinguish between a single electron and an electron accompanied by any number of zero-momentum photons, as the corresponding states carry the same electric charge, energy and momentum. An (infinite) degeneracy of states implies that a naive application of perturbation theory may run into difficulties, a phenomenon that is, for instance, also known from applications in quantum mechanics. According to the Kinoshita-Lee-Nauenberg (KLN) theorem [18, 19] the divergences that are in principle present in partial transition probabilities, must cancel when averaging over a suitable set of degenerate states. This theorem encompasses in fact the older Bloch-Nordsieck [20] theorem.

Observables sufficiently inclusive to allow a sum over a sufficiently large ensemble of degenerate states for the KLN cancellations to occur, are known as *infrared safe*. How large an ensemble should be depends on the experimental process that one is considering. Of course in electron-positron annihilation at high energies, the *total* cross section (where one sums over *all* possible finite states) certainly constitutes an infrared safe quantity, so reliable predictions in perturbative QCD should be possible.

Let us, then, examine the first three terms in the perturbation series for R [21], in the limit of zero fermion mass (owing to the KLN theorem the quark mass could be suppressed without encountering infrared divergences)

$$\begin{aligned}
 R(t) = & \left(\sum_f Q_f^2 \right) \left\{ 1 + \frac{\alpha_s(t)}{4\pi} 3C_2(R) \right. \\
 & + \left(\frac{\alpha_s(t)}{4\pi} \right)^2 \left[-\frac{1}{2}C_2^2(R) + \left(\frac{123}{2} - 44\zeta(3) \right) C_2(G) C_2(R) \right. \\
 & \left. \left. + n_f (-22 + 16\zeta(3)) C_2^2(R) \frac{3}{8} \right] \right\}, \tag{70}
 \end{aligned}$$

where $(\sum_f Q_f^2)$ denotes the square of the electric charges of the fermions and $C_2(G), C_2(R)$ are colour factors of SU(3). As before, t represents the logarithm of the ratio of two energy scales, one being the total center-of-mass energy q^2 of the incoming electron-positron pair and the other some reference scale. Obviously, the running coupling constant should be evaluated to the same order as the cross section. Through $\alpha_s(t)$ this result thus depends on the number of quark flavours n_f .

The Riemann zeta function invariably appears in higher-loop calculations. It is defined by $\zeta(z) = \sum_{n=1}^{\infty} 1/n^z$. The specific value encountered above is $\zeta(3) \approx 1.2020569$. Using these values, the numerical coefficients for SU(3) with $n_f = 5$ quark flavours yield

$$R(t) = \left(\sum_f Q_f^2 \right) \left(1 + \frac{\alpha_s(t)}{\pi} + 1.409 \left(\frac{\alpha_s(t)}{\pi} \right)^2 \right). \tag{71}$$

We see that the coefficient in front of the $(\alpha_s(t)/\pi)^2$ is not too large, and the perturbative description is well-behaved. As is clear from Fig. 9 the result above should be used with great caution in the vicinity of

heavy flavour thresholds, because bound states appear in $R(t)$, which are not describable in finite order perturbation theory.

Let us next discuss two important, technical but generic issues that arise in the derivation of results such as (71) in the context of dimensional regularization. The first concerns the integration over phase space. Because the quantities that one calculates are infrared safe, infrared divergences must cancel at the end of the calculation. This requires one to determine the full cross section in n dimensions and take the limit $n \rightarrow 4$ only at the end. In particular, also the phase-space integrals should be evaluated in n dimensions. The second issue is that the mass shell for massless particles poses problems in perturbative calculations. On-shell massless particles may split into perfectly collinear massless particles which then remain on their mass shells. This makes the mass shell ill-defined, and singularities appear, as we will see below. Moreover, there is a conceptual problem in that on-shell massless particles should correspond to asymptotic states. But in a confined theory such as QCD the massless partons do not correspond to *physical* states, which consist of massive hadrons. For infrared safe observables this is in fact not fatal to predictive power, but for calculations this is at least at an intermediate level a cumbersome feature. We now discuss these two aspects in turn.

In n dimensions the two-particle phase-space integral is defined by

$$I^{(n)}(s, m_3^2, m_4^2) = \int \frac{d^{n-1}p_3}{(2\pi)^{n-1}2\omega_3} \frac{d^{n-1}p_4}{(2\pi)^{n-1}2\omega_4} (2\pi)^n \delta^{(n)}(p_1 + p_2 - p_3 - p_4), \quad (72)$$

where $s = -(p_1 + p_2)^2$ and $_{3,4} = (\mathbf{p}_{3,4}^2 + m_{3,4}^2)^{1/2}$. We choose the centre-of-mass frame and decompose the full integral in one over the $n - 2$ angular variables (which we leave unperformed) and one over the length of the $(n - 1)$ -dimensional momentum vector $\mathbf{p}_3 = -\mathbf{p}_4$, which contains a delta function, and which we do perform. It yields

$$I^{(n)}(s, m_3^2, m_4^2) = \frac{1}{8\pi\sqrt{s}} \left[\frac{\lambda(s, m_3^2, m_4^2)}{16\pi^2 s} \right]^{\frac{n-3}{2}} \int d_{CM}, \quad (73)$$

where $\lambda(x, y, z) = x^2 + y^2 + z^2 - 2xy - 2xz - 2yz$. As usual this expression must be combined with the square of the invariant amplitude to yield a cross section or decay rate. Assuming that the invariant amplitude depends only on the deflection angle θ_{CM} between \mathbf{p}_1 and \mathbf{p}_3 , we can integrate over the remaining $n - 3$ angles, using the formula

$$\int d_{CM} = \frac{2\pi^{-1+\frac{1}{2}n}}{\Gamma(\frac{1}{2}n - 1)} \int_0^\pi d\theta_{CM} [\sin \theta_{CM}]^{n-3}, \quad (74)$$

where the integral on the left-hand side runs over all $n - 2$ angles, while the integral on the right-hand side contains only the deflection angle. Typically one needs the integral for $m_4 = 0$, reflecting emission of a massless particle. Replacing m_3 by m and introducing the variables $x = m^2/s$ and $y = \frac{1}{2}(1 + \cos \theta)$ the combined result for the phase-space integral reads

$$I^{(n)}(s, m^2, 0) = \frac{1}{8\pi} \left(\frac{m^2}{4\pi} \right)^{-2+\frac{1}{2}n} \frac{x^{2-\frac{1}{2}n} (1-x)^{n-3}}{\Gamma(\frac{1}{2}n - 1)} \int_0^1 dy [y(1-y)]^{-2+\frac{1}{2}n}, \quad (75)$$

which has the correct dimension of a mass to the power $n - 4$. For $n > 2$ this expression is free of singularities. Corresponding expressions can be derived for multi-particle phase-space integrals. Formulae like (75) are obviously needed for calculating decay rates and cross sections in arbitrary dimension, the squared invariant amplitudes for which are then functions of y . The y -integral can be evaluated by using the relation

$$\int_0^1 dy y^{p-1} (1-y)^{q-1} = B(p, q) = \frac{\Gamma(p)\Gamma(q)}{\Gamma(p+q)}, \quad (76)$$

where $B(p, q)$ is the Euler beta-function. Depending on the invariant amplitude of the process, infrared divergences can then appear as poles in the Gamma function, just as for virtual corrections.

The second issue involves the definition of the mass shell for massless particles in dimensional regularization. To this end we let us turn to the evaluation of a typical one-loop self-energy diagram This

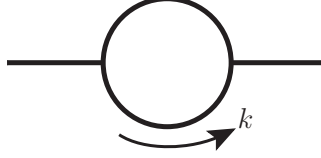


Fig. 14: A typical one-loop self-energy diagram

involves an integral of the type

$$I(k^2, m_1^2, m_2^2) = \frac{1}{(2\pi)^n} \int \frac{d^n q}{((q + \frac{1}{2}k)^2 + m_1^2)((q - \frac{1}{2}k)^2 + m_2^2)}. \quad (77)$$

We imagine k to be the momentum of a massless particle that is off-shell and put $m_1 = m_2 = 0$. Using Feynman parameters one obtains

$$I(k^2, 0, 0) = \frac{i}{16\pi^2} \Gamma(2 - \frac{1}{2}n) \left(\frac{k^2}{4\pi}\right)^{-2 + \frac{1}{2}n} \int_0^1 dx [x(1-x)]^{-2 + \frac{1}{2}n}. \quad (78)$$

The x integral can be evaluated using (76) and becomes $(\Gamma(\frac{1}{2}n - 1))^2 / \Gamma(n - 2)$, so that

$$I(k^2, 0, 0) = \frac{i}{16\pi^2} \frac{\Gamma(2 - \frac{1}{2}n)\Gamma(\frac{1}{2}n - 1)^2}{\Gamma(n - 2)} \left(\frac{k^2}{4\pi}\right)^{-2 + \frac{1}{2}n}. \quad (79)$$

This expression exhibits poles for both large and small values of n , signaling ultraviolet and infrared singularities respectively. The last factor in (79) shows that the result is in fact ambiguous when approaching the mass shell, $k^2 \rightarrow 0$. When considering infrared divergences one assumes $n > 4$ so that the integral is in fact zero on the mass shell. Hence, one can omit self-energy loop corrections for massless external particles. In fact, their zero contribution can be shown to be due to a perfect cancellation between a UV divergence and a collinear divergence. However, one must still include the UV counterterms on the external lines. The sum of the two is then in fact the collinear divergence, which in turn will cancel in a calculation of infrared safe quantities.

3.4 Jets

Besides event shapes there is another important class of infrared safe observables that uses the notion of a jet. In high-energy e^+e^- collisions the photon couples directly to a quark-antiquark pair, and the latter are then produced back-to-back in the e^+e^- cm frame, with high momentum. As the quarks begin to fly apart they undergo the complicated fragmentation or hadronization process that leads to colourless hadronic final states. One could therefore expect the final hadrons to follow the line of flight of the quarks to produce two streams of back-to-back particles, as depicted in Fig. 15. The angular distribution of the quarks is $1 + \cos^2 \theta$, where θ is the polar angle between a quark and the beam direction. The angular distribution of the hadrons should then have roughly the same dependence on $\cos \theta$. Indeed this is the case.

In the context of considering the effect of higher orders, one may ask how this angular distribution is changed by the emission of an additional gluon. Remember that the contribution due to gluon emission contains soft and collinear divergences, to be cancelled via the KLN theorem. Intuitively, one would

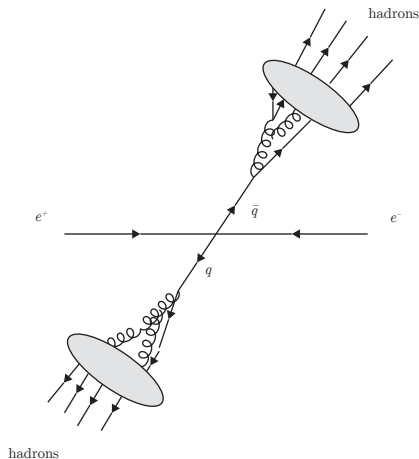


Fig. 15: Two jets of hadrons arising from quark-antiquark production in an e^+e^- collision. The blobs represent the hadronization process.

think that one does not need to integrate over *all* possible gluon emission energies and angles; if we only integrate the gluon emission rate over a small angle close to the quark or antiquark direction the collinear divergence should already cancel with the divergence contained in the virtual contribution, leaving a contribution depending on the size of the angular range. Also, if we allow a (very) soft gluon to be emitted and add this contribution to that from the virtual contribution we expect that the infrared divergences will cancel too. The result will then still depend on one angle and one energy. One could therefore define a two-jet event as one where almost all of the energy, namely $(1 - \epsilon)\sqrt{s}$, is contained in two small cones of semi-angle δ , where ϵ and δ are fixed, and can be reasonably large, as shown in Fig. 16. An explicit calculation of the corrections to the (anti)quark angular distribution shows that the

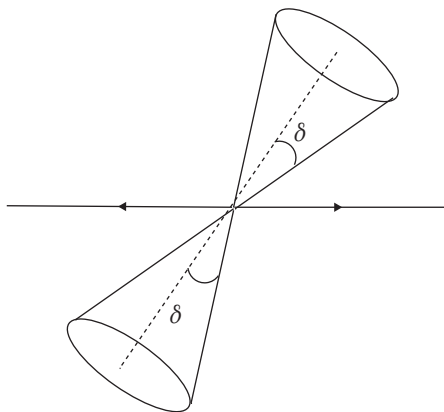


Fig. 16: Two jets defined by an opening angle δ

angular distribution is still proportional to $1 + \cos^2 \theta$ but the coefficient in front is modified by the factor

$$1 - \frac{\alpha_s(q^2)C_2(R)}{\pi} \left[(4 \ln 2\epsilon + 3) \ln \frac{\pi^2}{3} - 5/2 + 0(\epsilon) + 0(\delta) \right]. \quad (80)$$

As one would expect, if one would take the limit ϵ and $\delta \rightarrow 0$ divergences show up again in this factor, so one must be careful to choose ϵ or δ small but large enough that the α_s correction in (80) is still relatively small. In this way, due to Sterman and Weinberg [22], the jet angular distribution is well-defined and has been successfully compared with experiment.

One may now generalize the definition of a jet such that singularities still cancel, but that their definitions are more easily implemented in both experimental measurements and theoretical calculations, the latter in the form of a Monte Carlo program. To this end one constructs an iterative algorithm for combining the measured hadrons (or computed partons) into jets. The starting point of such an algorithm is a list of particles (hadrons or partons) with their energies and angles. For example, in one algorithm, for all particle pairs i and j one then calculates the quantity $y_{ij} = 2E_i E_j (1 - \cos \theta_{ij})/s$. All y_{ij} 's are now compared with a chosen value y_{cut} . For each y_{ij} that is smaller than y_{cut} the two momenta of particles i and j are combined according some chosen prescription, for instance ‘‘add the four-momenta’’. Particles i and j are then removed from the list, but their combination is returned to the list as a new ‘pseudoparticle’. The procedure is repeated until no two (pseudo)particles have an y_{ij} that is smaller than y_{cut} . This subdivides the experimentally measured or theoretically simulated events into a number of clustered jets, of which one can study the properties. One should be aware however that not all algorithms are infrared safe for all collider types.

This concludes our discussion of higher orders for collider processes with quarks and gluons only in the final state. We now turn to the case where there are strongly interacting particles in the initial state as well.

3.5 The Drell-Yan process

The Drell-Yan process [23] is, and has been, an important reaction in particle physics. It involves the production of a lepton-antilepton pair in proton-(anti)proton collisions,

$$p + \bar{p}/p \rightarrow l + \bar{l} + X$$

where X denotes the rest of the final state. Leptons are relatively easy to detect and through this reaction a number of important discoveries such as of the J/Ψ and the Υ mesons (and therefore of the charm and bottom quarks), and of the W and Z vector bosons were made. From a theoretical point of view, its QCD corrections are prototypical for any high-energy cross section with initial state hadrons, and it is from this perspective that we shall discuss these corrections here. For simplicity we will only examine the QCD corrections to the single differential cross section in the lepton pair invariant mass Q , i.e. $d\sigma/dQ^2$. Therefore the process is inclusive in all the hadron final states, which renders the KLN theorem for the QCD corrections in principle operative (as we will see, only for the final state). To calculate the corrections we consider the reaction at the partonic level, where the lowest order approximation only involves only quark-antiquark annihilation into a virtual photon, which then couples to the lepton-antilepton pair. The total cross section for quark-antiquark annihilation in the reaction $q(p_1) + \bar{q}(p_2) \rightarrow l(q_1) + \bar{l}(q_2)$ can be computed as

$$\sigma_{q\bar{q}}^{(0)}(\hat{s}) = \frac{1}{4N_c^2} \frac{1}{2\hat{s}} \int \frac{d^3 q_1}{(2\pi)^3 2\omega_1} \int \frac{d^3 q_2}{(2\pi)^3 2\omega_2} (2\pi)^4 \delta(p_1 + p_2 - q_1 - q_2) \sum |\mathcal{M}|^2, \quad (81)$$

where $\hat{s} = -(p_1 + p_2)^2 = -(q_1 + q_2)^2 = Q^2$, the sum is over all initial and final spin and colour indices, and initial state spins and colours are averaged over.

We remind the reader that the hadronic cross section follows by convoluting this result with partonic densities in the incoming hadrons, as in sections 2.2 and 3.1. We write $\hat{s} = \xi_1 \xi_2 s$, where $\xi_{1,2}$ are parton momentum fractions and s is the collider cm energy squared. Also we introduce the variable $\tau = Q^2/s$ so that

$$\frac{d\sigma_{pp}^{(0)}(\tau)}{dQ^2} = \sum_{i,j} \int_{\xi_{1,\min}}^1 d\xi_1 \int_{\xi_{2,\min}}^1 d\xi_2 f_{i/p}(\xi_1) f_{j/p}(\xi_2) \frac{d\sigma_{ij}^{(0)}(\xi_1, \xi_2)}{dQ^2}, \quad (82)$$

where the f 's are the parton distribution functions for the quarks and antiquarks in the proton and antiproton. The sum runs over all quarks and antiquarks in both the proton and antiproton, while $\xi_{1,\min} = \tau$, and $\xi_{2,\min} = \tau/\xi_1$. We return to this formula towards the end of this section.

The only Feynman diagram to compute is the one photon exchange diagram for which the square of the amplitude yields

$$\sum |\mathcal{M}|^2 = e^4 Q_f^2 \text{Tr}(\gamma_\mu \not{p}_1 \gamma_\nu \not{p}_2) \text{Tr}(\gamma_\mu \not{q}_2 \gamma_\nu \not{q}_1) \frac{1}{\hat{s}^2}. \quad (83)$$

The charge of quark flavour f is $Q_f e$, and the final trace is over the unit N_c -dimensional matrix labelled by the colour indices. It is not difficult to work out (83). Moreover the integration over the lepton trace in (81) can be done by applying the so-called Lenard identity (here given in n dimensions)

$$\int d^n q_1 \delta(q_1^2) \int d^n q_2 \delta(q_2^2) \delta^n(q - q_1 - q_2) q_1^\mu q_2^\nu = \left(\frac{-q^2}{4}\right)^{(n-4)/2} \frac{\pi^{(n-1)/2}}{\Gamma((n+1)/2)} \frac{1}{32} (q^2 \eta^{\mu\nu} + 2q^\mu q^\nu). \quad (84)$$

The final result, in 4 dimensions,

$$\sigma_{q\bar{q}}^{(0)}(\hat{s}) = \frac{4\pi\alpha^2}{3N_c\hat{s}}, \quad (85)$$

is only a function of \hat{s} . The differential cross section with respect to $Q^2 = -(q_1 + q_2)^2$ can now be derived using

$$\frac{d\sigma_{q\bar{q}}^{(0)}(Q^2)}{dQ^2} = \left[\frac{4\pi\alpha^2}{3N_c(Q^2)^2} \right] \delta\left(1 - \frac{Q^2}{\hat{s}}\right). \quad (86)$$

Indeed, as a check

$$\sigma_{q\bar{q}}^{(0)}(\hat{s}) = \int \frac{d\sigma_{q\bar{q}}^{(0)}(Q^2)}{dQ^2} dQ^2 = \frac{4\pi\alpha^2}{3N_c} \int \frac{dQ^2}{(Q^2)^2} \delta\left(1 - \frac{Q^2}{\hat{s}}\right) = \frac{4\pi\alpha^2}{3N_c\hat{s}}. \quad (87)$$

Note that (86) is no longer a function but a distribution as it is proportional to a δ -function with argument proportional to $\hat{s} - Q^2$. Therefore as far as the lowest order formula is concerned we can write either $d\sigma_{q\bar{q}}^{(0)}/dQ^2$ or $d\sigma_{q\bar{q}}^{(0)}/d\hat{s}$. The expression in square brackets in (86) we will refer to as $\sigma_\gamma^{(0)}$.

For the calculation of the QCD corrections we would prefer not to include the part of the diagram where the photon decays into leptons, which is common to all diagrams to any order in QCD perturbation theory. One can account for that by computing the ratio K of the squared amplitude for the process $q(p_1) + \bar{q}(p_2) \rightarrow \gamma^*(q)$ ($q^2 = -Q^2$) and the $q(p_1) + \bar{q}(p_2) \rightarrow l\bar{l}(q)$ at lowest order as follows

$$\sigma^{(0)}(l\bar{l}) = K \sigma^{(0)}(\gamma^*). \quad (88)$$

The factor K can be computed in dimensional regularization. It is valid to all orders in perturbative QCD, because it only involves the electroweak final state. We shall not give the expression here, but thanks to (88) we can now suffice with computing the cross section for γ^* production.

Let us now evaluate the next order corrections to (82). We consider the quark-antiquark channel and calculate the processes involving the virtual corrections to the Born reaction, and the counterterm contributions. In Fig. 17 we show these, and also contributions to the quark-gluon channel, which are typically smaller. The Feynman diagrams must be evaluated in n -dimensions and a colour matrix must be added at the quark gluon vertex. We split the correction as follows

$$\frac{d\sigma_{q\bar{q}}^{(1)}}{dQ^2} = \frac{d\sigma_{q\bar{q}}^{(1)}}{dQ^2}|_{\text{virtual}} + \frac{d\sigma_{q\bar{q}}^{(1)}}{dQ^2}|_{\text{real}}. \quad (89)$$

Incidentally, we use n -dimensional regularization also for infrared divergences, and consider the quark and anti-quark to be massless and on-shell. To see how this affects the loop integrals, let present the

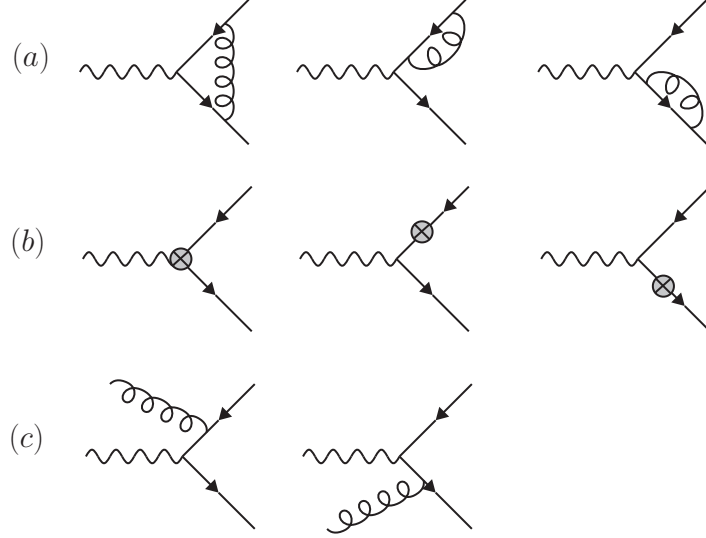


Fig. 17: The Feynman diagrams for the first order QCD corrections to the partonic Drell-Yan reaction in the quark-antiquark collisions producing an off-shell photon. Shown are (a) loop contributions (b) counterterm contributions, and (c) radiative graphs. The leptons into which the photon decays are not shown. Time runs from right to left in this figure.

result for $J(t, 0, 0)$, the scalar vertex function, where $t = -Q^2$. It occurs in the first diagram in Fig. 17a and is defined by

$$J(t, 0, 0) = \frac{1}{(2\pi)^n} \int \frac{d^n q}{((p+q)^2)((p'+q)^2)(q^2)}, \quad (90)$$

where $p^2 = p'^2 = 0$. The integral may be computed using standard methods in dimensional regularization. The result is

$$J(t, 0, 0) = i(4\pi)^{-\frac{n}{2}} \left(\frac{-t}{\mu^2}\right)^{\frac{n-6}{2}} (\mu^2)^{\frac{n-6}{2}} \frac{\Gamma(3-n/2)\Gamma^2(n/2-1)}{\Gamma(n-3)} \times \frac{4}{(n-4)^2}, \quad (91)$$

where we have inserted a mass scale μ to make the integral have the correct dimension in n space-time dimensions. Notice that the last factor shows a double pole in $n-4$, arising from the overlap of an infrared and a collinear singularity, when the virtual gluon both becomes soft and collinear to either the incoming quark or anti-quark. Also a two-denominator integral occurs when including numerator factors in the leftmost graph of Fig. 17a. It reads

$$I(k^2, 0, 0) = \frac{1}{(2\pi)^n} \int \frac{d^n q}{((q+\frac{1}{2}k)^2)((q-\frac{1}{2}k)^2)}, \quad (92)$$

with $k^2 = Q^2$, and the result of doing the integral is

$$I(-t, 0, 0) = i(4\pi)^{-\frac{n}{2}} \left(\frac{-t}{\mu^2}\right)^{\frac{n-4}{2}} (\mu^2)^{n/2-2} \frac{\Gamma(3-n/2)\Gamma^2(n/2-1)}{\Gamma(n-2)} \times \frac{2}{4-n}. \quad (93)$$

Again it features a pole in $n-4$. Note that it is not always obvious from superficial inspection to see whether a $1/(n-4)$ pole has an ultraviolet, infrared or collinear origin. However, in general, a UV divergence occurs after the n -dimensional integral over the loop momentum, while the IR and collinear singularities arise from the integrations over the Feynman parameters. The full result for the vertex graph in Fig. 17a including numerator factors, reads, after substituting $n = 4 + \varepsilon$

$$\Lambda(p', p) = e^3 \gamma_\mu i(4\pi)^{-2} \left(\frac{-t}{4\pi\mu^2}\right)^{\varepsilon/2} (\mu^2)^{\varepsilon/2} \frac{\Gamma(1-\varepsilon/2)\Gamma^2(1+\varepsilon/2)}{\Gamma(2+\varepsilon)}$$

$$\times \left[\frac{8}{\varepsilon^2} + \frac{2}{\varepsilon} + 1 \right]. \quad (94)$$

Besides the vertex graph we should also consider other virtual contributions, namely the one-loop gluon self-energy corrections to the incoming on-shell quark and anti-quark, as well as contributions from counterterms. However, none of these contribute to the present calculation. To see this, consider first the self-energy contribution for an on-shell massless fermion

$$\Sigma(p) = -i\not{p} - g^2 \int \frac{d^n q}{(2\pi)^n} \frac{(-i\not{p})(-i\not{p} - i\not{q})(-i\not{p})}{(p+q)^2 q^2}. \quad (95)$$

Using $p^2 = 0$ this reduces to

$$\Sigma(p) = -i\not{p} - i\not{p} g^2 \int \frac{d^n q}{(2\pi)^n} \frac{2p \cdot q}{(p+q)^2 q^2}. \quad (96)$$

Writing

$$2p \cdot q = (q+p)^2 - q^2, \quad (97)$$

we see that the $\mathcal{O}(g^2)$ correction vanishes, by the rules of dimensional regularization, in which scaleless loop integrals may be consistently set to zero.

Besides the loop diagrams also the $\mathcal{O}(\alpha_s)$ counterterms in the Lagrangian must be included in the virtual contributions, shown in Fig. 17b. This is so even when a loop graph itself is zero, such as for the quark and antiquark self energy corrections. There are in fact three counterterm diagrams in the Lagrangian, indicated in Fig. 17b. The quark colours, when including initial quark colour averaging, here merely lead to a common factor $C_2(R)/N_c$ for all three contributions. The counterterm contributions for the self energy corrections must be included with a factor 1/2 due to the need to normalize the scattering amplitude using the residue at the pole. When one does this, the counterterm contributions cancel against each other.

So, remarkably, in the end only the triangle diagram contributes to the virtual contribution, and we have the result

$$\begin{aligned} \frac{d\sigma_{q\bar{q}}^{(1)}}{d\hat{s}} \Big|_{\text{virtual}} &= \sigma_\gamma^{(0)} Q_f^2 \frac{1}{2\pi} C_2(R) \left(\frac{4\pi\mu^2}{\hat{s}} \right)^{-\varepsilon/2} \frac{\Gamma(1+\varepsilon/2)}{\Gamma(1+\varepsilon)} \\ &\times \left[-\frac{8}{\varepsilon^2} + \frac{6}{\varepsilon} - 8 + \frac{2\pi^2}{3} + \mathcal{O}(\varepsilon) \right] \delta(1-x), \end{aligned} \quad (98)$$

where $x = \hat{s}/s$. We have used the expansion $\Re(-1)^{\varepsilon/2} = \Re \exp(i\varepsilon\pi/2) \simeq 1 - \pi^2\varepsilon^2/8$. (We dropped the imaginary part $\varepsilon i\pi/2$ since we only need the real part of the virtual contributions in the interference with the Born diagram.) The other π^2 terms in (98) follow from expansion of the Gamma functions

$$\Gamma(1-\varepsilon/2)\Gamma(1+\varepsilon/2) = 1 + \frac{\pi^2}{6} \frac{\varepsilon^2}{4} + \mathcal{O}(\varepsilon^3). \quad (99)$$

Next we must consider the real gluon bremsstrahlung graphs which as far as the partonic channel is concerned contribute to the two-to-two body scattering cross section for $q(p_1) + \bar{q}(p_2) \rightarrow \gamma(q) + g(k)$. Now since $\hat{s} = -(p_1 + p_2)^2$ is the square of the total centre-of-mass energy and $Q^2 = -q^2 = (q_1 + q_2)^2$ is the invariant mass of the dilepton pair then $\hat{s} \neq Q^2$. It is convenient to rewrite the Mandelstam invariants in terms of the two variables $x = Q^2/s$ and $y = (1 + \cos\theta)/2$. This yields the relations $s = Q^2/x$, $\hat{t} = -Q^2(1-x)(1-y)/x$, and $\hat{u} = -Q^2(1-x)y/x$. In this bremsstrahlung correction we will have contributions from the region $x = Q^2/s < 1$, whereas the virtual and counterterm diagrams only contribute at $x = 1$.

Let us introduce a convenient shorthand notation for an l -particle n -dimensional phase-space measure

$$\int_{\text{PS}l} dq_1 \cdots dq_l = (2\pi)^{n+l(1-n)} \int \frac{d^{n-1}q_1}{2q_1^0} \cdots \frac{d^{n-1}q_l}{2q_l^0} \delta^{(n)}(P - \sum_i^l q_i), \quad (100)$$

where we have left the masses of each particle unspecified. We need to evaluate

$$\frac{d\sigma_{q\bar{q}}^{(1)}}{dQ^2}|_{\text{real}} = \frac{1}{8N_c^2 \hat{s}} \int_{\text{PS}3} dk dq_1 dq_2 \delta^{(n)}(p_1 + p_2 - k - q_1 - q_2) \sum |\mathcal{M}|^2, \quad (101)$$

where \mathcal{M} is the matrix element of the two-to-three body reaction $q(p_1) + \bar{q}(p_2) \rightarrow l(q_1) + \bar{l}(q_2) + g(k)$. The three-body phase-space integral can be factorized into two two-body phase-space integrals by inserting

$$1 = \int \frac{dQ^2}{2\pi} \int d^n q \delta^{(n)}(q - q_1 - q_2) (2\pi) \delta(q^2 - Q^2), \quad (102)$$

into the integral. Then we write the integral over dq as a $n - 1$ dimensional integral using $\delta(q^2 - Q^2)$. If we use the notation $p = p_1 + p_2$ then the integrals can be written as

$$\frac{d\sigma_{q\bar{q}}^{(1)}}{dQ^2}|_{\text{real}} = \frac{1}{16\pi N_c^2 \hat{s}} \int_{\text{PS}2} dk dq \int_{\text{PS}2} dq_1 dq_2 \sum |\mathcal{M}|^2, \quad (103)$$

where the first phase space-integral has a δ -function $\delta^{(n)}(p - q - k)$ and the second one $\delta^{(n)}(q - q_1 - q_2)$. This enables us again to factor off the decay of the γ^* into the lepton-antilepton pair, leading to the equation (88) but now also for the real emission contribution.

The square of the partonic matrix element summed over all initial and final spins and polarizations can then be written in terms of the Mandelstam invariants for the reaction $q(p_1) + \bar{q}(p_2) \rightarrow \gamma(q) + g(k)$. These we will call $s = -(p_1 + p_2)^2$, $t = -(p_1 - k)^2$, and $u = -(p_2 - k)^2$, which satisfy $s + t + u = -Q^2$. Note that a term involving a new mass scale μ will be required because the QCD coupling constant g has mass dimension $(4 - n)/2$ in n -dimensions. There is no need to write an n -dimensional generalization for the QED coupling constant so we can keep e in four dimensions. The answer in terms of $n = 4 + \varepsilon$ reads

$$\begin{aligned} \frac{d\sigma_{q\bar{q}}^{(1)}}{d\hat{s}}|_{\text{real}} &= \sigma_\gamma^{(0)} Q_f^2 \frac{1}{2\pi} C_2(R) \left(\frac{4\pi\mu^2}{\hat{s}} \right)^{-\varepsilon/2} \frac{\Gamma(1 + \varepsilon/2)}{\Gamma(1 + \varepsilon)} \frac{4}{\varepsilon} \\ &\quad \times \left[2x^{1-\varepsilon/2} (1-x)^{-1+\varepsilon} + x^{-\varepsilon/2} (1-x)^{1+\varepsilon} \right]. \end{aligned} \quad (104)$$

A collinear pole in ε resulting from the angular integral is now explicit. If we integrate over the variable x , which we must to form the hadronic cross section, a second pole will appear from the region $x \rightarrow 1$. That is the infrared pole. After integration there are therefore double pole terms from overlapping divergences and single pole terms from the either soft or the collinear singularities. Using the KLN theorem to cancel these pole terms against the contributions from the virtual graphs, which only exist for $x = 1$ would be convenient, especially before doing the integration over x . So, we would need a way of combining the contributions from the virtual and bremsstrahlung graphs as functions of x .

One way to do this is to split off a small piece in (104) between $x = 1 - \delta$ and $x = 1$ and call this the "soft" bremsstrahlung piece. In this small range near unity one can substitute $x = 1$ whenever this is allowed and simply do the x integral yielding terms in $\ln \delta$ as well as poles in ε . These pieces can then be added to the contributions from the virtual graphs. The remaining "hard" bremsstrahlung integral over the range 0 to $1 - \delta$ is finite, and can be taken in $n = 4$ dimensions. Integration will then yield a term involving $\ln \delta$ which should cancel with the corresponding $\ln \delta$ term in the virtual graphs. This method is called the phase-space slicing method.

We will employ another method. We would like a relation that expresses the double pole terms immediately in terms of $\delta(1-x)$. Such a relation does exist but in the sense of distributions, namely when multiplied by a smooth function $F(x)$ and integrated between 0 and 1 (like the δ -function itself). Assume the function $F(x)$ has a Taylor expansion near $x = 1$ so we can write $F(x) = F(1) + F(x) - F(1)$, where the difference between the last two terms is proportional to the finite derivative of $F(x)$ at $x = 1$. Let us consider therefore

$$\int_0^1 dx \frac{F(x)}{(1-x)^{1-\varepsilon}} = F(1) \int_0^1 dx \frac{1}{(1-x)^{1-\varepsilon}} + \int_0^1 dx \frac{F(x) - F(1)}{(1-x)^{1-\varepsilon}}. \quad (105)$$

The first integral yields $F(1)\varepsilon^{-1}$. We can rewrite this again as an integral over dx with the argument $\delta(1-x)$. In the second integral we can expand the denominator so it yields

$$\begin{aligned} \int_0^1 dx \frac{F(x) - F(1)}{(1-x)^{1-\varepsilon}} &= \int_0^1 dx \frac{F(x) - F(1)}{(1-x)} \\ &+ \varepsilon \int_0^1 dx [F(x) - F(1)] \frac{\ln(1-x)}{(1-x)} + O(\varepsilon^2), \end{aligned} \quad (106)$$

near $\varepsilon = 0$. Therefore we have the identity

$$\begin{aligned} \int_0^1 dx \frac{F(x)}{(1-x)^{1-\varepsilon}} &= \frac{1}{\varepsilon} \int_0^1 dx F(x) \delta(1-x) + \int_0^1 dx \frac{F(x) - F(1)}{1-x} \\ &+ \varepsilon \int_0^1 dx [F(x) - F(1)] \frac{\ln(1-x)}{1-x} + O(\varepsilon^2). \end{aligned} \quad (107)$$

This we will write in shorthand notation as

$$\frac{1}{(1-x)^{1-\varepsilon}} = \frac{1}{\varepsilon} \delta(1-x) + \left[\frac{1}{1-x} \right]_+ + \varepsilon \left[\frac{\ln(1-x)}{1-x} \right]_+ + O(\varepsilon^2), \quad (108)$$

where on the right hand side we see so-called "plus" distributions. Note that this result is exact for a lower integration limit $x = 0$. If the lower limit is not zero then there are additional finite terms involving logarithms of this lower limit.

Our final result for the gluon radiation graphs therefore follows by expanding the terms in the square bracket in (104) in powers of ε and using (108). We find

$$\begin{aligned} \frac{d\sigma_{q\bar{q}}^{(1)}}{d\hat{s}} \Big|_{\text{real}} &= \sigma_\gamma^{(0)} Q_f^2 \frac{1}{2\pi} \left(\frac{4\pi\mu^2}{\hat{s}} \right)^{-\varepsilon/2} \frac{\Gamma(1+\varepsilon/2)}{\Gamma(1+\varepsilon)} \left[\frac{8}{\varepsilon^2} \delta(1-x) \right. \\ &+ \frac{4}{\varepsilon} (1+x^2) \left[\frac{1}{1-x} \right]_+ + 4(1+x^2) \left[\frac{\ln 1-x}{1-x} \right]_+ \\ &\left. - 2(1+x^2) \frac{\ln x}{1-x} + O(\varepsilon) \right]. \end{aligned} \quad (109)$$

Now we have isolated the term in $\delta(1-x)$ containing the double pole we see that it cancels the corresponding term from the virtual graphs in (98). These are the overlap terms containing both soft and collinear divergences and they cancel as expected from the KLN theorem. The single pole term in ε however cannot possibly cancel against a virtual contribution, as it is not purely a $\delta(1-x)$ term. Therefore we are left with an uncancelled collinear singularity.

Finally we can finally sum (98) and (109) and find

$$\frac{d\sigma_{q\bar{q}}^{(1)}}{d\hat{s}} = \sigma_\gamma^{(0)} Q_f^2 \frac{1}{2\pi} C_2(R) \left(\frac{4\pi\mu^2}{\hat{s}} \right)^{-\varepsilon/2} \frac{\Gamma(1+\varepsilon/2)}{\Gamma(1+\varepsilon)}$$

$$\begin{aligned} & \times \left\{ \frac{4}{\varepsilon} \left((1+x^2) \left[\frac{1}{1-x} \right]_+ + \frac{3}{2} \delta(1-x) \right) + 4(1+x^2) \left[\frac{\ln(1-x)}{1-x} \right]_+ \right. \\ & \left. - 2(1+x^2) \frac{\ln x}{1-x} + (4\zeta(2) - 8)\delta(1-x) + \mathcal{O}(\varepsilon) \right\}, \end{aligned} \quad (110)$$

with $\zeta(2) = \pi^2/6$. The remaining pole term in ε implies that the KLN theorem is inoperable when there are collinear singularities in the initial partonic state. How are we then going to make sense of this result?

First, let us observe that if one expands all functions in (110) in ε one finds

$$\begin{aligned} \frac{d\sigma_{q\bar{q}}^{(1)}}{d\hat{s}} &= \sigma_\gamma^{(0)} Q_f^2 \frac{1}{2\pi} C_2(R) 2 \left(\frac{2}{\varepsilon} - \ln 4\pi + \gamma_E \right) \left((1+x^2) \left[\frac{1}{1-x} \right]_+ \right. \\ & \left. + \frac{3}{2} \delta(1-x) \right) + \mathcal{O}(\varepsilon^0) \\ &= \sigma_\gamma^{(0)} Q_f^2 \frac{1}{2\pi} C_2(R) 2 \left(\frac{2}{\varepsilon} - \ln 4\pi + \gamma_E \right) \left[\frac{1+x^2}{1-x} \right]_+ + \mathcal{O}(\varepsilon^0). \end{aligned} \quad (111)$$

Next, we realize that this expression should be substituted into the convolution (82). At this point one may, in a sense, *renormalize* (or rather: *factorize*) the parton distributions in (82) as

$$f_{q/A}(\xi) = \int_0^1 dz \int_0^1 dy f_{q/A}(y, \mu_F) \Phi_{q\bar{q}}^{-1}(z, \mu_F) \delta(\xi - zy), \quad (112)$$

with μ_F the factorization scale, introduced in the previous section, and $\Phi_{q\bar{q}}$ a transition function. This function is analogous to the Z -factors for UV renormalization in section 2.3.2.

To first order, the above relation can be written as

$$\begin{aligned} f_{q/A}(\xi) &= f_{q/A}(\xi, \mu_F) - \int_\xi^1 \frac{dz}{z} f_{q/A} \left(\frac{\xi}{z}, \mu_F \right) \\ & \times \left\{ \frac{\alpha_s(\mu) C_2(R)}{2\pi} \frac{1}{\varepsilon} \left(\frac{4\pi\mu^2}{\mu_F^2} \right)^{-\varepsilon/2} \left[\frac{1+z^2}{1-z} \right]_+ \right\}. \end{aligned} \quad (113)$$

Collecting terms we see indeed, as we announced, the collinear singularities cancel after renormalization of the parton distribution by the transition functions, leaving a finite remainder. The final result is

$$\begin{aligned} \frac{d\sigma_{q\bar{q}}^{(1)}}{d\hat{s}} &= \sigma_\gamma^{(0)} Q_f^2 \frac{1}{2\pi} C_2(R) \\ & \times \left\{ 2 \ln \left(\frac{Q^2}{\mu_F^2} \right) \left[\frac{1+z^2}{1-z} \right]_+ + 4(1+x^2) \left[\frac{\ln(1-x)}{1-x} \right]_+ \right. \\ & \left. - 2(1+x^2) \frac{\ln x}{1-x} + (4\zeta(2) - 8)\delta(1-x) \right\}. \end{aligned} \quad (114)$$

This result we can now insert into (82), use NLO PDF's and predict the Drell-Yan cross section.

3.6 Factorization

The fact that the initial state divergences cancel through a renormalization/factorization of the PDFs, as in (112) is a one-loop manifestation of the QCD factorization theorem [8]. This is the full QCD generalization of the parton model formula, and states that for IR safe cross sections, the initial state collinear divergences can be consistently removed in this way. The consistency lies in the fact that this factorization does not depend on the process, i.e. that it is *always the same set* of Φ_{ij} functions, computed to the appropriate order. This aspect is the one that preserves predictive power: indeed if we

devote certain set of observables to infer the PDF's, as we discussed extensively in section 3.1, we can use these for any other reaction and predict the outcome. To cover the details of the factorization proof for the inclusive Drell-Yan cross section would take us too far. However, it is worthwhile to point out that factorization proofs for other observables (differential cross sections, cross sections near phase space edges, or with vetoed phase space regions) are an active and important area of research [24, 25].

4 Modern methods

In this section I discuss a number of modern methods in the application of perturbative QCD, focussing mostly on spinor helicity techniques, and the essence of the recent ‘‘NLO revolution’’. For lack of space I shall not discuss the enormous strides made in Monte Carlo methods and applications in recent years.

4.1 Spinor methods, recursion relations

At high center-of-mass energies, final states produced in particle colliders usually contain many more than two particles. Calculations of such processes are long and complicated because one must write down the individual amplitudes for the Feynman graphs and then square the result, which involves all the cross products between them. In this section we describe methods to shorten these calculations by using clever choices for external line polarizations and simplifications owing to the masslessness of the particles. We also note that at high energies most of the final state particles can be considered massless, so that in order to represent fermions we may make use of a chiral spinor basis because at large momenta chirality and helicity are related. In that case many external helicities configurations are in fact simply not allowed by parity invariance. There are moreover many relations among the amplitudes so the number of amplitudes to compute is not overly large. An interesting thing to note is that by specifying all external line quantum numbers, the expression for each helicity amplitude is simply a complex number. This can then obviate the need for analytically spin-summing over the absolute value squared of the invariant amplitudes, and allow this task to be handled by a computer, reducing the amount of laborious computation further.

Let us see how the use of spinors of definite chirality or helicity can significantly simplify the calculation of Feynman diagrams with massless fermions and gauge bosons. We will also use the freedom of gauge choice for external gauge fields to maximal advantage. I try to give a reasonably explicit and self-contained presentation of these helicity spinor methods. We shall need the Dirac gamma matrices γ^μ , γ^5 and the charge conjugation matrix C in the Weyl basis:

$$\begin{aligned}\gamma^k &= \begin{pmatrix} 0 & \sigma_k \\ \sigma_k & 0 \end{pmatrix}, \quad k = 1, 2, 3; & \gamma^0 &= \begin{pmatrix} 0 & \mathbb{1} \\ -\mathbb{1} & 0 \end{pmatrix}, \\ \gamma^5 &= \gamma_5 = -i\gamma^0\gamma^1\gamma^2\gamma^3 = \begin{pmatrix} \mathbb{1} & 0 \\ 0 & -\mathbb{1} \end{pmatrix}, & C &= i\gamma^1\gamma^3 = \begin{pmatrix} \sigma_2 & 0 \\ 0 & \sigma_2 \end{pmatrix}.\end{aligned}\quad (115)$$

The explicit form of the u and v spinors in this basis is

$$\begin{aligned}u(\mathbf{P}, \xi) &= \frac{e^{i\pi/4}}{\sqrt{2(m + \omega(\mathbf{P}))}} \begin{pmatrix} [(m + \omega(\mathbf{P}))\mathbb{1} - \mathbf{P} \cdot \boldsymbol{\sigma}]\xi \\ -i[(m + \omega(\mathbf{P}))\mathbb{1} + \mathbf{P} \cdot \boldsymbol{\sigma}]\xi \end{pmatrix}, \\ v(\mathbf{P}, \bar{\xi}) &= \frac{e^{i\pi/4}}{\sqrt{2(m + \omega(\mathbf{P}))}} \begin{pmatrix} -[(m + \omega(\mathbf{P}))\mathbb{1} - \mathbf{P} \cdot \boldsymbol{\sigma}]\bar{\xi} \\ -i[(m + \omega(\mathbf{P}))\mathbb{1} + \mathbf{P} \cdot \boldsymbol{\sigma}]\bar{\xi} \end{pmatrix},\end{aligned}\quad (116)$$

with $\bar{\xi} = i\sigma_2\xi^*$. The momentum $P^\mu = \omega(\mathbf{P}), \mathbf{P}$ is the on-shell momentum of the fermion, and the charge conjugation matrix is used to define the charge conjugate spinor

$$\psi^c \equiv C^{-1}\bar{\psi}^T. \quad (117)$$

Having this explicit form will allow us to derive a number of useful identities which make calculations with massless particle must more efficient. The following identity,

$$[(m + \omega(\mathbf{P}))\mathbb{1} \pm \mathbf{P} \cdot \boldsymbol{\sigma}]^2 = 2(m + \omega(\mathbf{P})) [\omega(\mathbf{P})\mathbb{1} \pm \mathbf{P} \cdot \boldsymbol{\sigma}] \quad (118)$$

suggests that there is a more systematic way to write these spinors. To see this let us define σ_μ and $\bar{\sigma}_\mu$ as four-vector arrays of 2×2 hermitian matrices,

$$\sigma_\mu = (-\mathbb{1}, \boldsymbol{\sigma}), \quad \bar{\sigma}_\mu = (-\mathbb{1}, -\boldsymbol{\sigma}), \quad (P \cdot \sigma)(P \cdot \bar{\sigma}) = -P^2 = m^2. \quad (119)$$

In terms of these matrices one has the identities

$$\begin{aligned} (i\not{P} \pm m) &= \begin{pmatrix} \pm m\mathbb{1} & iP \cdot \boldsymbol{\sigma} \\ -iP \cdot \bar{\boldsymbol{\sigma}} & \pm m\mathbb{1} \end{pmatrix}, \\ -P^\mu \sigma_\mu &= \omega(\mathbf{P})\mathbb{1} - \mathbf{P} \cdot \boldsymbol{\sigma}, \\ -P^\mu \bar{\sigma}_\mu &= \omega(\mathbf{P})\mathbb{1} + \mathbf{P} \cdot \boldsymbol{\sigma}. \end{aligned} \quad (120)$$

Observe that $-P \cdot \sigma$ and $-P \cdot \bar{\sigma}$ are hermitian positive definite matrices with eigenvalues equal to $\omega(\mathbf{P}) \pm |\mathbf{P}|$.

Let us now consider the case of massless spinors. In that case the matrices $-P \cdot \sigma$ and $-P \cdot \bar{\sigma}$ have one zero eigenvalue and become equal to $2\omega(\mathbf{P})$ times a projection operator, as follows from (118). Indeed, the massless limit of (116) equals

$$\begin{aligned} u(\mathbf{P}, \xi) &= \frac{e^{i\pi/4}}{\sqrt{2\omega(\mathbf{P})}} \begin{pmatrix} (-P \cdot \sigma) \xi \\ -i(-P \cdot \bar{\sigma}) \xi \end{pmatrix}, \\ v(\mathbf{P}, \bar{\xi}) &= \frac{e^{i\pi/4}}{\sqrt{2\omega(\mathbf{P})}} \begin{pmatrix} -(-P \cdot \sigma) \bar{\xi} \\ -i(-P \cdot \bar{\sigma}) \bar{\xi} \end{pmatrix}. \end{aligned} \quad (121)$$

Before proceeding, let us introduce the light-cone basis for a generic massless momentum p^μ . In this basis the components p^0 and p^3 are replaced by

$$p^+ = \frac{p^0 + p^3}{\sqrt{2}}, \quad p^- = \frac{p^0 - p^3}{\sqrt{2}}, \quad (122)$$

where the two remaining components are denoted by the two-component vector $p_\perp = (p^1, p^2)$. In this basis

$$p^2 = -2p^+p^- + p_\perp^2. \quad (123)$$

The advantage of this basis is clear when considering a massless particle moving along the 3-axis. In the standard basis the momentum four-vector has two non-zero components, namely p^0 and p^3 , but in the light-cone basis there is only one non-vanishing component (i.e. either p^+ or p^-), which helps with the calculations as we will see below.

The positive frequency solution is degenerate and can be further classified using the chirality projectors $P_L = (1 + \gamma_5)/2$ and $P_R = (1 - \gamma_5)/2$, which project onto the upper and lower two components of the spinor, respectively. Thus we have the left- and right-handed solutions

$$u_L(\mathbf{P}, \xi) = \frac{e^{i\pi/4}}{\sqrt{2\omega(\mathbf{P})}} \begin{pmatrix} (-P \cdot \sigma) \xi \\ 0 \end{pmatrix}, \quad u_R(\mathbf{P}, \xi) = \frac{e^{-i\pi/4}}{\sqrt{2\omega(\mathbf{P})}} \begin{pmatrix} 0 \\ (-P \cdot \bar{\sigma}) \xi \end{pmatrix}, \quad (124)$$

and likewise for the spinors v_L and v_R . We can specify further the two-component spinors ξ . We note that $-P \cdot \sigma$ and $-P \cdot \bar{\sigma}$ project onto negative and positive helicity eigenstates, respectively. For instance, from

$$(-P \cdot \sigma)\xi = (|\vec{P}| - \vec{P} \cdot \vec{\sigma})\xi, \quad (125)$$

we see that the right hand side is only non-zero for ξ a negative helicity, ξ_- . Because $-P \cdot \sigma$ and $-P \cdot \bar{\sigma}$ are projectors, we can, without loss of generality, choose a convenient basis for the ξ_{\pm} spinors independent of momentum. We choose ξ_- (ξ_+) such that, in the frame where \vec{P} is along the z -axis, u_L (u_R) has j_3 eigenvalue $-\frac{1}{2}$ ($+\frac{1}{2}$), in correspondence with the helicity-chirality relation $2h = -\gamma_5$. We thus choose

$$\xi_- = \begin{pmatrix} 0 \\ 1 \end{pmatrix}, \quad \xi_+ = \begin{pmatrix} 1 \\ 0 \end{pmatrix}. \quad (126)$$

In this case we have for $u_L(P, \xi)$ and $u_R(P, \xi)$

$$u_L(\mathbf{P}, \xi) = \frac{e^{i\pi/4}}{\sqrt{2P^0}} \begin{pmatrix} -P_T^* \\ \sqrt{2}P^+ \\ 0 \\ 0 \end{pmatrix}, \quad u_R(\mathbf{P}, \xi) = \frac{e^{-i\pi/4}}{\sqrt{2P^0}} \begin{pmatrix} 0 \\ 0 \\ \sqrt{2}P^+ \\ P_T \end{pmatrix}. \quad (127)$$

For the rest of this section we change from chirality to helicity labels, and allow for a change in normalization

$$u_L \equiv \frac{1}{c_-} u_-, \quad u_R \equiv \frac{1}{c_+} u_+. \quad (128)$$

Once can show that in order to have $u_{\pm}(P)^\dagger u_{\pm}(P) = 2P^0$ one must, up to phases, choose $c_- = 2^{1/4} \sqrt{P^0/P^+}$ and $c_+ = 2^{1/4} \sqrt{P^0/P^-}$. We choose the phases of u_{\pm} now such that

$$u_-(\mathbf{P}, \xi) = 2^{1/4} \begin{pmatrix} -\sqrt{P^-} e^{-i\phi_p} \\ \sqrt{P^+} \\ 0 \\ 0 \end{pmatrix}, \quad u_+(\mathbf{P}, \xi) = 2^{1/4} \begin{pmatrix} 0 \\ 0 \\ \sqrt{P^+} \\ \sqrt{P^-} e^{i\phi_p} \end{pmatrix}. \quad (129)$$

where the phase ϕ_p is defined through

$$P_T = e^{i\phi_p} \sqrt{2P^+P^-}. \quad (130)$$

Having constructed quite explicit forms for helicity spinors we now use them to derive useful computational rules. Arguments of spinors we now indicate with lower-case four-momenta. To begin, we define *spinor products* together with bra-ket notation, as follows

$$i\bar{u}_-(k)u_+(p) \equiv \langle k-|p+ \rangle \equiv \langle kp \rangle, \quad (131)$$

and

$$i\bar{u}_+(k)u_-(p) \equiv \langle k+|p- \rangle \equiv [kp]. \quad (132)$$

One may show that

$$\langle kp \rangle = (e^{i\phi_k} \sqrt{2k^-p^+} - e^{i\phi_p} \sqrt{2k^+p^-}), \quad (133)$$

and

$$[kp] = \langle kp \rangle = (e^{-i\phi_k} \sqrt{2k^-p^+} - e^{-i\phi_p} \sqrt{2k^+p^-}), \quad (134)$$

so that

$$\langle kp \rangle = -\langle pk \rangle, \quad [kp] = -[pk], \quad \langle kp \rangle^* = [kp], \quad (135)$$

and

$$\langle kp \rangle [kp] = -2k \cdot p. \quad (136)$$

The real benefits of working with helicity spinors come to the fore when also the polarization vectors $\varepsilon^\mu(k, \lambda)$ of massless spin-1 particles with momentum k and helicity λ are expressed in terms of them. To see how this works, we first choose the frame in which the on-shell massless gauge boson momentum has only a + component. In this frame only the ε^1 and ε^2 components are meaningful, corresponding to the two helicity states of the massless vector field. For the chosen frame the third component of the spin is identical to the helicity, and the transversality condition $k \cdot \varepsilon(k) = 0$ becomes

$$k^+ \varepsilon^-(k, \lambda) = 0, \quad (137)$$

which implies that $\varepsilon^0 = \varepsilon^3$. From this explicit solution one observes that $(\varepsilon_\mu(k, +))^*$ has negative helicity. Our normalization is such that

$$(\varepsilon_\mu(k, +))^* = \varepsilon_\mu(k, -). \quad (138)$$

and

$$\varepsilon(k, +) \cdot \varepsilon(k, -) = -1. \quad (139)$$

We will also use the notation

$$\varepsilon^\mu(k, \pm) = \varepsilon_\pm^\mu(k). \quad (140)$$

Let us now demonstrate that we may write the polarization vector indeed in terms of spinors of fixed helicity, as follows

$$\varepsilon_+^\mu(k, p) = A_+ \overline{u}_+(k, +) \gamma^\mu u(p, +) \equiv -i A_+ \langle k+ | \gamma^\mu | p+ \rangle, \quad (141)$$

and similarly for negative helicity. Note the extra momentum p , called the *reference momentum*, of the second u spinor. It is in fact arbitrary, with $p^2 = 0$, we will discuss it further below. From the explicit form of the helicity spinors in (129) and the form of the solutions one may derive

$$A_+ = \frac{-i}{\sqrt{2} \langle kp \rangle}, \quad A_- = \frac{-i}{\sqrt{2} [kp]}. \quad (142)$$

Recall that any multiple of k^μ may be added to the expressions for the photon polarizations without changing the amplitude, as this is just a gauge transformation.

From the explicit form of the u and v spinors (129), one can prove the following series of identities

$$\langle k+ | p+ \rangle = 0, \quad (143)$$

$$\langle k+ | \gamma^\mu | p- \rangle = \langle k+ | \gamma_5 | p+ \rangle = 0, \quad (144)$$

$$\langle k+ | \gamma^\mu | k+ \rangle = 2k^\mu, \quad (145)$$

$$\langle k+ | \gamma^\mu | p+ \rangle = \langle p- | \gamma^\mu | k- \rangle, \quad (146)$$

and similarly with all helicities reversed. These identities are remarkably useful in practical calculations with helicity spinors. Another very important property for this is Fierz reordering, with which one may “recouple” the spinors. Consider the following expression

$$\langle 1+ | \gamma^\mu | 2+ \rangle \langle 3- | \gamma_\mu | 4- \rangle, \quad (147)$$

where we have abbreviated $|k_1+ \rangle = |1+ \rangle$ etc. This is in fact the most general form for such a contraction of spinor products. Let us define the following complete set of 16 matrices

$$O_I = \{1, \gamma_5, \gamma^\mu, i\gamma^\mu \gamma_5, \sigma^{\mu\nu}\}, \quad (148)$$

with the orthogonality property

$$\frac{1}{4} \text{Tr} [O_I O_J] = \delta_{IJ}, \quad I = 1 \dots 5. \quad (149)$$

We can insert this relation into (147), which may then be written as

$$\frac{1}{4} \sum_I \langle 1+|\gamma^\mu O_I \gamma_\mu|4-\rangle \langle 3-|O_I|2+\rangle. \quad (150)$$

Because of the chirality properties of the bra's and kets, only the two diagonal O_I yield a non-zero result, 1 and γ_5 , and they moreover yield the same result. Hence the Fierz recoupling identity reads simply

$$\langle 1+|\gamma^\mu|2+\rangle \langle 3-|\gamma_\mu|4-\rangle = 2\langle 1+|4-\rangle \langle 3-|2+\rangle, \quad (151)$$

where e.g. $\langle 1+|$ has been recoupled to $|4-\rangle$ in the spinor product. With this identity we can now check the normalization of the polarization vectors and find

$$\varepsilon^+(k, p) \cdot \varepsilon^-(k, p) = -A_+ A_- \langle k+|\gamma^\mu|p+\rangle \langle k-|\gamma_\mu|p-\rangle = 1, \quad (152)$$

and similarly that $\varepsilon_\pm(k, p) \cdot \varepsilon_\pm(k, p) = 0$. The identities involving the sum over spin polarizations read in terms of helicity spinors

$$\not{k} = |k+\rangle \langle k+| + |k-\rangle \langle k-|. \quad (153)$$

One can derive the completeness relation for the polarization vectors in the representation (141)

$$\sum_{\lambda=\pm} \varepsilon_\lambda^\mu(k, p) (\varepsilon_\lambda^\nu(k, p))^* = \eta^{\mu\nu} - \frac{p^\mu k^\nu + p^\nu k^\mu}{p \cdot k}, \quad (154)$$

and that a change in reference momentum amounts to a different gauge choice

$$\varepsilon_+^\mu(k, p) - \varepsilon_+^\mu(k, q) = \frac{\sqrt{2}\langle pq\rangle}{\langle kp\rangle\langle kq\rangle} k^\mu. \quad (155)$$

We have now sufficient ingredients to demonstrate the efficiency of using helicity spinors in computing invariant amplitudes for a few examples. For each amplitude we shall discuss the result for various sets of helicities for the external particles. We shall also take each external particle as massless so that helicity is a conserved quantum number. For convenience we choose momenta of the external particles outgoing, and express possible anti-fermion spinors in terms of u spinors using $v_+ = u_-$ and $v_- = u_+$.

The reaction $e^+e^- \rightarrow \mu^+\mu^-$

We first consider the reaction

$$e^-(k_1) + e^+(k_2) \rightarrow \mu^-(k_3) + \mu^+(k_4), \quad (156)$$

mediated via a photon. The invariant amplitude may be represented as

$$\mathcal{M}(1^{\lambda_1}, 2^{\lambda_2}, 3^{\lambda_3}, 4^{\lambda_4}), \quad (157)$$

where we have indicated only the label of each external line momentum, and the associated helicity. Using the rules derived in this section we have

$$\mathcal{M}(1^+, 2^-, 3^+, 4^-) = (ie)^2 \langle 2-|\gamma^\mu|1-\rangle \frac{-i}{s_{12}} \langle 3+|\gamma_\mu|4+\rangle, \quad (158)$$

where we used the notation $s_{ij} = -(k_i + k_j)^2$. Using the Fierz identity (151) and the shorthand notation of (131) and (132) this can be written as

$$\mathcal{M}(1^+, 2^-, 3^+, 4^-) = 2ie^2 \frac{[24]\langle 31\rangle}{\langle 12\rangle[12]}. \quad (159)$$

Using momentum conservation this may be further rewritten as

$$\mathcal{M}(1^+, 2^-, 3^+, 4^-) = 2ie^2 \frac{[13]^2}{[12][34]}. \quad (160)$$

It may be readily verified that

$$\mathcal{M}(1^-, 2^+, 3^-, 4^+) = 2ie^2 \frac{\langle 13 \rangle^2}{\langle 12 \rangle \langle 34 \rangle}. \quad (161)$$

The expressions in (160) and (161) are quite compact, and can be transformed into each other by either a parity transformation or a charge conjugation. For any other helicity configuration the amplitude actually vanishes.

The reaction $e^+e^- \rightarrow \mu^+\mu^-\gamma$

In this second example we study the production of a muon pair together with a photon in electron positron annihilation

$$e^-(k_1) + e^+(k_2) \rightarrow \mu^-(k_3) + \mu^+(k_4) + \gamma(k_5) \quad (162)$$

The photon can be radiated off any of the four external fermion lines, leading to the four diagrams shown in Fig. 18. Let us list another useful identity, not difficult to prove, for a positive helicity massless vector

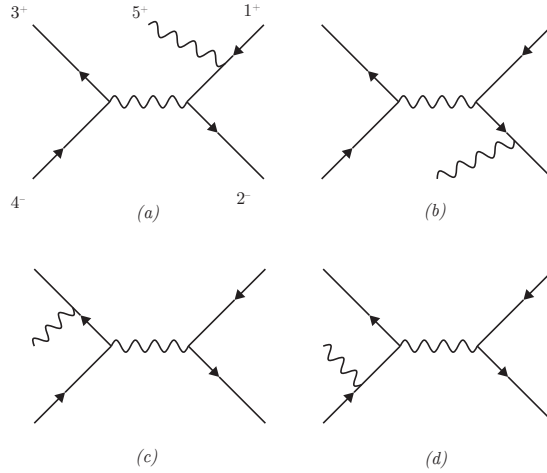


Fig. 18: Feynman diagrams contributing a particular helicity amplitude, indicated in diagram (a), for $e^+e^- \rightarrow \mu^+\mu^-\gamma$ at lowest order. All momenta are outgoing, and time runs from right to left.

boson with polarization $\varepsilon_+^\mu(k, p)$ emitted from a fermion by

$$\not{\varepsilon}_+(k, p) = \frac{i\sqrt{2}}{\langle kp \rangle} (|p+\rangle\langle k+| + |k-\rangle\langle p-|). \quad (163)$$

For the negative helicity case one has, in analogy

$$\not{\varepsilon}_-(k, p) = \frac{-i\sqrt{2}}{[kp]} (|k+\rangle\langle p+| + |p-\rangle\langle k-|). \quad (164)$$

The invariant amplitude reads

$$\mathcal{M}(1^{\lambda_1}, 2^{\lambda_2}, 3^{\lambda_3}, 4^{\lambda_4}, 5^{\lambda_5}). \quad (165)$$

Given that each external line can have two helicity values, it might seem that this process allows thirty-two different independent helicity amplitudes. However, helicity conservation and invariance under charge conjugation and parity transformation ensure that there is in fact only one independent amplitude. We thus consider the helicity amplitude

$$\mathcal{M}(1^+, 2^-, 3^+, 4^-, 5^+), \quad (166)$$

and choose as k_4 as reference momentum for the outgoing photon. Diagram (a) then reads

$$\mathcal{M}_a(1^+, 2^-, 3^+, 4^-, 5^+) = (ie)^3 \langle 2^- | \gamma^\mu \frac{-i(\not{1} + \not{5})}{-s_{15}} \not{\epsilon}_+(k_5, k_4) | 1^- \rangle \times \frac{-i}{s_{34}} \langle 3^+ | \gamma_\mu | 4^+ \rangle. \quad (167)$$

Using the results in eqs. (163) and (164) we find

$$\mathcal{M}_a(1^+, 2^-, 3^+, 4^-, 5^+) = -2\sqrt{2}e^3 \frac{\langle 24 \rangle^2 [23]}{\langle 15 \rangle \langle 45 \rangle \langle 34 \rangle [34]}. \quad (168)$$

For diagram (b) we find similarly

$$\mathcal{M}_b(1^+, 2^-, 3^+, 4^-, 5^+) = 2\sqrt{2}e^3 \frac{\langle 24 \rangle^2 [13]}{\langle 25 \rangle \langle 45 \rangle \langle 34 \rangle [34]}, \quad (169)$$

while for (c) we have

$$\mathcal{M}_c(1^+, 2^-, 3^+, 4^-, 5^+) = 2\sqrt{2}e^3 \frac{\langle 24 \rangle^2}{\langle 12 \rangle \langle 35 \rangle \langle 45 \rangle}. \quad (170)$$

Notice that with our choice of reference momentum we have

$$\mathcal{M}_d(1^+, 2^-, 3^+, 4^-, 5^+) = 0. \quad (171)$$

Adding up the contributions we find

$$\mathcal{M}(1^+, 2^-, 3^+, 4^-, 5^+) = 2\sqrt{2}e^3 \frac{\langle 24 \rangle^2}{\langle 12 \rangle} \left(\frac{[34]}{\langle 15 \rangle \langle 45 \rangle [12]} + \frac{1}{\langle 35 \rangle \langle 45 \rangle} \right). \quad (172)$$

Again this is a nice, compact result, a complex number fully expressed in terms of helicity spinors.

Without further proof we can list what is perhaps the most famous result in tree-level QCD amplitudes calculations [26]: the so-called maximal helicity violating (MHV) amplitudes (aka. Parke-Taylor amplitudes) for n -gluon scattering. One may first organize the full tree-level invariant amplitude in the colour quantum number as

$$M_n(p_i, \lambda_i, a_i) = g^{n-2} \sum_{\sigma \in S_n/Z_n} (T_{\sigma(a_1)} \dots T_{\sigma(a_n)}) A_n \left(\sigma(p_1^{\lambda_1}), \dots, \sigma(p_n^{\lambda_n}) \right). \quad (173)$$

where the sum is over all permutations σ modulo the cyclic ones. The amplitudes A_n are called ‘‘colour-ordered’’. Such amplitudes [27–29] are considerably easier to calculate. First, if all gluons have the same helicity, say $+$, then the amplitude is zero. The same holds if one of them has helicity $-$. With two helicities $-$, we have the MHV amplitude. The stunningly simple expression (a result of millions of Feynman diagrams if n is large enough) for the colour-ordered amplitude reads

$$A_n(1^+, \dots, i^-, \dots, j^-, \dots, n^+) = i \frac{\langle ij \rangle^4}{\langle 12 \rangle \langle 23 \rangle \dots \langle n-1, n \rangle \langle n1 \rangle}. \quad (174)$$

When flipping all $-$ to $+$ and vice versa, all one has to do is replace the angled brackets by squared ones.

Helicity spinor methods are now a standard tool in the computation of QCD scattering amplitudes for the LHC. It is worth mentioning that among the very interesting developments in QCD in recent years has been the realization of recursion relations among these amplitudes [30, 31], after new insights were gained after phrasing them in terms of so-called twistors [32, 33]. Such recursion relations, besides the still very powerful, and often faster [34, 35], earlier ones by Berends and Giele [28] have been important in extending analytical and numerical computational power to high-multiplicity amplitudes.

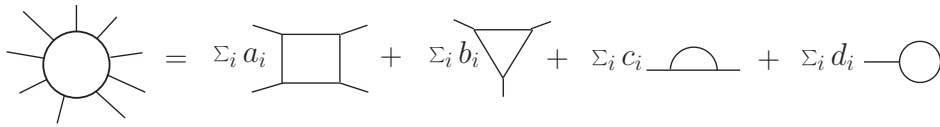


Fig. 19: Expansion of n -leg one-loop amplitude in sum of tadpoles, bubbles, triangles and boxes.

4.2 The NLO revolution

I will here briefly touch upon recent ideas that have spurred what is sometimes referred to as the NLO revolution. An extensive and clear review by some of the instigators is Ref. [36]. For many years the bottleneck in computing NLO cross sections for many external lines were the one-loop diagrams for the virtual part of the cross section. They become increasingly hard to calculate when the number of external lines grows from 4 to 5, 6 etc. Because of similar arguments just mentioned for the case of high-multiplicity tree-level amplitudes one can restrict oneself to a smaller set of diagrams having a particular colour order. The objects to compute have, besides the denominator factors due to the propagators in the loop, a numerator containing dot products among external momenta, polarization vectors, and the loop momentum. Hence, the integral over the loop momentum has possibly a number of loop momenta in the numerator, with open Lorentz- indices.

Such tensor integrals can be reduced to scalar integrals in a well-defined procedure [37]. New stable and efficient reduction techniques for tensor integrals have been proposed in Refs. [38, 39], and have found much use.

One may also express external vectors in terms of a basis set of four. In this procedure also denominators are cancelled, reducing the n -point function to lower-point ones. This leads to an expansion of the amplitude in terms of scalar functions down from n -point ones. Furthermore, up to (here irrelevant) $\mathcal{O}(\epsilon)$ terms, five- and higher point functions can be expressed in terms of four-point functions and lower [40–42]. The price to pay is that for these lower point functions the external momenta are not subsets but rather combinations of the original, massless external momenta. These combinations then are not massless. The upshot is that one has, schematically

$$A_n^{\text{one-loop}} = \sum_{j \in B} c_j \mathcal{I}_j \quad (175)$$

where B is a basis set that consists of a certain set of box-, triangle and bubble integrals with or without massive external legs [43], and the c_j are rational functions of dot products of external momenta and polarization vectors, see Fig. 19. With a generic representation (175) in hand, the task of calculating $A_n^{\text{one-loop}}$ is then mapped to the task of find the coefficients c_j .

For this one may use unitarity methods [44]. In Eq. (175) the elements of the basis set on the *right hand side* may have branchcuts in the invariants on which the logarithms and dilogarithms in the \mathcal{I}_j depend. For instance, a particular integral may have terms of the type $\ln(-s_{ij}/\mu^2)$, with $s_{ij} = p_{ij}^2 = (p_i + p_j)^2 = 2p_i \cdot p_j$, which clearly has a branchcut in the s_{ij} variable.

On the other hand, one can also examine a particular discontinuity across a particular branch cut for a particular invariant, or channel, for *the left-hand side* in Eq. (175), which is done by cutting the amplitude and replacing cut propagators in the loop by delta functions.

$$\frac{1}{p^2 + i\epsilon} \rightarrow -i2\pi \delta(p^2) \quad (176)$$

This amounts to taking the imaginary part. From the comparison of both sides the coefficients c_j can then be determined. Essentially, one thus determines the function $A_n^{\text{one-loop}}$ from its poles and cuts. This

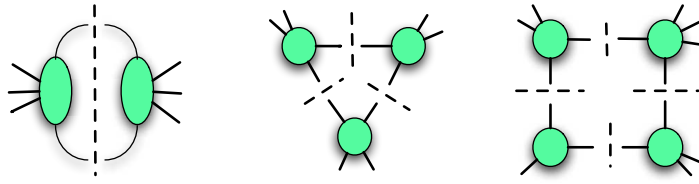


Fig. 20: Generalized unitarity

is vastly more efficient than computing every term fully by itself, and is the key insight that spurred the NLO revolution.

However, there are important subtleties. Using four-dimensional momenta in the cuts leaves an ambiguity in the form of a rational function. Using a $n = 4 + \epsilon$ version of the unitary method [45, 46] avoids this, but this is somewhat more cumbersome to use. A number of other methods have been devised to fix this ambiguity, such as using recursion relations [30, 31], or using D -dimensional unitarity [47, 48]. Particularly fruitful is the use of complex kinematics, which allows non-vanishing, non-trivial three-point amplitudes. This allows taking multiple cuts of a box integral, such as in Fig. 20, which goes under the name “generalized unitarity”. By so doing, one may determine the coefficients c_j purely algebraically [49], since the four delta-functions fix the loop momentum.

An effective way of solving Eq. (175) was proposed in Ref. [50], and is known as the OPP method. Writing the equivalent of Eq. (175) at the *integrand* level, the coefficients of the box etc integral can then be extracted by choosing different values of the loop momentum, and perform the inversion numerically.

Furthermore, numerical [51, 52] and semi-numerical [53] techniques for loop integrals have progressed to the level where much work is taken care of for the user through programs like Blackhat [54], Cuttools [55], or Rocket [56] and MCFM [57]. The level of automation, including the matching to parton showers, has now been stepped up tremendously, with the POWHEG Box [58] and aMC@NLO-MadGraph5 [59] framework. They have brought NLO calculations now to the general user.

As this snapshot of the NLO revolution suggests, the area of NLO calculations was a very lively marketplace of ideas and methods. Although it is still a bustling place, attention is now shifting to exporting the revolution to NNLO.

4.3 Aspects of NNLO

Here I will not say much, as this falls out of the scope of the lectures. Many of the conceptual issues in earlier sections play a role here as well. The accounting of singularities in a flexible way is much harder at this order. An equation as (175) does not yet fully exist for this order, though impressive progress is being made [60]. Nevertheless, results were obtained first already many years ago for DIS [61], Drell-Yan [62] and some time later for Higgs production [63–65]. Recently the latter was even computed to NNNLO using powerful and clever methods involving threshold expansions [66].

Essential for any NNLO calculation for hadron colliders are the NNLO (3-loop) Altarelli-Parisi splitting functions. These were calculated some time ago [9, 10] thanks also to the powers of the computer algebra program FORM [67, 68].

For top quark pair production [69] the first full two-to-two QCD process calculated to NNLO was completed recently (more about this below). Many other results are now appearing (see e.g. [70] for NNLO results on jet cross sections), the review of which would take us too far afield, and would anyway be out of date in very short order.

This concludes our discussions of finite order QCD methods and results. Let us now turn to aspects of QCD resummation, and all-order results.

5 All orders

“Resummation” is shorthand for all-order summation of classes of potentially large terms in quantum field perturbation theory. To review status and progress in a field defined so generally is an impossibly wide scope, and I will restrict myself to certain types in QCD, related of course to observables at high-energy hadron colliders.

Let us first form an impression of what resummation is and what it does. Let $d\sigma$ be a (differential) cross section with the schematic perturbative expansion

$$d\sigma = 1 + \alpha_s(L^2 + L + 1) + \alpha_s^2(L^4 + L^3 + L^2 + L + 1) + \dots \quad (177)$$

where α_s is the coupling, also serving as expansion parameter, L is some logarithm that is potentially large. In our discussion we focus on gauge theories, and on the case with at most two extra powers of L per order, as Eq. (177) illustrates. An extra order corresponds to an extra emission of a gauge boson, the two (“Sudakov”) logs resulting from the situation where the emission is simultaneously soft and collinear to the parent particle direction.

Denoting $L = \ln A$, we can next ask what A is. In fact, A will in general depend on the cross section at hand. For example, for a thrust (T) distribution $A = 1 - T$, while for $d\sigma(p\bar{p} \rightarrow Z + X)/dp_T^Z$ $A = M_Z/p_T^Z$. It should be pointed out already here that A is not *necessarily* constructed out of measured variables but can also be a function of unobservable partonic momenta that are to be integrated over. E.g. for inclusive heavy quark production A could be $1 - 4m^2/(x_1x_2S)$ in hadron collisions with energy \sqrt{S} , where x_1, x_2 are partonic momentum fractions. When L is numerically large so that even for small α_s , the convergent behaviour of the series is endangered, resummation of the problematic terms into an analytic form might provide a remedy, and thereby extend the theory’s predictive power to the range of large L . In general the resummed form of $d\sigma$ may be written schematically as

$$d\sigma_{res} = C(\alpha_s) \exp [Lg_1(\alpha_s L) + g_2(\alpha_s L) + \alpha_s g_3(\alpha_s L) + \dots] + R(\alpha_s) \quad (178)$$

where $g_{1,2,\dots}$ are computable functions. The series $C(\alpha_s)$ multiplies the exponential, and $R(\alpha_s)$ denotes the remainder.

The key aspect of resummation is finding the functions g_i . With only g_1 one has leading logarithmic resummation (LL), with also g_2 NLL etc. For NNLL resummation the matching function C must also be known to next order in α_s .

5.1 Resummation basics, eikonal approximation, webs

Well-developed arguments exist for the exponentation properties of the Drell-Yan cross section near threshold [71, 72]. Some are based on identifying further evolutions equations [71, 73] based on refactorizations of the cross section into different regions only sensitive to either collinear, soft or hard corrections. This has been made into a formidable systematic programme based on effective field theory [74–77].

The connection between refactorization and resummation is already illustrated by perturbative renormalization, in which the general relation of unrenormalized and renormalized Green functions of fields ϕ_i carrying momenta p_i is

$$G_{\text{un}}(p_i, M, g_0) = \prod_i Z_i^{1/2}(\mu/M, g(\mu)) G_{\text{ren}}(p_i, \mu, g(\mu)). \quad (179)$$

M is an ultraviolet cutoff, and $g(\mu)$ and g_0 are the renormalized and bare couplings respectively. The independence of G_{un} from μ and G_{ren} from M may be used to derive renormalization group equations,

$$\mu \frac{d \ln G_{\text{ren}}}{d\mu} = - \sum_i \gamma_i(g(\mu)), \quad (180)$$

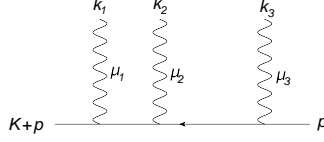


Fig. 21: Soft photon emission from an energetic line

in which the anomalous dimensions $\gamma_i = (1/2)(\mu d/d\mu) \ln Z_i$ appear as constants in the separation of variables, free of explicit dependence on either μ or M . The solution to (180)

$$G_{\text{ren}}(p_i, 1, g(M)) = G_{\text{ren}}(p_i, M/\mu_0, g(\mu_0)) \exp \left[- \sum_i \int_{\mu_0}^M \frac{d\mu}{\mu} \gamma_i(g(\mu)) \right], \quad (181)$$

is clearly an exponential. While in this example the factorization involves separation of UV modes from finite energy ones, for the resummation we discuss in this section one (re)factorizes collinear modes from soft-, anticollinear and hard modes. In a manner similar to this example differential equations may be set up whose solution, in terms of appropriate exponentials of (double) integrals over anomalous dimensions, is the resummed cross section [73].

To see the appearance of exponentials in a different way we can observe that in the refactorization approach the soft or eikonal part of the observable is isolated in a well-defined way. One may then use the property that moments of the eikonal DY cross section exponentiate at the level of integrands [72, 78–80], with exponents consisting of so-called *webs*. These are selections of cut diagrams under criteria defined by graphical topology (irreducibility under cuts of the eikonal lines) and with possibly modified colour weights. Each web is a cut diagram, and can be integrated over the momentum k that it contributes to the final state.

To see how webs work, let us first consider the abelian case¹⁰. Webs are phrased in terms of eikonal Feynman rules. In order to derive these one may consider a single hard massless external line of final on-shell momentum p , originating from some unspecified hard interaction described by $\mathcal{M}_0(p)$. The hard line may emit a number n of soft photons with momenta k_i , as depicted in Fig. 21, where k_1 is emitted closest to the hard interaction. We shall take the emitting particle to be a scalar (the argument for fermions is very similar). For this case the hard interaction is dressed according to

$$\mathcal{M}^{\mu_1 \dots \mu_n}(p, k_i) = \mathcal{M}_0(p) \frac{1}{(p + K_1)^2} (2p + K_1 + K_2)^{\mu_1} \dots \frac{1}{(p + K_n)^2} (2p + K_n)^{\mu_n}, \quad (182)$$

where we have introduced the partial momentum sums $K_i = \sum_{m=i}^n k_m$.

The eikonal approximation in this case can simply be defined as the leading-power contribution to the amplitude when the photon momenta $k_i^{\mu_i} \rightarrow 0$, $\forall i$, in both numerator and denominator. In this limit, eq. (182) becomes

$$\mathcal{M}^{\mu_1 \dots \mu_n}(p, k_i) = \mathcal{M}_0(p) \frac{p^{\mu_1} \dots p^{\mu_n}}{(p \cdot K_1) \dots (p \cdot K_n)}. \quad (183)$$

The eikonal factor is insensitive to the spin of the emitting particles. One may also notice that the eikonal factor does not depend on the energy of the emitter, since it is invariant under rescalings of the hard momentum p^μ : at leading power in the soft momenta, one is effectively neglecting the recoil of the hard particle against soft radiation.

The eikonal factor can be further simplified by employing Bose symmetry. Indeed for the physical quantity depending on the amplitude $\mathcal{M}^{\mu_1 \dots \mu_n}(p, k_i)$, one must sum over all diagrams corresponding to

¹⁰This text is derived from section 2 in [81].

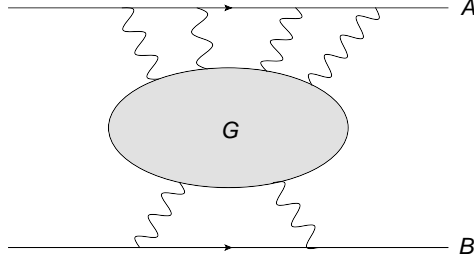


Fig. 22: A process involving two eikonal lines A and B, interacting through the exchange of soft gluons forming diagram G.

permutations of the emitted photons along the hard line. Having done this, the eikonal factor multiplying $\mathcal{M}_0(p)$ on the *r.h.s.* of (183) will be replaced by the symmetrized expression

$$E^{\mu_1 \dots \mu_n}(p, k_i) = \frac{1}{n!} p^{\mu_1} \dots p^{\mu_n} \sum_{\pi} \frac{1}{p \cdot k_{\pi_1}} \frac{1}{p \cdot (k_{\pi_1} + k_{\pi_2})} \dots \frac{1}{p \cdot (k_{\pi_1} + \dots + k_{\pi_n})}, \quad (184)$$

where the sum is over all permutations of the photon momenta, and k_{π_i} is the i^{th} momentum in a given permutation. There are $n!$ permutations, and each gives the same contribution to any physical observable. This becomes manifest using the *eikonal identity*

$$\sum_{\pi} \frac{1}{p \cdot k_{\pi_1}} \frac{1}{p \cdot (k_{\pi_1} + k_{\pi_2})} \dots \frac{1}{p \cdot (k_{\pi_1} + \dots + k_{\pi_n})} = \prod_i \frac{1}{p \cdot k_i}. \quad (185)$$

Using (185), the eikonal factor $E^{\mu_1 \dots \mu_n}(p, k_i)$ arising from n soft emissions on an external hard line becomes simply

$$E^{\mu_1 \dots \mu_n}(p, k_i) = \prod_i \frac{p^{\mu_i}}{p \cdot k_i}, \quad (186)$$

which is manifestly Bose symmetric and invariant under rescalings of the momenta $\{p_i\}$. In practice, each eikonal emission can then be expressed by the effective Feynman rule

$$\begin{array}{c} k \\ \text{wavy line} \\ \text{---} p \end{array} = \frac{p^\mu}{p \cdot k} \quad (187)$$

These Feynman rules can be obtained by replacing the hard external line with a Wilson line along the classical trajectory of the charged particle. In abelian quantum field theories this is given by the expression

$$\Phi_\beta(0, \infty) = \exp \left[ie \int_0^\infty d\lambda \beta \cdot A(\lambda\beta) \right], \quad (188)$$

where β is the dimensionless four-velocity corresponding to the momentum p . (For non-abelian gauge theory the gauge field is a matrix $A_\mu = A_\mu^a T_a$ with T_a matrices that represent the generators of the group. Because the exponent is an integral over a matrix-valued function, the exponential is a path-ordered expression.) This expresses the fact that soft emissions affect the hard particle only by dressing it with a gauge phase. Having constructed the effective Feynman rules, one may proceed to demonstrate the exponentiation of soft photon corrections as follows. As an example, we consider graphs of the form shown in Fig. 22, at a fixed order in the perturbative expansion. Fig. 22 consists of two eikonal lines, labelled A and B, each of which emits a number of soft photons. One may envisage lines A and B

as emerging from a hard interaction, and one may consider the graph G either as a contribution to an amplitude, or to a squared amplitude (in which case some of the propagators in G will be cut).

Diagram G can be taken as consisting only of soft photons and fermion loops. Photons originating from one of the two eikonal lines must land on the other one, or on a fermion loop inside G . Indeed, a photon cannot land on the same eikonal line, as in that case the diagram is proportional to $p^\mu p_\mu = 0$.

Using eikonal Feynman rules, one finds that graphs of the form of Fig. 22 contribute to the corresponding (squared) amplitude a factor

$$\mathcal{F}_{AB} = \sum_G \left[\prod_i \frac{p_A^{\mu_i}}{p_A \cdot k_i} \right] \left[\prod_j \frac{p_B^{\nu_j}}{p_B \cdot l_j} \right] G_{\mu_1 \dots \mu_n; \nu_1 \dots \nu_m}(k_i, l_j), \quad (189)$$

where k_i, l_j are the momenta of the photons emitted from lines A and B respectively, with $i = 1, \dots, n$ and $j = 1, \dots, m$.

Given that we have already summed over permutations in order to obtain the eikonal Feynman rules, each diagram G can be uniquely specified by the set of connected subdiagrams it contains, as indicated schematically in Fig. 23, where each possible connected subdiagram $G_c^{(i)}$ occurs N_i times. According to the standard rules of perturbation theory, diagram G has a symmetry factor corresponding to the number of permutations of internal lines which leave the diagram invariant. This symmetry factor is given by

$$S_G = \prod_i S_i^{N_i} (N_i)!, \quad (190)$$

where S_i is the symmetry factor associated with each connected subdiagram $G_c^{(i)}$, and the factorials account for permutations of identical connected subdiagrams, which must be divided out. Contracting Lorentz indices as in (189), the eikonal factor \mathcal{F}_{AB} may be written as

$$\mathcal{F}_{AB} = \sum_{\{N_i\}} \prod_i \frac{1}{N_i!} \left[\mathcal{F}_c^{(i)} \right]^{N_i}, \quad (191)$$

where

$$\mathcal{F}_c^{(i)} = \frac{1}{S_i} \left(\prod_q \frac{p_A^{\mu_q}}{p_A \cdot k_q} \right) \left(\prod_r \frac{p_B^{\nu_r}}{p_B \cdot l_r} \right) G_{\mu_1 \dots \mu_{n_q}; \nu_1 \dots \nu_{m_r}}^{(i)}(k_q, l_r), \quad (192)$$

is the expression for each connected subdiagram, including the appropriate symmetry factor. Recognising (191) as an exponential series, it follows that

$$\mathcal{F}_{AB} = \exp \left[\sum_i \mathcal{F}_c^{(i)} \right]. \quad (193)$$

We conclude that soft photon corrections exponentiate in the eikonal approximation, and the exponent is given by the sum of all connected subdiagrams. Having seen the abelian case, the non-abelian case for the eikonal cross section is not all that much more difficult, though we shall not treat it here.

Following arguments similar to that for the abelian case [79] [78, 80, 82–84] one may in fact arrive at the result that the eikonal cross section is a sum over eikonal diagrams D

$$\sigma^{(\text{eik})} = \exp \left[\sum_W \sum_{D, D'} \mathcal{F}(D) R_{DD'}^{(W)} C(D') \right], \quad (194)$$

where a mixing matrix R connects the momentum space parts of the diagrams $\mathcal{F}(D)$ and their colour factors $C(D)$ in an interesting way. A very recent, pedagogical review of this and other aspects of webs can be found in [85].

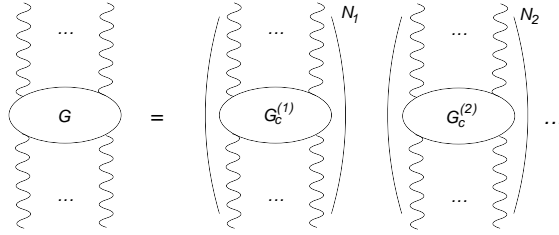


Fig. 23: Decomposition of a soft photon graph into connected subdiagrams $G_c^{(i)}$, each of which occurs N_i times.

The functions g_i that constitute the resummation are usually not only defined by the eikonal cross section. Hard collinear modes in the higher-order corrections can be resummed in different ways, through so-called jet functions. These are in fact also universal, so that by now constructing a resummed cross section is often a matter of putting the right set of all-order functions together. Some automation of this has already been undertaken [86, 87] and is at present being worked on further by various groups.

5.2 Some applications in threshold resummation: heavy quark production, Higgs production

The very general arguments in the previous section can be applied to transverse momentum resummation and threshold resummation. Here we focus on the latter. An illuminating study of the effects of threshold resummation was given in Ref. [88]. One can represent the partonic resummed cross section in moment space as

$$\sigma_{DY}(N, Q^2) = H(Q) \exp[G_{DY}(N, Q)] \quad (195)$$

$$G_{DY} = 2 \ln N g_1(2\lambda) + g_2(2\lambda) + \alpha_s g_3(2\lambda) + \dots \quad (196)$$

$$\lambda = \beta_0 \alpha_s \ln N, \quad (197)$$

which was already more schematically given in (178), and where

$$g_1(\lambda) = \frac{C_F}{\beta_0 \lambda} [\lambda + (1 - \lambda) \ln(1 - \lambda)]. \quad (198)$$

In Fig. 24 [88] convergence properties for both the exponent and the resummed cross section are shown (for toy PDF's) when increasing the logarithmic accuracy of the exponent, and of the hadronic K factor. One observes good convergence as the logarithmic accuracy of the resummation is increased. For the inverse Mellin transform, required to compute the hadronic cross section in momentum space, one may use the so-called minimal prescription [89].

Very similar to Drell-Yan is Higgs production, in the large top mass limit where there is essentially a pointlike gluon-gluon-Higgs coupling. A recent N³LL threshold resummed result [90] is shown in Fig. 25.

We conclude this section with the already mentioned NNLO top quark cross section results, matched to a NNLL threshold resummed calculation for this observable [91]. For the resummed part an added complication is the accounting for colour, as all four external particles are coloured. This issue was solved in Refs. [73, 92, 93], we shall not go into the technical aspects of this. The result of the very impressive, and important calculation [69] is shown in Fig. 26

6 Conclusions

In these lectures I have discussed many aspects of QCD, from the conceptual to the practical, that are relevant for understanding and appreciating its role in the physics of particle colliders. These aspects are often quite technical in nature, and no doubt I have done poor justice to them in the limited space

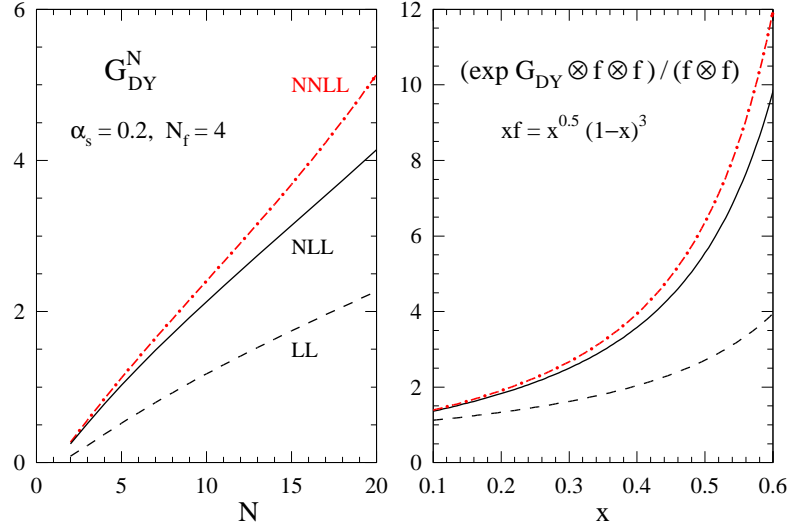


Fig. 24: Convergence behavior of Drell-Yan partonic and hadronic cross section [88]

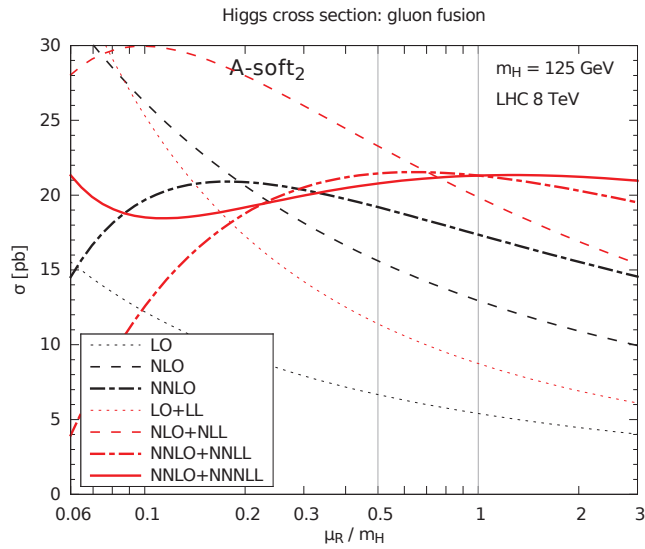


Fig. 25: A recent result [90] for the N^3LL cross section for Higgs production. One observes the notably less dependence of the result on the renormalization scale μ_R .

available. Nevertheless, some attention must be given to these, in order to assess the strengths and weaknesses of theoretical results. This is of crucial importance when confronting these results with data. With the focus of theory and measurement turning towards precision, having paid this attention should be all the more valuable.

Nevertheless I hope that readers are not blinded by the technicalities, but are able to sharpen their intuition regarding how QCD behaves a bit further. Both technical understanding and intuition will be fruitful in the theory-experiment collaborations, joint workshops etc in which they may find themselves at times, and upon which much of the success of the LHC research programme depends.

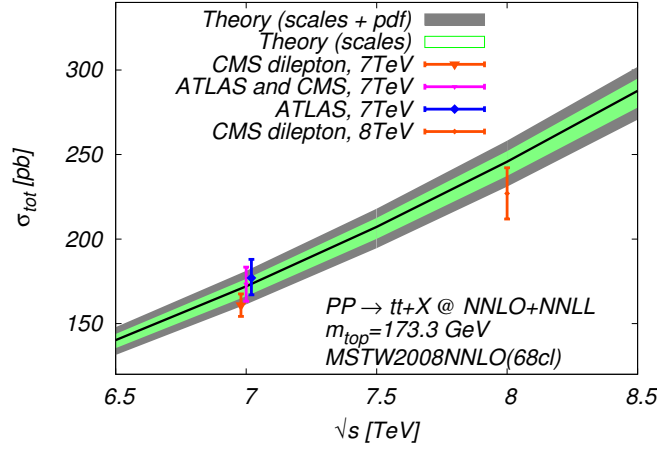


Fig. 26: Theoretical prediction for the LHC as a function of the collider c.m. energy, compared to available measurement from ATLAS and/or CMS at 7 and 8 TeV.

Acknowledgements

I would like to thank the organizers of the CERN Summer School for the excellent environment they created at the school, and for their forbearance towards these notes. I thank the students of the school for their interest and lively participation in the lectures and question sessions.

Appendices

A Conventions and useful formulae

Units

We use here $\hbar = 1$ and $c = 1$. Energy can be converted to inverse distance and vice versa by the relation $1 = 197.3 \text{ MeV fm}$, with 1 fm (“fermi” or “femtometer”) equal to 10^{-15} m , and $c = 2.998 \cdot 10^8 \text{ m/s}$.

Cross sections are expressed in nanobarns (nb), picobarns (pb) etc, where $1 \text{ b} = 10^{-24} \text{ cm}^2$.

The metric tensor we use in this course is

$$\eta^{\mu\nu} = \text{diag}(-1, 1, 1, 1) \quad (\text{A.1})$$

Cross sections and decay rates

The cross section for the scattering of two incoming massless particles with momenta k_1 and k_2 to n particles with momenta $\{p_i\}$ is given by

$$\sigma = \frac{1}{2s} \overline{\sum_{\text{spins}}} \int |\mathcal{M}|^2 dPS(n) \quad (\text{A.2})$$

where the bar indicates initial spin averaging and

$$dPS(n) = \prod_{j=1}^n \frac{d^3 p_j}{(2\pi)^3 2E_j} \times (2\pi)^4 \delta \left(k_1 + k_2 - \sum_i^n p_i \right) \quad (\text{A.3})$$

If there are j identical particles among the n , there is an extra factor $1/j!$. For the case $n = 2$, in the center of momentum frame, and with both outgoing particles having equal mass m

$$dPS(2) = \frac{1}{16\pi} \sqrt{1 - \frac{4m^2}{s}} d\cos\theta, \quad (\text{A.4})$$

where θ is the polar angle of one of the outgoing particles with respect to the collision axis.

The width for the decay of a particle with mass Q and 4-momentum k to n particles with 4-momenta $\{p_i\}$ reads

$$\Gamma = \frac{1}{2Q} \sum_{\text{spins, (colours...)}} \int |\mathcal{M}|^2 dPS(n). \quad (\text{A.5})$$

If there are j identical particles among the n , there is an extra factor $1/j!$. For the case $n = 2$, in the center of momentum frame

$$dPS(2) = \frac{1}{16\pi Q^2} \sqrt{\lambda(Q^2, m_1^2, m_2^2)} d\cos\theta, \quad (\text{A.6})$$

where θ is the polar angle of one of the outgoing particles with respect to some arbitrary axis, and $\lambda(x, y, z) = x^2 + y^2 + z^2 - 2xy - 2xz - 2yz$.

Dirac algebra

Dirac equation in x-space:

$$(\not{\partial} + m)\psi(x) = 0 \quad (\text{A.7})$$

Dirac equation in momentum space for u and v spinors:

$$(i\not{p} + m)u(p, s) = 0, \quad (i\not{p} - m)v(p, s) = 0 \quad (\text{A.8})$$

$$\{\gamma^\mu, \gamma^\nu\} = 2\eta^{\mu\nu} \quad (\text{A.9})$$

where on the right hand side the 4 by 4 unit matrix in spinor space is implied. An often-used identity based on this is

$$\not{p}\not{p} = p^2. \quad (\text{A.10})$$

Other useful relations:

$$\gamma^0 = -i \begin{pmatrix} 1 & 0 \\ 0 & -1 \end{pmatrix}, \quad \vec{\gamma} = -i \begin{pmatrix} 0 & \vec{\sigma} \\ -\vec{\sigma} & 0 \end{pmatrix}, \quad (\text{A.11})$$

$$(\gamma^\mu)^\dagger = \gamma^0 \gamma^\mu \gamma^0, \quad (\text{A.12})$$

$$\gamma_5 = i\gamma_0\gamma_1\gamma_2\gamma_3, \quad (\text{A.13})$$

$$\gamma_5 = \begin{pmatrix} 0 & 1 \\ 1 & 0 \end{pmatrix}, \quad (\text{A.14})$$

$$\{\gamma_5, \gamma^\mu\} = 0, \quad (\text{A.15})$$

$$\gamma^\mu \not{a} \gamma_\mu = -2\not{a}, \quad \gamma^\mu \not{a} \not{b} \gamma_\mu = 4a \cdot b, \quad \gamma^\mu \not{a} \not{b} \not{c} \gamma_\mu = -2\not{a} \not{b} \not{c}, \quad (\text{A.16})$$

$$\begin{aligned} \text{Tr}(\gamma^\mu) &= \text{Tr}(\gamma_5) = 0, & \text{Tr}(\gamma^\mu \gamma^\nu \gamma^\rho) &= 0, \\ \text{Tr}(\gamma_5 \gamma_\mu) &= \text{Tr}(\gamma_5 \gamma_\mu \gamma_\nu) = \text{Tr}(\gamma_5 \gamma_\mu \gamma_\nu \gamma_\rho) = 0, \end{aligned} \quad (\text{A.17})$$

$$\text{Tr}(\gamma^\mu \gamma^\nu) = 4\eta^{\mu\nu}, \quad \text{Tr}(\gamma^\mu \gamma^\nu \gamma^\rho \gamma^\sigma) = 4(\eta^{\mu\nu} \eta^{\rho\sigma} - \eta^{\mu\rho} \eta^{\nu\sigma} + \eta^{\mu\sigma} \eta^{\nu\rho}), \quad (\text{A.18})$$

$$\text{Tr}(\gamma_\mu \gamma_\nu \gamma_\rho \gamma_\sigma \gamma_5) = -4i\epsilon_{\mu\nu\rho\sigma}, \quad \epsilon_{0123} = +1. \quad (\text{A.19})$$

Conjugate spinor:

$$\bar{\psi} = i\psi^\dagger \gamma^0. \quad (\text{A.20})$$

With this definition the term

$$\bar{\psi} \psi \quad (\text{A.21})$$

is hermitean, since γ^0 is anti-hermitean. The chiral (left- and righthanded) projections of a fermion are defined by

$$\begin{aligned}\psi_L &= \left(\frac{1+\gamma_5}{2}\right)\psi, \\ \psi_R &= \left(\frac{1-\gamma_5}{2}\right)\psi.\end{aligned}\tag{A.22}$$

A parity transform on a spinor is defined by

$$P : \psi(x) \rightarrow \gamma_0 \psi(\tilde{x}),\tag{A.23}$$

with $\tilde{x} = (x^0, -\vec{x})$. Complex-conjugation of general spinor-trace:

$$(\bar{u}(p)\gamma_{\mu_1}\cdots\gamma_{\mu_n}u(p'))^* = (-)^n (\bar{u}(p')\gamma_{\mu_n}\cdots\gamma_{\mu_1}u(p)),\tag{A.24}$$

$$(\bar{u}(p)\gamma_{\mu_1}\cdots\gamma_{\mu_n}\gamma_5u(p'))^* = -(-)^n (\bar{u}(p')\gamma_5\gamma_{\mu_n}\cdots\gamma_{\mu_1}u(p)).\tag{A.25}$$

Unitary groups and their Lie algebras

The U(1) Lie algebra has only 1 generator t , which we choose hermitean. Acting on a d-dimensional vector t may be represented as the d-dimensional unit matrix. The group elements are then

$$\exp(i\alpha t).\tag{A.26}$$

The SU(2) Lie algebra has 3 generators t_i , $i = 1, 2, 3$. If we choose the t_i hermitean, then in the fundamental representation $t_i^{(F)} = \sigma_i/2$, with σ_i the Pauli matrices

$$\sigma_1 = \begin{pmatrix} 0 & 1 \\ 1 & 0 \end{pmatrix} \quad \sigma_2 = \begin{pmatrix} 0 & -i \\ i & 0 \end{pmatrix} \quad \sigma_3 = \begin{pmatrix} 1 & 0 \\ 0 & -1 \end{pmatrix}.\tag{A.27}$$

The group elements are

$$U = \exp(i\xi^i t_i).\tag{A.28}$$

Note that for the fundamental representation

$$\sigma_2 U \sigma_2 = U^* = (U^\dagger)^T.\tag{A.29}$$

Note that the SU(2) Lie-algebra is isomorphic to the SO(3) Lie-algebra, whose generators $t_i = -iS_i$ read, in the fundamental representation:

$$S_1 = \begin{pmatrix} 0 & 0 & 0 \\ 0 & 0 & 1 \\ 0 & -1 & 0 \end{pmatrix} \quad S_2 = \begin{pmatrix} 0 & 0 & -1 \\ 0 & 0 & 0 \\ 1 & 0 & 0 \end{pmatrix} \quad S_3 = \begin{pmatrix} 0 & 1 & 0 \\ -1 & 0 & 0 \\ 0 & 0 & 0 \end{pmatrix}.\tag{A.30}$$

The SU(3) Lie algebra has 8 generators t_i , $i = 1, \dots, 8$, which are not needed explicitly. Lie algebra generators in general obey the commutation relations

$$[t_i, t_j] = i f_{ijk} t_k,\tag{A.31}$$

with the f_{ijk} the structure constants for the given group. The kj matrix element of the generator $t_i^{(A)}$ in the adjoint representation is defined as

$$\left[t_i^{(A)}\right]_{kj} = i f_{ijk}.\tag{A.32}$$

Note that we can always choose anti-hermitean generators t' by multiplying the hermitean versions t by i . In that case the group elements for $SU(2)$ e.g. are

$$\exp(\xi^i t'_i) . \quad (\text{A.33})$$

Representations of $SU(2)$, etc. groups are often indicated by $\underline{2}, \dots$ indicating the size of the matrices of that representation. Trivial or singlet representation are then indicated with $\underline{1}$.

Some other group theory factors (the so-called Casimir factors):

$$\begin{aligned} SU(2) : \quad C_A &= 2, \quad C_F = \frac{3}{4}, \\ SU(3) : \quad C_A &= 3, \quad C_F = \frac{4}{3}. \end{aligned}$$

For the fundamental representation of $SU(N)$ we have

$$\text{Tr} [t_i^{(F)} t_j^{(F)}] = \frac{1}{2} \delta_{ij} . \quad (\text{A.34})$$

Standard Model quantities

The amount of electric charge (in units of e) Q , the hypercharge Y and the third component of weak isospin t_3 are related by

$$Y = 2(Q - t_3) . \quad (\text{A.35})$$

In the Standard Model the generator of the $U(1)$ of hypercharge is conventionally written as

$$\frac{1}{2} Y , \quad (\text{A.36})$$

and is then represented on d -dimensional vectors as $1/2$ times the hypercharge eigenvalue times the unit matrix.

The gauge couplings associated with the $SU_{J_W}(2)$ and $U_Y(1)$ gauge groups are traditionally denoted g and g' respectively. In terms of these couplings the unit of electric charge is

$$e = \frac{g g'}{\sqrt{g^2 + g'^2}} = g \sin \theta_W = g' \cos \theta_W , \quad (\text{A.37})$$

with $\sin^2 \theta_W \simeq 0.226$.

The gauge fields are mixed as follows:

$$B_\mu = \cos \theta_W A_\mu - \sin \theta_W Z_\mu, \quad W_\mu^3 = \cos \theta_W Z_\mu + \sin \theta_W A_\mu, \quad (\text{A.38})$$

$$W_\mu^1 - i W_\mu^2 = \sqrt{2} W_\mu^+, \quad W_\mu^1 + i W_\mu^2 = \sqrt{2} W_\mu^- . \quad (\text{A.39})$$

The Fermi constant is defined by

$$G_F = \frac{g^2}{4\sqrt{2}m_W^2} = \frac{1}{\sqrt{2}v^2} \simeq 1.2 \times 10^{-5} \text{ GeV}^2 . \quad (\text{A.40})$$

Vector boson masses in GeV:

$$m_Z = \frac{gv}{2 \cos \theta_W} = 91.1876 \pm 0.0021, \quad m_W = \frac{gv}{2} = 80.385 \pm 0.015 . \quad (\text{A.41})$$

The photon and gluon are massless.

Heavy quark masses in GeV:

$$m_c = 1.5, \quad m_b = 5, \quad m_t = 175. \quad (\text{A.42})$$

u, d, s are massless.

Lepton masses in GeV:

$$m_\tau = 1.7, \quad m_\mu = 0.105, \quad m_e = 0.0005. \quad (\text{A.43})$$

QCD scale in GeV:

$$\Lambda_{QCD} \simeq 0.2. \quad (\text{A.44})$$

Assorted Feynman rules

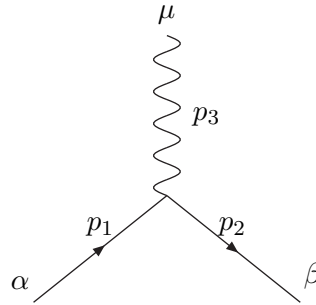
All momenta in vertex Feynman rules are incoming here.

– Fermion propagator

$$\alpha \xrightarrow{\quad \rightarrow p \quad} \beta$$

$$\frac{1}{i(2\pi)^4} \frac{(-i\not{p} + m)_{\beta\alpha}}{p^2 + m^2 - i\epsilon} \quad (\text{A.45})$$

– Electron-electron photon vertex



$$i(2\pi)^4 \delta(p_1 + p_2 + p_3) (-ie) \gamma_{\beta\alpha}^\mu \quad (\text{A.46})$$

where the three momentum vectors (not drawn) are pointing to the vertex.

- Outgoing fermion: $\bar{u}(p, s)$ Row spinor
- Outgoing anti-fermion: $v(p, s)$ Column spinor
- Incoming fermion: $u(p, s)$ Column spinor
- Incoming antifermion: $\bar{v}(p, s)$ Row spinor
- Outgoing vector boson: $\epsilon_\mu^*(k, \lambda)$
- Incoming vector boson: $\epsilon_\mu(k, \lambda)$

In Feynman diagrams, always start where the charge vector top of the fermion lines *ends* (i.e. start with a row spinor), and work your way back against the charge flow.

Integrate over internal momenta: $\int d^4 k_i$

Completeness relations for spin sums over polarization spinors and polarization vectors, associated with external particles

$$\sum_s u_\alpha(p, s) \bar{u}_\beta(p, s) = (-i\not{p} + m)_{\alpha\beta}, \quad (\text{A.47})$$

$$\sum_s v_\alpha(p, s) \bar{v}_\beta(p, s) = (-i\not{p} - m)_{\alpha\beta}, \quad (\text{A.48})$$

with m the fermion mass, α, β are spinor indices.

For photons the sum over the two physical polarizations gives

$$\sum_\lambda \epsilon^\mu(k, \lambda) \epsilon^{*\nu}(k, \lambda) = \eta^{\mu\nu} - \frac{k^\mu \bar{k}^\nu + k^\nu \bar{k}^\mu}{k \cdot \bar{k}}, \quad (\text{A.49})$$

where the sum is over the physical spin only, and we define

$$k^\mu = (k^0, \vec{k}), \quad \bar{k}^\mu = (-k^0, \vec{k}). \quad (\text{A.50})$$

The photon propagator is (κ is the gauge parameter here)

$$\Delta_{\mu\nu}(k) = \frac{1}{i(2\pi)^4} \frac{1}{k^2 - i\epsilon} \left(\eta_{\mu\nu} - \left(1 - \frac{1}{\kappa^2}\right) \frac{k_\mu k_\nu}{k^2} \right). \quad (\text{A.51})$$

The scalar field propagator is simply

$$\Delta(p) = \frac{1}{i(2\pi)^4} \frac{1}{p^2 + m^2 - i\epsilon}. \quad (\text{A.52})$$

For massive vector bosons the sum over the three physical polarizations gives

$$\sum_\lambda \epsilon^\mu(k, \lambda) \epsilon^{*\nu}(k, \lambda) = \eta^{\mu\nu} + \frac{k^\mu k^\nu}{M^2}. \quad (\text{A.53})$$

Loop integrals

$$\frac{1}{A_1 A_2} = \int_0^1 dx_1 \int_0^1 dx_2 \frac{\delta(1 - x_1 - x_2)}{[x_1 A_1 + x_2 A_2]^2}. \quad (\text{A.54})$$

The result for the integral

$$I(n, \alpha) = \int d^n q \frac{1}{(q^2 + m^2 - i\epsilon)^\alpha} \quad (\text{A.55})$$

is

$$I(n, \alpha) = i\pi^{n/2} \frac{\Gamma(\alpha - (n/2))}{\Gamma(\alpha)} (m^2)^{(n/2) - \alpha}. \quad (\text{A.56})$$

The Euler gamma function $\Gamma(z)$ has the following relevant properties:

$$\Gamma(z+1) = z\Gamma(z), \quad \Gamma(1) = 1, \quad (\text{A.57})$$

$$\ln \Gamma(1+z) \simeq -z\gamma_E + \mathcal{O}(z^2), \quad \gamma_E = 0.577\dots \quad (\text{A.58})$$

References

- [1] H1 and ZEUS Collaboration, F. D. Aaron *et al.*, “Combined Measurement and QCD Analysis of the Inclusive e^+p Scattering Cross Sections at HERA,” *JHEP* **1001** (2010) 109, 0911.0884.
- [2] J. Callan, C. G. and D. J. Gross, “High-energy electroproduction and the constitution of the electric current,” *Phys. Rev. Lett.* **22** (1969) 156–159.
- [3] R. D. Ball, V. Bertone, S. Carrazza, C. S. Deans, L. Del Debbio, *et al.*, “Parton distributions with LHC data,” *Nucl.Phys.* **B867** (2013) 244–289, 1207.1303.
- [4] “The durham hepdata project,”.
- [5] B. De Wit and J. Smith, *Field Theory in Particle Physics Volume 1*. North-Holland, Amsterdam, Netherlands, 1986.
- [6] P. A. Baikov, K. G. Chetyrkin, and J. H. Kühn, “Five-Loop Running of the QCD coupling constant,” 1606.08659.
- [7] S. Forte and G. Watt, “Progress in the Determination of the Partonic Structure of the Proton,” *Ann.Rev.Nucl.Part.Sci.* **63** (2013) 291–328, 1301.6754.
- [8] J. C. Collins, D. E. Soper, and G. Sterman, “Factorization of hard processes in qcd,”. in *Perturbative Quantum Chromodynamics*, A.H. Mueller ed., World Scientific, Singapore, 1989.
- [9] S. Moch, J. A. M. Vermaseren, and A. Vogt, “The three-loop splitting functions in qcd: The non-singlet case,” *Nucl. Phys.* **B688** (2004) 101–134, hep-ph/0403192.
- [10] A. Vogt, S. Moch, and J. A. M. Vermaseren, “The three-loop splitting functions in qcd: The singlet case,” *Nucl. Phys.* **B691** (2004) 129–181, hep-ph/0404111.
- [11] A. D. Martin, W. J. Stirling, R. S. Thorne, and G. Watt, “Parton distributions for the LHC,” *Eur. Phys. J.* **C63** (2009) 189–285, 0901.0002.
- [12] J. Rojo, A. Accardi, R. D. Ball, A. Cooper-Sarkar, A. de Roeck, *et al.*, “The PDF4LHC report on PDFs and LHC data: Results from Run I and preparation for Run II,” 1507.00556.
- [13] K. Fabricius, I. Schmitt, G. Kramer, and G. Schierholz, “Higher order perturbative qcd calculation of jet cross- sections in e^+e^- annihilation,” *Zeit. Phys.* **C11** (1981) 315.
- [14] G. K. J. F. Vermaseren, J. A. M. and S. J. Oldham, “Perturbative QCD calculation of jet cross-sections in e^+e^- annihilation,” *Nucl.Phys.* **B187** (1981) 301.
- [15] Z. Kunszt, “Comment on the $\mathcal{O}(\alpha_s^2)$ corrections to jet production in e^+e^- annihilation,” *Phys. Lett.* **B99** (1981) 429.
- [16] R. K. Ellis, D. A. Ross, and A. E. Terrano, “The perturbative calculation of jet structure in e^+e^- annihilation,” *Nucl. Phys.* **B178** (1981) 421.
- [17] A. Gehrmann-De Ridder, T. Gehrmann, E. W. N. Glover, and G. Heinrich, “NNLO corrections to event shapes in e^+e^- annihilation,” *JHEP* **12** (2007) 094, 0711.4711.
- [18] T. Kinoshita, “Mass singularities of Feynman amplitudes,” *J. Math. Phys.* **3** (1962) 650–677.
- [19] T. D. Lee and M. Nauenberg, “Degenerate Systems and Mass Singularities,” *Phys. Rev.* **133** (1964) B1549–B1562.
- [20] F. Bloch and A. Nordsieck, “Note on the Radiation Field of the electron,” *Phys. Rev.* **52** (1937) 54–59.
- [21] C. K. G. K. J. H. Baikov, P. A. and J. Rittinger, “Adler function, sum rules and Crewther relation of order $\mathcal{O}(\alpha_s^4)$: the singlet case,” *Phys. Lett.* **B714** (2012) 62–65, 1206.1288.
- [22] G. F. Sterman and S. Weinberg, “Jets from quantum chromodynamics,” *Phys. Rev. Lett.* **39** (1977) 1436.
- [23] S. D. Drell and T.-M. Yan, “Partons and their applications at high-energies,” *Annals Phys.* **66** (1971) 578.
- [24] J. R. Forshaw, M. H. Seymour, and A. Siodmok, “On the Breaking of Collinear Factorization in

- QCD,” *JHEP* **11** (2012) 066, 1206.6363.
- [25] S. Catani, D. de Florian, and G. Rodrigo, “Factorization violation in the multiparton collinear limit,” *PoS LL2012* (2012) 035, 1211.7274.
- [26] S. J. Parke and T. R. Taylor, “An amplitude for n gluon scattering,” *Phys. Rev. Lett.* **56** (1986) 2459.
- [27] F. A. Berends, W. T. Giele, and H. Kuijf, “Exact expressions for processes involving a vector boson and up to five partons,” *Nucl. Phys.* **B321** (1989) 39.
- [28] F. A. Berends and W. T. Giele, “Recursive calculations for processes with n gluons,” *Nucl. Phys.* **B306** (1988) 759.
- [29] M. L. Mangano, “The Color Structure of Gluon Emission,” *Nucl. Phys.* **B309** (1988) 461.
- [30] R. Britto, F. Cachazo, and B. Feng, “New recursion relations for tree amplitudes of gluons,” *Nucl. Phys.* **B715** (2005) 499–522, hep-th/0412308.
- [31] R. Britto, F. Cachazo, B. Feng, and E. Witten, “Direct proof of tree-level recursion relation in Yang-Mills theory,” *Phys. Rev. Lett.* **94** (2005) 181602, hep-th/0501052.
- [32] E. Witten, “Perturbative gauge theory as a string theory in twistor space,” *hep-th/0312171* (2003) hep-th/0312171.
- [33] F. Cachazo, P. Svrcek, and E. Witten, “Mhv vertices and tree amplitudes in gauge theory,” *JHEP* **09** (2004) 006, hep-th/0403047.
- [34] C. Duhr, S. Hoche, and F. Maltoni, “Color-dressed recursive relations for multi-parton amplitudes,” *JHEP* **08** (2006) 062, hep-ph/0607057.
- [35] M. Dinsdale, M. Ternick, and S. Weinzierl, “A comparison of efficient methods for the computation of Born gluon amplitudes,” *JHEP* **03** (2006) 056, hep-ph/0602204.
- [36] Z. Bern, L. J. Dixon, and D. A. Kosower, “On-Shell Methods in Perturbative QCD,” *Annals Phys.* **322** (2007) 1587–1634, 0704.2798.
- [37] G. Passarino and M. J. G. Veltman, “One Loop Corrections for e+ e- Annihilation Into mu+ mu- in the Weinberg Model,” *Nucl. Phys.* **B160** (1979) 151.
- [38] A. Denner and S. Dittmaier, “Reduction schemes for one-loop tensor integrals,” *Nucl. Phys.* **B734** (2006) 62–115, hep-ph/0509141.
- [39] T. Binoth, J. P. Guillet, G. Heinrich, E. Pilon, and C. Schubert, “An algebraic / numerical formalism for one-loop multi-leg amplitudes,” *JHEP* **10** (2005) 015, hep-ph/0504267.
- [40] W. L. van Neerven and J. A. M. Vermaseren, “Large loop integrals,” *Phys. Lett.* **B137** (1984) 241.
- [41] Z. Bern, L. J. Dixon, and D. A. Kosower, “Dimensionally regulated one loop integrals,” *Phys. Lett.* **B302** (1993) 299–308, hep-ph/9212308.
- [42] Z. Bern, L. J. Dixon, and D. A. Kosower, “Dimensionally regulated pentagon integrals,” *Nucl. Phys.* **B412** (1994) 751–816, hep-ph/9306240.
- [43] R. K. Ellis and G. Zanderighi, “Scalar one-loop integrals for QCD,” *JHEP* **02** (2008) 002, 0712.1851.
- [44] Z. Bern, L. J. Dixon, D. C. Dunbar, and D. A. Kosower, “One loop n point gauge theory amplitudes, unitarity and collinear limits,” *Nucl. Phys.* **B425** (1994) 217–260, hep-ph/9403226.
- [45] Z. Bern, L. J. Dixon, D. C. Dunbar, and D. A. Kosower, “One-loop self-dual and N = 4 superYang-Mills,” *Phys. Lett.* **B394** (1997) 105–115, hep-th/9611127.
- [46] Z. Bern and A. G. Morgan, “Massive loop amplitudes from unitarity,” *Nucl. Phys.* **B467** (1996) 479–509, hep-ph/9511336.
- [47] C. Anastasiou, R. Britto, B. Feng, Z. Kunszt, and P. Mastrolia, “Unitarity cuts and reduction to master integrals in d dimensions for one-loop amplitudes,” *JHEP* **03** (2007) 111, hep-ph/0612277.
- [48] A. Brandhuber, S. McNamara, B. J. Spence, and G. Travaglini, “Loop amplitudes in pure

- Yang-Mills from generalised unitarity,” *JHEP* **10** (2005) 011, hep-th/0506068.
- [49] R. Britto, F. Cachazo, and B. Feng, “Generalized unitarity and one-loop amplitudes in $N = 4$ super-Yang-Mills,” *Nucl. Phys.* **B725** (2005) 275–305, hep-th/0412103.
- [50] G. Ossola, C. G. Papadopoulos, and R. Pittau, “Reducing full one-loop amplitudes to scalar integrals at the integrand level,” *Nucl. Phys.* **B763** (2007) 147–169, hep-ph/0609007.
- [51] Z. Nagy and D. E. Soper, “Numerical integration of one-loop Feynman diagrams for N -photon amplitudes,” *Phys. Rev.* **D74** (2006) 093006, hep-ph/0610028.
- [52] C. Anastasiou, S. Beerli, and A. Daleo, “Evaluating multi-loop Feynman diagrams with infrared and threshold singularities numerically,” *JHEP* **05** (2007) 071, hep-ph/0703282.
- [53] R. K. Ellis, W. T. Giele, and G. Zanderighi, “Semi-numerical evaluation of one-loop corrections,” *Phys. Rev.* **D73** (2006) 014027, hep-ph/0508308.
- [54] C. F. Berger *et al.*, “One-Loop Calculations with BlackHat,” 0807.3705.
- [55] G. Ossola, C. G. Papadopoulos, and R. Pittau, “CutTools: a program implementing the OPP reduction method to compute one-loop amplitudes,” *JHEP* **03** (2008) 042, 0711.3596.
- [56] W. T. Giele and G. Zanderighi, “On the Numerical Evaluation of One-Loop Amplitudes: the Gluonic Case,” 0805.2152.
- [57] J. M. Campbell and R. K. Ellis, “Radiative corrections to $Z b$ anti- b production,” *Phys. Rev.* **D62** (2000) 114012, hep-ph/0006304.
- [58] S. Alioli, P. Nason, C. Oleari, and E. Re, “A general framework for implementing NLO calculations in shower Monte Carlo programs: the POWHEG BOX,” *JHEP* **06** (2010) 043, 1002.2581.
- [59] J. Alwall, R. Frederix, S. Frixione, V. Hirschi, F. Maltoni, *et al.*, “The automated computation of tree-level and next-to-leading order differential cross sections, and their matching to parton shower simulations,” *JHEP* **1407** (2014) 079, 1405.0301.
- [60] H. Johansson, D. A. Kosower, and K. J. Larsen, “An Overview of Maximal Unitarity at Two Loops,” *PoS LL2012* (2012) 066, 1212.2132.
- [61] E. B. Zijlstra and W. L. van Neerven, “Order α_s^2 qcd corrections to the deep inelastic proton structure functions f_2 and f_L ,” *Nucl. Phys.* **B383** (1992) 525–574.
- [62] R. Hamberg, W. L. van Neerven, and T. Matsuura, “A complete calculation of the order α_s^2 correction to the drell-yan k factor,” *Nucl. Phys.* **B359** (1991) 343–405.
- [63] C. Anastasiou and K. Melnikov, “Higgs boson production at hadron colliders in nnlo qcd,” *Nucl. Phys.* **B646** (2002) 220–256, hep-ph/0207004.
- [64] R. V. Harlander and W. B. Kilgore, “Next-to-next-to-leading order higgs production at hadron colliders,” *Phys. Rev. Lett.* **88** (2002) 201801, hep-ph/0201206.
- [65] V. Ravindran, J. Smith, and W. L. van Neerven, “Two-loop corrections to higgs boson production,” *Nucl. Phys.* **B704** (2005) 332–348, hep-ph/0408315.
- [66] C. Anastasiou, C. Duhr, F. Dulat, F. Herzog, and B. Mistlberger, “Higgs boson gluon-fusion production in N³LO QCD,” 1503.06056.
- [67] J. A. M. Vermaseren, “The FORM project,” *Nucl.Phys.Proc.Suppl.* **183** (2008) 19–24, 0806.4080.
- [68] U. T. V. J. A. M. Kuipers, J. and J. Vollinga, “FORM version 4.0,” *Comput.Phys.Commun.* **184** (2013) 1453–1467, 1203.6543.
- [69] M. Czakon, P. Fiedler, and A. Mitov, “The total top quark pair production cross-section at hadron colliders through $\mathcal{O}(\alpha_s^4)$,” *Phys.Rev.Lett.* **110** (2013) 252004, 1303.6254.
- [70] A. Gehrmann-De Ridder, T. Gehrmann, E. Glover, and J. Pires, “Second order QCD corrections to jet production at hadron colliders: the all-gluon contribution,” *Phys.Rev.Lett.* **110** (2013), no. 16, 162003, 1301.7310.
- [71] G. Sterman, “Summation of large corrections to short distance hadronic cross-sections,” *Nucl.*

- Phys.* **B281** (1987) 310.
- [72] S. Catani and L. Trentadue, “Resummation of the QCD Perturbative Series for Hard Processes,” *Nucl. Phys.* **B327** (1989) 323.
- [73] H. Contopanagos, E. Laenen, and G. Sterman, “Sudakov factorization and resummation,” *Nucl. Phys.* **B484** (1997) 303–330, hep-ph/9604313.
- [74] C. W. Bauer, S. Fleming, D. Pirjol, and I. W. Stewart, “An effective field theory for collinear and soft gluons: Heavy to light decays,” *Phys. Rev.* **D63** (2001) 114020, hep-ph/0011336.
- [75] C. W. Bauer, D. Pirjol, and I. W. Stewart, “Soft-Collinear Factorization in Effective Field Theory,” *Phys. Rev.* **D65** (2002) 054022, hep-ph/0109045.
- [76] M. Beneke, A. P. Chapovsky, M. Diehl, and T. Feldmann, “Soft-collinear effective theory and heavy-to-light currents beyond leading power,” *Nucl. Phys.* **B643** (2002) 431–476, hep-ph/0206152.
- [77] T. Becher, A. Broggio, and A. Ferroglia, “Introduction to Soft-Collinear Effective Theory,” 1410.1892.
- [78] G. Sterman, “Infrared divergences in perturbative qcd. (talk),”. In *Tallahassee 1981, Proceedings, Perturbative Quantum Chromodynamics*, 22-40.
- [79] J. G. M. Gatheral, “Exponentiation of eikonal cross-sections in nonabelian gauge theories,” *Phys. Lett.* **B133** (1983) 90.
- [80] J. Frenkel and J. C. Taylor, “Nonabelian eikonal exponentiation,” *Nucl. Phys.* **B246** (1984) 231.
- [81] E. Laenen, L. Magnea, G. Stavenga, and C. D. White, “Next-to-eikonal corrections to soft gluon radiation: a diagrammatic approach,” *JHEP* **01** (2011) 141, 1010.1860.
- [82] E. Laenen, G. Stavenga, and C. D. White, “Path integral approach to eikonal and next-to-eikonal exponentiation,” 0811.2067.
- [83] E. Gardi, E. Laenen, G. Stavenga, and C. D. White, “Webs in multiparton scattering using the replica trick,” *JHEP* **11** (2010) 155, 1008.0098.
- [84] A. Mitov, G. Sterman, and I. Sung, “Diagrammatic Exponentiation for Products of Wilson Lines,” *Phys. Rev.* **D82** (2010) 096010, 1008.0099.
- [85] C. White, “An Introduction to Webs,” 1507.02167.
- [86] A. Banfi, G. P. Salam, and G. Zanderighi, “Principles of general final-state resummation and automated implementation,” *JHEP* **03** (2005) 073, hep-ph/0407286.
- [87] T. Becher, R. Frederix, M. Neubert, and L. Rothen, “Automated NNLL + NLO resummation for jet-veto cross sections,” *Eur.Phys.J.* **C75** (2015), no. 4, 154, 1412.8408.
- [88] A. Vogt, “Next-to-next-to-leading logarithmic threshold resummation for deep-inelastic scattering and the drell-yan process,” *Phys. Lett.* **B497** (2001) 228–234, hep-ph/0010146.
- [89] S. Catani, M. L. Mangano, P. Nason, and L. Trentadue, “The resummation of soft gluons in hadronic collisions,” *Nucl. Phys.* **B478** (1996) 273–310, hep-ph/9604351.
- [90] M. Bonvini and S. Marzani, “Resummed Higgs cross section at N³LL,” *JHEP* **1409** (2014) 007, 1405.3654.
- [91] M. Czakon, A. Mitov, and G. F. Sterman, “Threshold Resummation for Top-Pair Hadroproduction to Next-to-Next-to-Leading Log,” *Phys.Rev.* **D80** (2009) 074017, 0907.1790.
- [92] N. Kidonakis and G. F. Sterman, “Resummation for QCD hard scattering,” *Nucl. Phys.* **B505** (1997) 321–348, hep-ph/9705234.
- [93] R. Bonciani, S. Catani, M. L. Mangano, and P. Nason, “NLL resummation of the heavy-quark hadroproduction cross-section,” *Nucl. Phys.* **B529** (1998) 424–450, hep-ph/9801375. [Erratum-ibid.B803:234,2008].